Trinity College Dublin
Coláiste na Tríonóide, Baile Átha Cliath
The University of Dublin

Optimal Control Algorithms for Wave Energy Conversion

Author:

Giacomo Politi

Supervisor:

Prof. Biswajit Basu

Thesis submitted to the University of Dublin, Trinity College for the degree of Doctor of Philosophy

June 2022

Declaration of Authorship

I, Giacomo POLITI, declare that this thesis titled, "Optimal Control Algorithms for Wave Energy Conversion" has not been submitted as an exercise for a degree at this or any other university and it is entirely my own work.

I agree to deposit this thesis in the University's open access institutional repository or allow the library to do so on my behalf, subject to Irish Copyright Legislation and Trinity College Library conditions of use and acknowledgement.

I consent / do not consent to the examiner retaining a copy of the thesis beyond the examining period, should they so wish (EU GDPR May 2018).

Signed:

_____

Date:

_____

Abstract

The aim of this thesis is to design control strategies with the objective of power maximization for point absorber (PA) type of wave energy converter (WEC) devices, considering non-linearities and physical limitations on operational conditions. Novel formulations were developed for control algorithms to address some of the open challenges in wave energy conversion systems. Specifically, the areas of contribution are in the development of multi-resolution control, Linear Matrix Inequalities(LMI)-based control, control for nonlinear systems/time-varying systems and observer-based control. Multi-resolution control has only recently been proved successful in engineering but its application in the area of ocean energy is still unexplored. The broadbanded nature of sea waves is a perfect match where such approach and controllers are useful. A wavelet domain linear quadratic regulator has been formulated for WEC in this thesis, which assign appropriate weights emphasising the frequency bands of importance and an optimal solution is sought for control. LMI-based control instead has seen a substantial recent establishment in tackling multi-objective optimization control problems. The design of a WEC presents often many contrasting requirements, which can be effectively addressed by LMI-based control. These constraints can be either bounds on actuator forces or limitation on displacement strokes of Power-Take-Off systems. The feedback controllers designed with this feature in this thesis, enforce the energy harnessing requirement by the minimization of a performance index, conveniently represented by an H_2 and H_∞ norm of a transfer function. Another aspect considered in this dissertation is deveopment of controllers in the presence of WEC non-linearities. Nonlinear effects in modeling a PA are often too computationally demanding with respect to the design of control strategies, as they are to be computed in real time. This is one of the reasons why linear theories are so widely used in literature. Sometimes though, non-linearities can be significant and bring only a small additional computational burden, so control theories able to consider them will be successful. A control methodology based on a time-varying state space formulation is proposed which solves the Riccati differential equation forward in time. Remarkable improvements are seen compared to the standard LTI control. A further improved forward Riccati differential equation based controller in multi-resolution framework is also developed and advances the method. Multi-resolution strategies are seen to enhance the power performance by about 12% with equivalent control forces involved. With the application of constrained LMI-based control a significant boost of over 40% in energy harnessed was achieved for a given site. Application of nonlinear Forward Riccati Equation control demonstrates a three-fold boost in power for a given sea environment, with the application of the same magnitude of control forces.

Acknowledgements

Prof. Biswajit Basu I would like to sincerely thank my supervisor, professor Biswajit Basu, both on a professional and personal level for granting me the opportunity to undertake this Ph.D. I am grateful to his expertise and his flexibility, in allowing me to work at my own pace, and to coordinate work actions most effectively. I would also like to acknowledge his financial support in the latest stages of the Ph.D.

Marie-Curie-Sklodowska H2020 Programme Grateful acknowledgements to the financial support from project 675659-ICONN-H2020-MSCA-ITN-2015 which made this doctorate opportunity possible in the first place, as part of the European Commission Horizon 2020 program.

Prof. Alessandro Casavola and Andrea Staino Special thanks to Prof. Alessandro Casavola and Andrea Staino, key contributors in discussing, adjusting and perfecting the work hereby. Thanks for their availability, guidance and expertise, always valuable and crucial in most circumstances.

Civil, Structural and Environmental Engineering Department Special mention to my colleagues, Ph.D students Saptarshi Sarkar, Hoa Nguyen, Elia Cantoni and post-doctoral researchers Lea Duran, Himanchu Nagpal which I am very thankful to have shared office space with. I will never thank enough the inspiring discussions, and motivating confrontations this gave us the chance to have.

Family and Friends Last but not least, a deep thanks goes to my family, who continually offer love and support. To my dad, who proof-read my thesis. To my girlfriend Aline, who was on my side despite the distance. To my Dublin friends, which believed in me and supported me all throughout.

Contents

List of Figures

List of Tables

Acronyms

BEM Boundary Element Method. 19, 36, 38, 39, 52, 63, 72

BMI Bilinear Matrix Inequalities. 31, 32, 34, 104, 108–110, 112, 117, 121

DoF Degrees-of-Freedom. 14, 22, 36, 99

DWT Discrete Wavelet Transform. 28, 32, 36, 46, 49, 69, 71, 119, 120

FK Froude-Krylov. 19, 63–66

FRE Forward Riccati Equation. 1, 4, 7, 10, 32, 62, 63, 68, 72, 74–76, 121

IRF Impulse Response Function. 6, 38, 40–42, 64, 66

JONSWAP Joint North Sea Wave Analysis Project. 6, 41, 43, 52, 73, 111

LMI Linear Matrix Inequalities. 1, 4, 27–32, 34, 77, 78, 82, 83, 85–87, 90, 91, 97–101, 103, 104, 107–110, 113, 117, 119, 121

LQ Linear Quadratic. 4, 6–8, 32, 33, 35, 42, 46–48, 50–54, 56–59, 74, 76, 78, 88–99, 101, 103, 119–121

LQG Linear Quadratic Gaussian. 22, 27

LQR Linear Quadratic Regulator. 7, 28, 29, 52, 53, 69, 72, 74, 75

LQT Linear Quadratic Tracking. 7, 47, 49, 50, 55–57, 120

LTI Linear Time Invariant. 1, 32, 59, 62, 63, 77, 116

MIPC Maximum Induced Power Control. 8, 10, 33, 34, 77–81, 83, 90, 91, 101, 107, 111–114

MPC Model Predictive Control. 25, 26

MRA Multi-resolution Analysis. 6, 7, 28, 32, 35, 44, 47, 49–54, 56–58, 62, 63, 71, 74, 119–121

OWC Oscillating Water Column. 15, 16, 18

PA Point Absorber. 1, 7, 15, 16, 18, 19, 25, 27, 32–35, 44, 46, 59, 62, 73, 77, 78, 80, 99, 101, 120

PID Proportional Integral Derivative. 28

PMP Pontryagin Maximum Principle. 25

PTO Power-Take-Off. 1, 6, 9, 13–16, 19–27, 29, 36, 37, 44, 47, 63, 64, 79, 84, 91, 95, 98, 103, 113–115, 117

TV time-varying. 16, 26, 28, 32, 62, 75

WEC Wave Energy Converter. 1, 3, 6, 13–16, 18, 19, 21, 22, 24–30, 32, 35, 36, 39, 42, 44, 62, 63, 69, 75, 77, 78, 84, 91, 95, 101, 104, 111, 116, 119

Chapter 1

Introduction and Literature Review

This chapter provides the motivation behind the research conducted in the thesis and also presents some general background to the work. A broad review of the topics involved is given including the state-of-the-art in the related field of research performed. The contributions are articulated with respect to the research gaps identified and the achievements in the thesis are highlighted. The chapter also outlines the main aim and the objectives of the research, and concludes with an overview of the individual chapters and the structure of the thesis.

1.1 Background and Motivation

Economic sustainability of ocean wave-energy extraction is still the most pressing issue to be addressed in order to make this kind of resource commercially viable. One of the reasons why research has moved at a slower pace on wave energy, compared to other renewables as wind and solar, is the nature of the resource itself. Wave energy is in general a very dense source, as the amount of energy per square meter on the surface of the ocean can be even one order of magnitude higher than the solar energy present in the same area. Higher energy density though, requires the devices to be more resistant to be able to withstand the harsh and at times possibly damaging sea environment. Moreover, the most energetic areas are usually in remote parts of the sea, quite far away from the coast. This increases dramatically the costs of installation, operation and maintenance as well, given the necessity for moorings for deeper waters and longer power transmission cables to reach shore.

Oscillating body wave energy converters (WECs) absorb energy by means of the mechanical work done by the wave forces on oscillating structures. The power-take-off (PTO) applies a mechanical force on the body and converts part of the kinetic energy into a different form, such as electricity.

In the design of every feature of a WEC a key role is played by mathematical models, which are used as a main tool to estimate the devices response in terms of motion, power produced, and structural loads. Mathematical models are often at the very base of control algorithms development, needed to ensure the most convenient response of the devices to given conditions. The motivation of this thesis is in developing novel control design methodologies that can be readily applied to functioning devices in real time based on these mathematical models, so that the efficiency of the devices can be ultimately increased, bringing down the so called *Levelized Cost of Energy*. According to Ocean Energy Europe [1], in can be reduced to $110 EUR/MW$ by 2030 for wave energy sources. In other words, control algorithms are meant to enhance wave energy extraction to eventually increase the competitiveness of the resource with the other renewables and with standard non-renewable sources. Mathematical models in wave energy converters are naturally developed from traditional ocean engineering theory, where it is common to use linear models. This is mainly due to computational convenience, since the inclusion of one or more nonlinear effects normally requires a substantial increase in complexity and computational time. While this is generally not an issue with system of this complexity, it can become a critical matter when nonlinear effects are more thoroughly accounted for. This is definitely true when the WEC is allowed to oscillate in several Degrees of Freedom (DoF) or when a number of WECs are considered, where the computation of the hydrodynamic coefficients and system identification has to be carried out for each oscillating mode and for all the combinations between two oscillating modes. [1]

Unless accurate results are needed, for example on extreme events or loading studies, where fully-nonlinear CFD (computational fluid dynamics) or SPH (smoothed-particle-hydrodynamics) are used, it is convenient to prioritize the shortness of the computation time to allow the strategies to act in real time. Hence, the algorithms presented in this thesis are chosen so as to be suited for real-time implementation. This is eased by the latest technological achievements in processors industry. However, experimental testing and actual application of the algorithms presented onto real devices is left for future work. The interest of the writer was to embrace some of the existing issues which were believed to most severely limit the successful application of some existing control methods, and address them to make them viable for wave energy devices.

Another aspect of the studies in this thesis eventually questions the application of linear control. As discussed, a variety of effects can introduce nonlinearities in the model of a WEC, from the PTO to the fluid body interaction. While it is often reasonable to assume a linear behavior for the radiation forces, some studies have shown a wide disparity between linear and nonlinear models in terms of excitation forces [2], viscous forces [3] and hydro-static restoring forces [4]. This is particularly obvious in the case of the effect of a nonlinear restoring force on a standard geometry

[1] i.e when symmetry cannot be exploited, computations have to be carried out $n + n(n-1)/2$ times, where n is the number of oscillating moved of each device multiplied by the number of devices

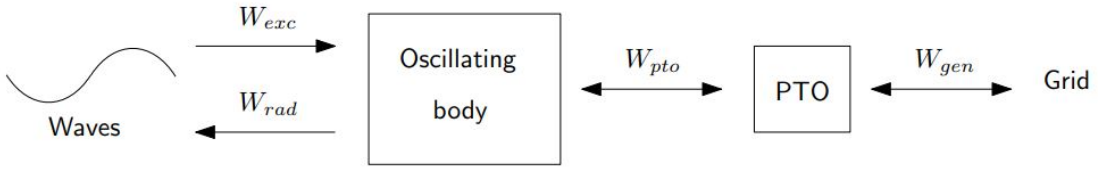

Figure 1.1: Energy transfer through an oscillating body wave energy converter

such as a sphere. When applying a linear control strategy, the performance deteriorates quickly and the necessity of an upgraded control method emerges. Work has been done on nonlinear control, but causal controllers for real time implementation on this kind of devices are still relying on either linear state space models or frequency-independent approximations of fluid body interactions.

1.2 Literature Review

1.2.1 Wave Energy Converters

Ocean waves as said, happen to have the highest energy density (per unit area) of all the renewable energy sources [5] and the total power that can be generated around the coast of the whole world is of the order of 1 TW, similar to the global electricity demand [6]. Recent research has shown that nearshore waves are only marginally less energetic compared to deep water waves [7]. This was a main drive to primarily focus on oscillating bodies in nearshore installations [8] for the new generation of wave energy converters (WECs). The debate on nearshore vs further from shore installations is still ongoing, but what is certain is that floating WECs drive much of the attention in the research field.

Point Absorbers (PA) and Oscillating Water Column (OWC) [9] type of devices have emerged among the most promising technologies proposed worldwide. For this reason they are among the most studied in literature. The peculiarity of PAs is to be relatively small, linear damped oscillators excited by ocean waves. They work as floating or submerged bodies, which are put into motion with a PTO machinery resisting to it. Relative motion between parts ensures the mechanical-to-electrical energy conversion, and this useful energy can be then transmitted to shore or to locally charge batteries/storage units. This is in contrast especially with the first generation of OWC type of devices which was built onshore and which absorbs energy by coupling the ocean water oscillation to an air turbine through compression and expansion of an air chamber. These latter technologies are still heavily studied, but as mentioned research is now more pushing towards floating structure solutions.

Over the last decades, a variety of technologies has been developed with the aim to exploit this abundant renewable energy. In most devices, the conversion process starts by transforming

the wave energy into mechanical energy of an oscillating system. Another usual common feature is the second stage of energy conversion, where the floating or submerged oscillating bodies drive a PTO mechanism, where the mechanical power is transformed into electricity in a way that is very much dependent on the technology of the machinery [10]-[11]-[12]-[13]. See Fig. 1.1 for a schematic representation of the energy conversion stages: the energy is transferred from waves to the prime mover by means of the work done by the incoming waves (W_{exc}), called excitation force. Neglecting the losses, some of the energy is returned to the sea by the radiation effects (W_{rad}) and part is absorbed by the PTO. A fraction of the energy absorbed by the PTO is delivered to the electrical grid by means of the work performed by the generator (W_{gen}) and the other fraction may be returned to the oscillating device.

According to the classification made in [14], there exists a third category of floating WECs, namely the so called overtopping devices, which is not discussed in the present thesis (see Fig. 1.2 for the classification). A comprehensive description of wave energy conversion technologies can be found in [15]. In the next section we will start by briefly introducing the first category, which is only mentioned in this thesis, the OWC. It is found relevant, as some of these devices can be modelled also as multibody-PA, so they possess few of the same properties and satisfy dynamic assumptions of single-bodied PA in linear domain.

Oscillating Water Column Devices

OWCs are among the first yet still regarded as some of the most promising concepts in the WECs literature. Many different solutions have been evaluated. An extensive literature exists in [12]. As mentioned, a main distinction can be made between fixed and floating structures, but in all cases this structure open to the sea underneath, traps the air above an inner free surface. Wave action then compresses and decompresses the trapped air (see Fig. 1.3(a), where a floating OWC is schematically represented) creating a time-varying pressure at the air-water interface. The air is then forced through a turbine, coupled with a generator. The most common type of turbines used are the bidirectional Wells turbines (see Fig. 1.3(b)).

As anticipated, some of the floating OWC devices keep some of the properties of the PA. This highly simplifies their modelling, and the concepts behind control and optimization procedures can be easily extended or replicated. These devices are known as spar buoy type. A full characterization of this kind is given in [17]. In [18], we can see how the dynamics of a two-body device exactly resembles that of an OWC, limited to wave-to-inner surface motion.

Spar-buoy-OWC kind of devices are to be controlled as well for optimizing their power performance at sea and their dynamics will determine the most effective way to do so. There are some strategies which are common to PA type of devices. One of the most known is latching. In [19]

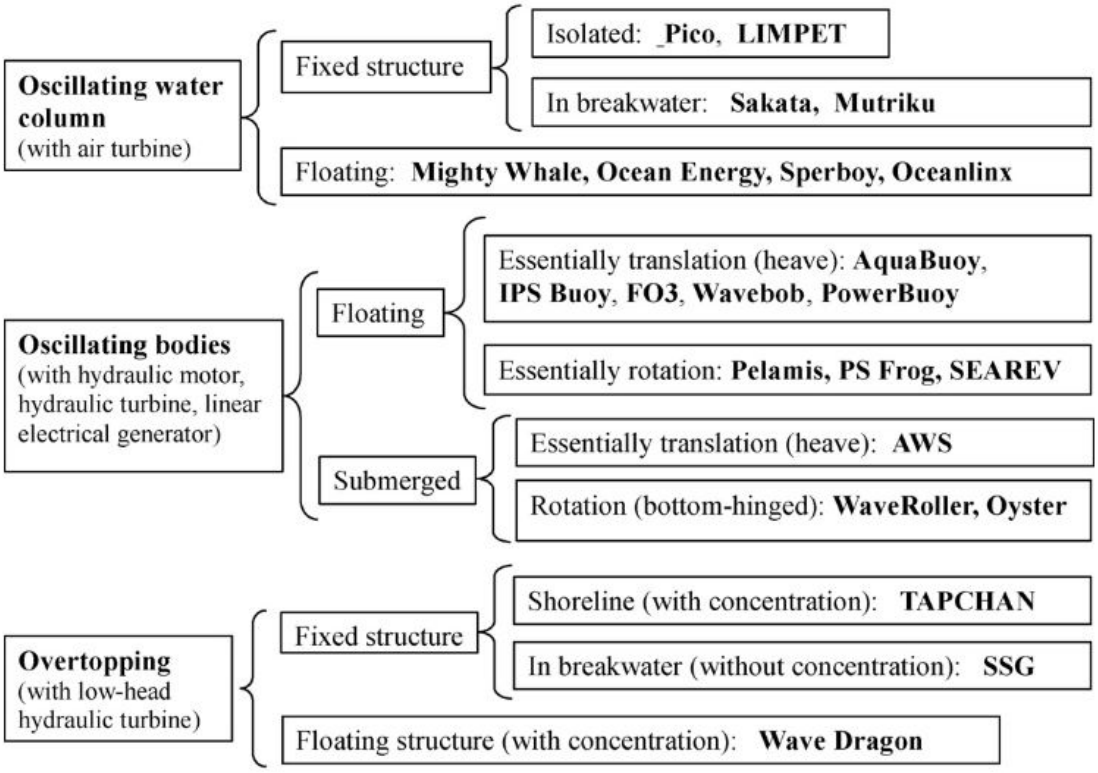

Figure 1.2: Categories of wave energy converters [14]

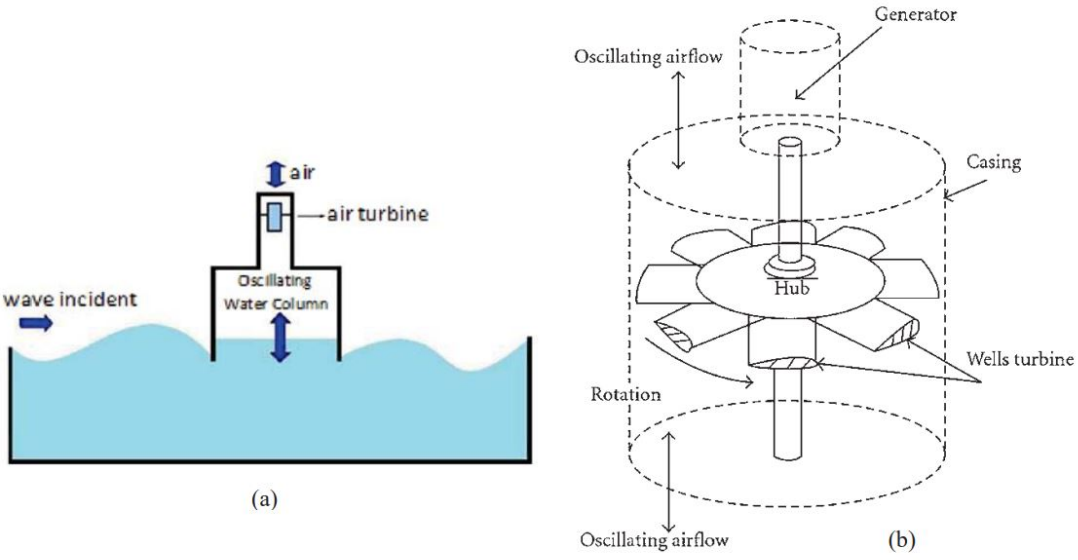

Figure 1.3: Schematic diagrams of (a) Oscillating Water Column and (b) Wells turbine. Image courtesy of [16]

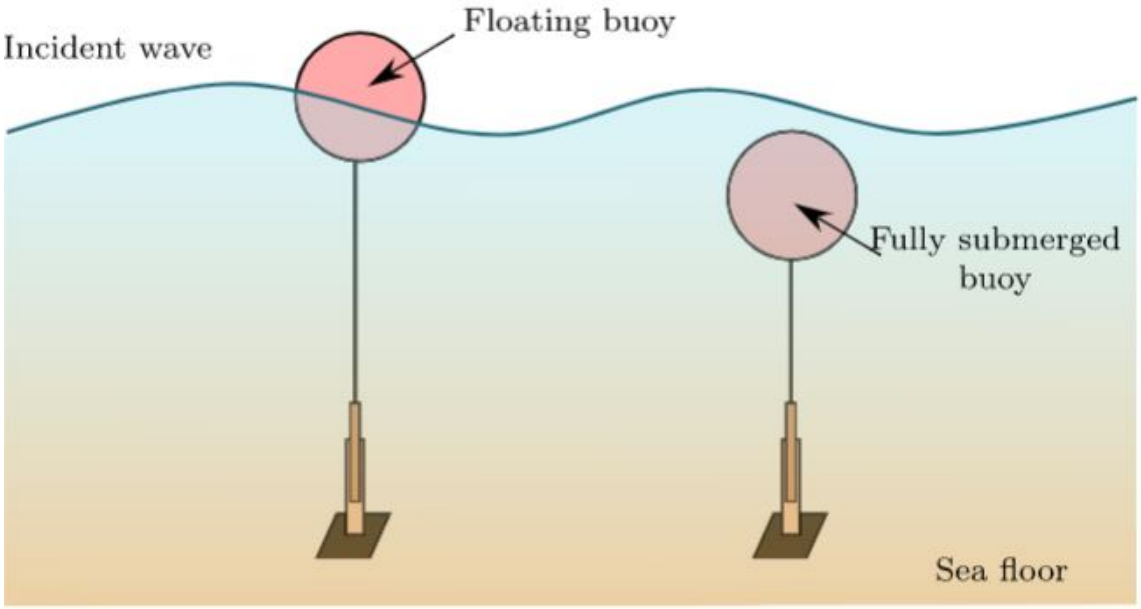

Figure 1.4: Schematic representation of the floating and fully submerged WECs that extract energy from oscillations in heave [26]

the application of latching control to a model of spar-buoy-OWC is discussed. However, the use of a special type of turbine and a receding horizon technique is needed though for a successful application.

Optimization of the shape of spar-buoy-OWC type of devices is made in [20] based on the maximization of wave energy extraction over real sea spectra. The system is modelled in frequency domain with dynamic constraints.

An interesting characterization worth mention is about a novel radial self-rectifying air turbine for this type of devices, explained in [21] and [22].

Studies on air chamber pressure models are undertaken in [23]- [24], as well as evaluation of combined efficiencies of the turbine and the generator in the electrical power output. Three performance indicators for air chambers have been introduced by [25].

Point Absorbers

textcolorredPoint Absorbers are central to this thesis, and the methodologies presented are applied to this kind of device. It is perhaps the simplest and for this reason the most studied class in literature. The broadest variety of results is available on its hydrodynamic modelling, geometrical optimization studies, material technologies, power-take-off machinery and of course control [6]. This makes comparisons and evaluation of control strategies straightforward. These are the main reasons behind this choice.

Among PA devices, designed to capture wave energy regardless of the direction of the wave

propagation, a sub-category is constrained to move only in the vertical direction, and the energy is harnessed from the motion relative to the seabed or to some submerged reaction body. Wave-structure interaction of such devices was tackled since the early days [27]. In Fig. 1.4 a representation of a floating and fully submerged PA device is provided.

Nowadays, potential flow theory is the most useful and popular numerical tool for modelling Wave Energy Converters; radiation/diffraction velocity potentials are easily calculated by boundary element method (BEM) solvers, using a discrete number of sources on the surfaces of the submerged bodies so as to fulfil all boundary conditions. Evans applied potential flow theory for regular waves to analytically study the hydrodynamics of oscillating body WECs [28]. Researchers contributed to potential flow algorithms throughout the years to model various types of oscillating body devices [29]-[30].

Assuming small body motion and a linear PTO dynamics it is possible to model numerically the WEC in frequency domain, using potential flow theory. In [31] the frequency domain approach has been used to analyse the power output for a two-body heave PA. Although the frequency domain analysis is relatively simple, one of the main drawbacks of its utilization is the impossibility to handle non-linearities, be they structural or of any other type. Besides, it is not possible to model the response of a device on a (real) broad-banded sea using frequency models. Control on a wave-by-wave basis is equally not possible.

It is hence necessary to perform a time domain analysis. The equation of motion for marine structures was initially proposed in [32], using potential flow theory. The equation contains a causal convolution integral to include the "memory effect" of the radiation damping. Approximations to this convolution term are now usually adopted, so that the integro-differential equation becomes an ordinary differential system, at the expense of introducing additional state variables [33]-[34].

In [35] the impact was studied of a nonlinear Froude-Krilov(FK) force on the dynamic response and power output of a cylidrically shaped and a spherical PA in regular waves. It was found that the FK force influences only marginally WECs with a constant cross-sectional area, while it affects significantly devices with a varying cross-section. This is one of the main subjects studied in chapter 3, where a control strategy developed for weakly-nonlinear models is successfully applied to a model of spherical Point Absorber.

The power take off unit

The PTO is designed to transform the energy associated with the oscillation of the primary hydrodynamic mover to a flow of energy with the right characteristics for being delivered to the electrical grid. There are a number of difficulties in this process that depend very much on the technology used. The power amplitude varies in time, but it must satisfy stringent requirements

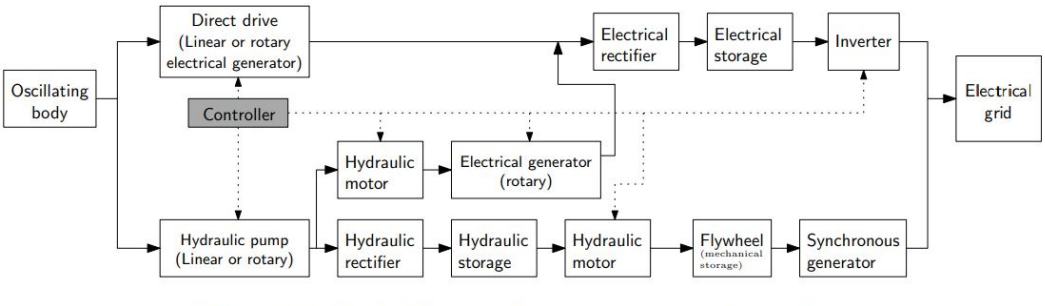

Figure 1.5: Block diagram of common PTO configurations [14]

(power quality) to be effectively delivered to the grid.

In particular, wave power is oscillatory by its nature, and the frequency and amplitude of those oscillations depends on stochastic meteorological factors. For this very reason the PTO always has to contain a rectifier and an element of storage: the rectifier is used to produce an unidirectional energy flow compensating the alternating nature of wave power, and the storage is used as decoupling element between the random source (waves) and the destination (grid).

The block diagram shown in Fig. 1.5 summarizes the structures of common PTOs. The slow alternating motion of the oscillating body will have to be transformed into an electric signal with constant voltage and frequency. The figure should be read from left to right. Depending on the device and the mode of oscillation, also the alternating motion can be linear or rotary.

The energy associated with the oscillating motion can be converted directly into an alternating current by using linear or rotary generators. The electrical rectifier and storage in this case produce a smooth DC signal, while the inverter generates the AC signal suitable for grid connection. If the mechanical energy is directly converted into electrical this is known on generators as *direct drive*; fewer components are required in this case, with better reliability and efficiency. Unfortunately large-dimensions generators are usually necessary to combine the slow motion of the primary absorber to generate the necessary PTO forces.

Hydraulic components can be used to transform the energy thanks to an alternating flow of fluid (oil), smoothed and rectified by accumulators and valves to drive a hydraulic motor at constant or variable speed. Depending on the motion of the hydraulic motor, if the speed is constant, then it can be connected to a synchronous generator, which usually provides good smoothing thanks to the inertia of its rotor. If needed, a flywheel can be added. If the speed is variable, then the hydraulic motor can drive the electrical generator at higher speed than a direct drive. The consequence is that the electrical generator is smaller than the one for a direct drive.

Reaction Force

An important characteristic for the classification of PTOs is their capability in terms of the force that they can generate. In fact, the amount of energy transferred by the primary absorber to the PTO can be controlled by acting on the PTO force. If a WEC is equipped with a control system which optimises the energy flow through the device, the control system usually acts on the PTO force to pursue this objective. Hence, the characteristics of the PTO are important for the energy absorption performance of a WEC. The capability of the PTO to exert the exact force specified by the control system is fundamental for the implementation of control algorithms. Direct drive solutions are characterized with good characteristics and dynamical properties. In fact, as assumed throughout this thesis, it is known that the force/torque exerted by the electrical generator can be controlled by acting on the current flowing through the coils. A wide choice of well established commercial solutions is available.

Another important characteristic is the bidirectional power capability, i.e. to reverse the energy flow from the PTO to the primary mover, and back to the water. This is more commonly called *reactive power*. The property is required by many control techniques for improving wave energy absorption. A PTO with this property is known as *active PTO*, while when it is not capable of this, it is known as *passive*. Passive PTOs are obviously simpler and cheaper.

1.2.2 Control of WECs

To be cost-effective and to produce a significant amount of power, WECs should be able to harness energy under different wave conditions. This means that the device should be able to work efficiently over a wide range of frequencies according to the shape of the wave spectra. To this end, control systems can be designed to adapt the dynamics of the WEC to the spectral characteristics of the waves for different sea states [36]. Classical control for wave-energy devices mainly aims at tuning the resonances of the devices at the wave peak frequencies [37]. A by now well known condition (see e.g. [38]) is indeed that the control action at optimal tuning should enforce the velocity of the device to be in phase with the excitation force.

However, it turns out that for real sea spectra, these techniques are not that efficient as they don't allow real time control on a wave-by-wave basis [39]. The main drawback resides in the *noncausality* of the involved transfer function as the application of controllers requires knowledge about the future motion of the device [40], [41].

The present and following paragraphs provide an overview of the control methods introduced in the literature for the control of WECs. First, we briefly recall the principles of reactive control. Then, control strategies are described, which share the common objective of the maximization of absorbed energy when no restriction is applied. Control strategies which instead take into account

constraints imposed by the physics of the problem are cited in the following paragraphs.

Reactive Control Overview

A control strategy resulting from some form of optimization is generally known as optimal control. Typically, the goal consists in maximizing the absorption of average power. In particular, the so called phase and amplitude control, and the reactive control (or impedance matching control, also known as complex conjugate control) aims at letting WECs absorb the maximum amount of energy from waves when the system is linear (as the models implemented in this thesis). The two control strategies lead to the same results in terms of motion, forces and converted power, following however, different procedures. Both require future knowledge of either the device motion or the wave force excitation. So both reside behind the drawback of noncausality. Phase and amplitude control calculates a reference velocity from knowledge of the excitation force. Reactive control calculates the PTO force from the velocity. In Fig. 1.6, a monochromatic wave impacts a vertical cylinder (the hydrodynamic model is discussed later in chapter 2); there we see the effect of reactive control on different quantities.

No further details are given on this matter. We limit ourselves to conclude that the reactance of the PTO is generally non-zero and this means that during some time intervals the PTO returns power to the oscillating body. In addition, large fluctuations of absorbed power are observed, as well as a large ratio between peak power $\hat{P}$ and average power $\bar{P}$. In order to make this possible, the PTO requires expensive components and this might reduce the economical convenience of the reactive control when applied on a WEC.

Typically, the amplitude and the phase of the force are controlled by adjusting some proportionality constants such as load spring, load damping and load inertia: this is the essence of complex-conjugate control. The effects of irregular waves on complex-conjugate control are analysed in [42] and [43]. Implementation of the technique requires predictions or measurements at distance from the device. The efficiency of these prediction techniques are studied in [44] and [45].

Causal approximations to the previous relationships are advantageous for several reasons. First, the overall control architecture is significantly simplified and, consequently, the related computational complexity reduced, easing a real-time implementation. Moreover, the uncertainty related to the prediction techniques is avoided. Causal approximations to the relations between the wave force and the wave elevation have been proposed by several authors [46],[47]. Non-predictive control has been implemented in [38], [48].

In [47], the authors developed an optimal causal control system of three DoF (surge, pitch and heave) based on a Linear Quadratic Gaussian (LQG) regulator. The control requires only the knowledge of past measurements and the spectral characteristics of the sea. They also discuss the

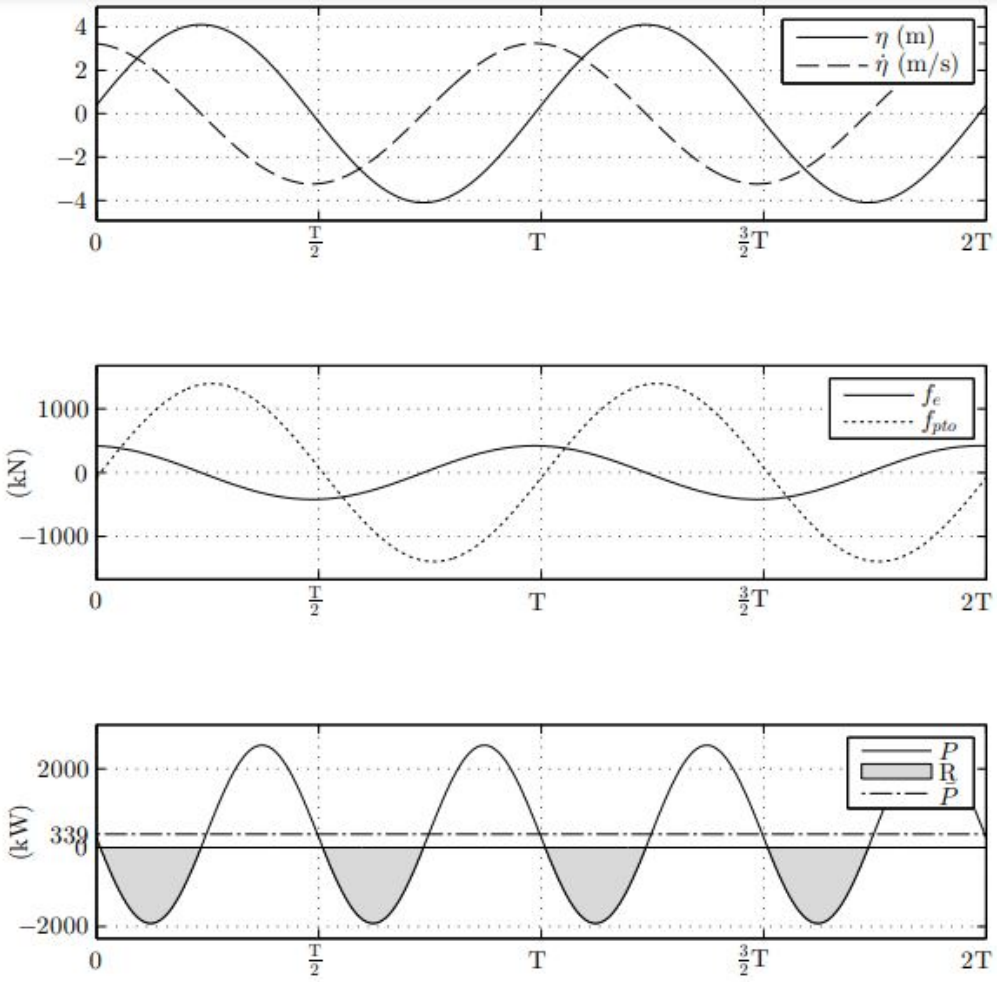

Figure 1.6: Position (η), velocity ($\dot{\eta}$), excitation force (f_e), PTO force (f_{PTO}), total absorbed power (P), average absorbed power ($\bar{P}$) on a vertical cylinder with model described in chapter 2, using reactive control, for monochromatic waves with period $T = 8s$. The grey area (R) indicated the PTO working in reactive mode.

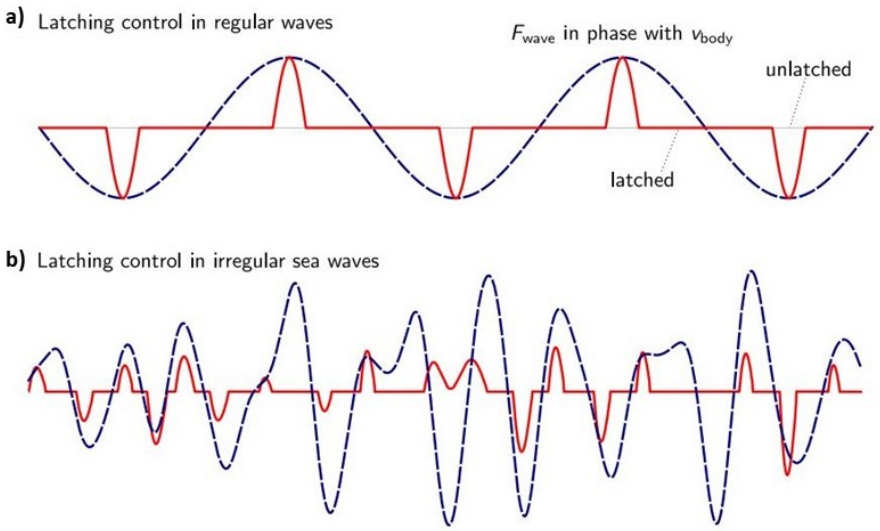

Figure 1.7: Latching control to tune the phases of the heaving velocity and the excitation force (a), latching control for a system subjected to irregular waves [52]

power factor for both reactive and causal control.

Latching and declutching control

Latching and declutching control strategies are the main tools used by methods based on the imposition of phase conditions.

The latching control proposed in [49] is an open-loop strategy. It is one of the most investigated and certainly one of the simplest methods [50], [51]. The idea is to latch the absorber motion when the velocity is zero and release it when the velocity and wave load are in phase, so that mechanical energy is supplied to the absorber (see Fig. 1.7). It was proven that latching control is very effective for oscillating-body WECs.

The fundamentals of latching control are presented in [53] and in the review of wave energy conversion [54]. The application of latching control to a heaving hemisphere has been discussed in [55] and [56], while the effects of latching on the grid have been investigated in [57].

Experimental realizations of latching prototypes are reported in [58] and [59]. The results from wave-tank testing are compared with a numerical model of vertical cylinder with hemispherical bottom.

The time interval when the device needs to be locked is called *latching time*; it is a critical variable which affects the conversion efficiency. Numerical optimization has been implemented in [60] to derive the latching duration in random seas.

An extension to latching, named *declutching* is proposed by Babarit [61] and it is applied to the SEAREV device to obviate an energy loss occurring in hydraulic PTOs, called Coulomb damping. Combination of latching and declutching is studied in [62] where a significant increase in energy

absorption is found compared to a separate latching and declutching application.

Other control strategies

In the early days, optimal control strategies on WECs in irregular waves focussed on the application of Pontryagin's maximum principle (PMP) and the numerical solution of the two-point boundary value problem [63]. PMP was used in [63]–[65]. The main problem of such indirect methods is that they attempt to solve analytically the necessary conditions for optimality, but they are problem specific and often with a small convergence region, hence requiring a good initial guess.

More recently, the wave energy community has adopted the popular Model Predictive Control (MPC) method [66]. Attempts to adopt discrete-time versions of its performance functional (object of the minimization problem) led to various modifications of the standard formulation, and in turn to the development of the so called direct transcription method, as generalized discretization framework.

In [67], the discretization is performed via mean weighted residuals. The first application of a direct transcription method to a wave-energy problem was reported in [68], which uses Fourier basis functions (and uses amplitude constraints only) to parametrize the device motion and the PTO force. In [69] instead, a pseudospectral method is used to approximate the motion and PTO force using polynomials, accompanied by an additional constraint to enforce periodicity.

A parameter optimization for a generic WEC (with respect to wave climate) is instead described in [70]. The WEC therein considered is a vertical cylinder with a limited range of motion and a linear damper. The influence of damping and stiffness are studied for sea state statistics of few test sites. It shows that the optimized device (under controlled conditions) performs significantly better.

A stochastic approach for the optimization of the PTO damping and spring coefficients on a Point Absorber is described in [71]. There, a linear-frequency-domain stochastic model of the WEC is developed and the optimal values for spring and damping coefficients are calculated once again by PMP. A device using a nonlinear hydraulic PTO is therein simulated, and the results are compared with the stochastic model in frequency domain.

In [72], the control of a PA with a linear generator is implemented via a Maximum Power Point Tracking algorithm. The algorithm compares the average power absorbed during a specific wave-cycle, and modifies the duty cycle of the electrical power mechanism accordingly. Both experimental laboratory and ocean results are reported.

Control of the system can be achieved also by adjusting the inertia, as described in [73], where mechanical amplification of oscillations are pursued by mass modulation, with water as a ballast. Power production and input-output stability are studied with respect to the mass modulation and

PTO damping.

Filter-design principles have been used to implement a wide bandwidth controller in [74], which aims at improving the independence of absorption performance from the sea conditions of the site where they are deployed. The authors claim that the wide-band response of the controller do not require a real-time tuning. In the present thesis, power maximization is always studied under the assumption of known sea-state conditions. This means that variations of such conditions always imply different control configurations. Although real ocean waves are, by nature, non-stationary phenomena, sea states are recognized to be slowly time-varying processes, meaning that their defining parameters are not altered more often than every few hours. It is believed that the slowly varying assumption of sea phenomena, justifies the philosophy of adjusting the control layout, when the spectral properties of the sea change substantially.

To conclude, it is compelling to mention the so called *survivability control* strategies. When the conditions of the sea become too severe, the control systems are generally programmed to shut down the device, in order to protect it. However, deciding when to deactivate the system is not obvious. In [75], the author claims an increase of the average annual power production is safely obtained, if the control system prevents to deactivate the device when not strictly necessary.

Constrained control

The optimal control problem in the real world always involves some form of sub-optimality, due to the uncertainty in the estimation procedure or other unforseen variations. Many authors who make use of non-causal techniques, have dealt with it by including auto-regressive models, receding horizon, or the well established MPC (the application on a PA model was presented in [66]). All of these strategies are, to some extent, sub-optimal. This means that a slightly smaller response and power output is to be expected compared to optimality. Nevertheless, external conditions are likely to push the device to operate beyond the physical limitations of the WEC, if no constraints are included.

Wave-energy converters contain mechanical components with limited operating ranges, may they be hydraulic PTOs or other machinery. These ranges necessarily involve force capabilities, length of strokes, velocities and other quantities, depending on the PTO device.

MPC still seems one of the most promising techniques in handling constraints but challenges still exist for its implementation at a practical level. The well known challenge of real-time computation with MPC is discussed in [76]. It was found that the performance of the MPC algorithm as well as of the receding horizon pseudospectral optimal control is found to suffer from high sensitivity to the approximation quality of the radiation force.

Beside MPC, handling constraints alongside the main objective of the controller is a task that

many authors have dealt with in many ways, starting from [77]. The possibility to cast them together in the same framework and build a multiobjective optimization was considered in [78] on a PA device. The problem was written as a LQG control, with the interesting property of being causal. Linear Matrix Inequalities (LMIs) were used to express the multi-objective optimization. The hard constraints were formulated in terms of variance, or more specifically the objective function included a penalty term proportional to the variance of the constraint violation.

In [77] a sub-optimal control law for WECs considering nonlinearities and constraints was presented, based on adaptive dynamic programming. Adaptive dyanamic programming was applied to solve the associated Hamilton-Jacobi-Bellman equation and the optimal cost and control force values are approximated with the help of a neural network.

There exists a rich literature on optimal constrained control strategies, but it mostly deals with frequency domain models and/or monochromatic waves, hence strategies not readily applicable to real devices. Eidsmoen [79] has presented a constrained version of the optimal controller, using Lagrange multipliers. The extracted power is obviously reduced when the stroke excursion limit is considered (compared to the unconstrained case), although the machine conversion-efficiency is seen to increase, meaning that the output energy is higher if compared to the total energy passing through the system.

Comparison of controllers

Literature on comparisons of control strategies is not missing as well. It is evident, that as a sub-optimal strategy latching control performs worse than the optimal control, however it performs substantially better than passive control. Detailed comparisons can be found in publications by Falnes [58] and [59].

A number of control methods are evaluated and compared in the publication by Hals [39], in the context of a model of heaving PA. Comparisons are made between model-predictive control, gain scheduling and extremum seeking, phase control by latching and clutching, linear damping and an approximate velocity tracking. Discussions are made with respect to the absorbed power, reactive power, implementation complexity, all based on simulation results. Strengths and weaknesses of each method are presented, suggestions on how to implement those controllers are provided, including tuning and constraints handling.

Control strategies can also be assessed with respect to the mechanical fatigue imposed on the machines they are implemented on. An analysis based on the *accumulated fatigue damage* metric [80] was carried out in a model of the Wavestar device, where the PTO is reduced to a mass-spring-damper. By tuning the controllers to different sea states (instead of keeping the configuration to a single setting) it was shown that the power production increases, but at the cost of a much larger

accumulated fatigue damage factor.

1.2.3 Advanced control strategies

Conventional control strategies for WEC devices have been broadly introduced in the previous section. Now, we present some more advanced control strategies relevant to this thesis. These are: multiresolution control, nonlinear control, LMI-based control and observer based control with regard to constrained wave energy conversion systems.

Multiscale Control Strategies

A relatively new class of controller, central for this thesis is that of the so called multiscale or multiresolution control strategies. As the name suggests, it is based on multiresolution analysis (MRA) or multiscale approximation. MRA is the design method of the most practically relevant Discrete Wavelet Transform (DWT). It was introduced by Stephane Mallat and Yves Meyer in 1988 and extensively treated by Mallat [81]. In the last decades, a few forward steps have been made in the application of PID to control theory, but there is still much to be investigated. In [82] it was shown that wavelet theory could be applied to a controller and thanks to the decomposition of the error signals into signals at different scales, the controller was able to show better noise rejection and smooth control performance than a PID. In [83] a multiscale PID control was also used for dynamic positioning of vessels under noise and environmental disturbances. The performance compared to a conventional PID with acceleration feedback, was again highly improved.

In [84], MRA was applied to slowly TV systems. A modified optimal control problem in a linear quadratic regulator (LQR) form was constrained to a band of frequency in wavelet domain. The band-dependent control-gain matrices obtained were applied on filtered time signals over an interval between initial time and current time. Thanks to the perfect decomposition/reconstruction property of MRA, the controller proved to be effective on the damping of forced vibrations even when basic LQR control fails. In [84] this controller is upgraded to an online formulation, so that the weights are updated in real time. It is demonstrated that the displacement response of vibrations is further significantly reduced for both single degree of freedom and multiple degrees of freedom systems.

The employment of multiresolution controllers though is still limited and much has to be discovered on their application. For example, no wavelet based control algorithm has been yet applied on wave energy devices.

Control of nonlinear WECs

Here we give some insight on the literature available on nonlinear effects in WEC models, and the role control strategies have. In the marine environment, nonlinearities have multiple causes, starting from the resource [85], the wave-device interaction [86], [2],[87] and the power take off system. Depending on the type of WEC and PTO, these nonlinearities can become significant, especially when the objective of control strategies is to amplify the device motion in order to maximize the power. A few studies have shown substantial differences between linear representations and experimental tests [88], compared to fully nonlinear models [89], or partially nonlinear models [2]. The computational effort usually increases noticeably with the number of nonlinear effects considered in the model while the gain in accuracy depends on the relevance of each of those [90]. The effect of nonlinear forces on WEC models has been investigated thoroughly in [91]. In [90] it is suggested a scenario where the behavior of WECs is summarized into three main regions: linear, nonlinear and highly nonlinear, depending on the ranges of motion. In [92] it is shown that nonlinear models are definitely needed in order to keep a good accuracy, especially when the devices operate close to resonance. Subsequently, WEC devices need an upgraded control methodology as well when the linear model description is not enough. In [77] it is shown how nonlinear controllers can make a significant difference even on the simplest devices.

LMI-based Control

Linear-matrix inequalities emerged in the 1990s as a powerful tool for optimal feedback design [93]. LMI-bsed control attracted a lot of interest since a wide variety of problems could be reduced to a few standard convex or quasiconvex optimization problems. These optimization problems could be solved very efficiently with recently made available codes based on interior-point or primal-dual techniques [94]. Applications of LMI-based control involve, just to mention a few

- construction of Lyapunov functions for stability and performance analysis;
- optimal system realization;
- interpolation problems, including scaling;
- multicriterion LQG/LQR;
- expression of H_2-H_∞ constraints;

We are going to place our interest mostly in the last two points.

As far as energy harnessing is concerned, in [95] it is shown how an LMI-based control allows to cast in the same multi-objective optimization different contrasting objectives related to a suspension

systems for cars. In particular, the energy maximization objective, can be expressed in terms of an H_∞ constraint.

For wave energy applications instead, in [78], Scruggs employs LMI-based control for a constrained power maximization problem of a WEC subject to linear dynamics. The strategy manages to cover simultaneously the two objectives of power maximization and the limitations (on displacements, force and voltage levels etc.). In [96], it is seen that hard constraints can be cast into the same LMI optimization with the concept of reachable sets in state space ellipsoids defined by a quadratic storage function. By avoiding saturation effects, the maximization of power criteria is simultaneously satisfied.

As seen in [5], in wave-energy-conversion systems and especially when applying control algorithms for power maximization, the required responses often stretch outside the linear regime and constraints are likely to be needed.

In other wave energy applications, LMI-based control is applied in the context of robust control: in uncertain systems, the uncertainty input/output channel can be approached with a H_∞ norm minimization. The minimization can be solved together with the usual power maximization objective thanks to the multi-objective formulation allowed by the LMI form. In [97] the controller is constrained to be stability-robust to unstructured uncertainties. The solution though results non-convex, requiring an iterative process to arrive at a local optimal solution.

Observer Based Control of WECs

An observer-based controller is a dynamic-feedback controller with a two-stage structure. First, the controller generates an estimate of the state variable of the system to be controlled, using the output and known input of the system; next the state estimate is treated as it was the state of the system itself and used as a static state feedback. In real applications, controllers are always of this kind.

In order to generate state estimates, what is needed is measurements. Measurements are all what can provide information to the control decision maker on short-term, medium-term or long-term time windows. In case of feedback control of WECs, measurements have to be conducted constantly, and the ability of the sensor to provide accurate frequent measurement data is crucial. The publication [98] reports the state of the art of the current measurement equipment used on open-sea trials. An obvious conclusion to that is that it is not trivial to measure any entity at sea, and almost every project that have reported their measurements at sea have also reported some kind of problem encountered due to the marine environment, may that be broken buoy lines [99], electrical equipment [100] or simply the difficulty to adjust to new conditions [101].

When it concerns measurements on the WEC devices themselves, things become even more

complicated as there are even fewer data collection systems for the specific needed entities in control mechanisms. The most common quantities measured are perhaps electric power, air pressure, device motion and acceleration. The measurement methods also can be very different (GPS, linear position sensors, accelerometers, optical systems).

Feedback control strategies as said, need access to signals updated in real time, and for their deployment it is fundamental to have measurement equipment able to provide those signals to the controllers. Knowing exactly what measure is available and what not, and how accurately/frequently can be measured is fundamental on a general basis.

Bilinear Matrix Inequalities Constrained Observer Design

Observer design of linear systems is highly complicated by the introduction of hard constraints. In [102] a method is proposed for a linear system with limitations on the input. The observer parameters are optimized with respect to the system performance and some assumptions on the solution make it possible to obtain an LMI formulation, from which the computation of the observer gain is straightforward.

When multiple hard constraints are to be taken into account, despite the main system being linear, the observer design is shown to be Bilinear Matrix Inequalities- (BMI) based. Less literature is available on the solution of BMIs and convergence is not granted given that they are in general non-convex. In [103], the problem of solving BMIs in the optimal control design field (using successive resolutions of properly defined LMIs) is described. The method is known as "LMI-based coordinate descent method". The problem is indeed solved independently for each coordinate at each step using an LMI optimization, while the other coordinate is fixed. No method based on this idea has been proven to formally converge to the global optimum of the BMI problem, or to a local optimum in general. It has been, however, shown that one can obtain a sequence of progressively improved solutions thanks to the successful choice of the initial guess.

In [104], the BMI problem is reduced to that of finding a feasible point in a Biaffine Matrix Inequality constraint. Hence, it is basically the bilinear version of the Linear (Affine) Matrix Inequality programming problem. It is approached as a biconvex global optimization problem by minimizing the maximum eigenvalue of a biaffine combination of symmetric matrices.

Other techniques have been investigated for the solution of BMI problems. Convexification methods known as sequential convex programming or the nonsmooth maximum eigenvalue minimization are introduced in [105],[106]. They show, together with the augmented Lagrangian approach in [107] that the selection of a feasible initial point can be a nontrivial matter.

In [108], BMI optimization problems are converted to polynomial-time solvable surrogates. That is shown by developing a family of penalty functions which can be incorporated in the

objective of the semi-definite programming, using any arbitrary initial point. If the point is close enough to the feasible set, then the penalized relaxations are guaranteed to produce feasible points for the initial BMIs.

1.3 Aim and Objectives

The main aim of a WEC controller is to maximize the energy absorbed by the device.

The aim of the present research is to design control strategies for a PA device to maximize the energy absorbed with real time implementation, considering non-linearities and physical constraints in operational conditions. Following that aim, the objectives are set as (1) to design constrained optimal control strategies with state feedback for maximizing induced power; (2) to investigate the efficacy of the constrained control strategies with generator losses and multiple objectives to optimize considering varying sea-state conditions; (3) to test the applicability of the constrained optimal controllers with the implementation of a suitable observer; (4) to consider the non-linearities in the device dynamics and design an appropriate controller algorithm; (5) to develop controllers for WECs manifesting TV system properties which also account for the non-causality.

1.4 Contributions

In this section, we summarize the contributions of the present work.

Two control algorithms for power maximization are presented in the context of multi-resolution analysis for a linear time invariant PA device. The first algorithm computes a reference trajectory and it is based on the tracking of such trajectory through wavelet decomposition of the tracking error signal. DWT ensures to attain a computationally efficient perfect reconstruction of the signal. The second algorithm explicitly includes a term associated with the electrical power in the objective function of the optimal control problem. The control is again designed based on MRA analysis with discrete wavelets. The two methods embrace two common LQ configurations in wave energy application and simulation results show that the MRA-based techniques are able to outperform their respective conventional LQ controller.

A non-linear control strategy is developed targeting a PA with time-varying/nonlinear dynamics. A forward propagating differential Riccati equation technique has been formulated in time-varying/nonlinear environment as the need for system matrices is circumvented. A re-formulation of the technique in wavelet domain has been proposed and has been shown to effectively boost the power performance of a PA device with nonlinear restoring force when compared to a multi-resolution LTI control and a baseline FRE control.

In the context of LMI-based optimization, two novel state feedback constrained ($S-H_2$ and $S-$

H_∞) control methodologies are proposed following a Maximum Induced Power Control approach. The multi-objective capability of the control allows to consider constraints, and the performance index of the minimization based on a causal relation, allows real time implementation. The result is a dramatic energy harvested gain compared to a more conventional LQ control for a given site, since LQ control is unable to consider constraints.

1.5 Thesis Outline

The thesis is organized in five chapters following this one.

In Chapter 2 two multi-scale strategies are presented. They are implemented on a linear model of cylindrical Point Absorber moving in heave. The objective of the strategies is power maximization. The model of the device is first outlined, with given approximations on the radiation force as a finite order state space system, and a causal reduction of the wave elevation/wave force relation - crucial throughout all the thesis, to ensure causality. The relationship is then also represented by a finite order state space system. The first method is based on the tracking of a reference trajectory. The trajectory is obtained via a model-order reduction to keep the control real time implementable. The second method then follows, based on direct power maximization. Eventually, numerical simulations provide results on the comparisons between the multi-scale version of the two methodologies and their corresponding simple baseline control. Discussion between the two methods is also given. In conclusion, a comparison between the two methods and optimal control is highlighted.

Chapter 3 deals with the multiscale (forward propagating) Riccati-equation control method. Since cylindrical devices are known to be accurately described by linear equations, it is preferred to focus on spherical shapes, where nonlinearities cannot be neglected. In fact, floating spheres translating in heave present substantial nonlinear effects due to their varying cross sectional area. The hydrodynamic model of the floating sphere in heave is first introduced, with particular focus on the nonlinear effects given by the hydro-static restoring force. The control method is then described in terms of architecture, objective and tuning. Computational cost of the proposed control methodology is very fast compared to the processing power of available units, so it is deemed noncritical. Finally, the numerical simulations are presented and results discussed on the comparison between the proposed strategy, its correspondent simple baseline forward-Riccati control, and the previously developed linear multi-scale LQ, from Chapter 2.

In Chapter 4, the topic of constrained control is introduced. Whereas control methods in Chapters 2 and the subsequent Chapter are based on their tuning to ensure that system variables don't exceed some limits, in Chapter 4 and in Chapter 5 two methodologies are proposed to ensure

that this condition is not violated on a varying sea scenario. Their difference lies in the system norm minimization they employ, being the first following an H_2 norm and the second H_∞. The consequences of this difference are highlighted in the results. It is assumed that the controllers are applied to a cylindrical PA. The two novel control architectures presented are based on the so called Maximum Induced Power Control concepts to ensure maximum power harnessing. MIPC is applied based on considerations from the generator dynamics. Generator details are given, from which the MIPC concepts are recalled and then the implementation of the control follows. The computation of the feedback control is based on an optimization problem which is mathematically described by LMIs. The power maximization objective results from the minimization of the H_2 and H_∞ norm of a performance index. The hard constraints are defined by additional LMIs. The optimization problem casting these requirements is unequivocally defined. The strategies are finally tested on simulations with actual measurements data gathered from a site on the west coast of Ireland. Results are given in terms of average power harnessed for each sea state simulated in comparison with a more standard LQ control. Overall energy absorption is also computed for the site. Where constraints are breached, the device is not supposed to be operational so no energy can be harnessed. At the very end, a closer look to the generator current and velocity of the shaft is given, to assess their behavior also in relation to limits imposed. Observations regarding the gap of the controllers from the non-causal optimum are also given.

Chapter 5 deals with constrained optimization and design of the observer based controller for the PA in Chapter 4. The extension from state-feedback to observer based control is put into place: the measurement equipment clearly defines the measured quantities. With that in mind, the observer dynamics and error dynamics are outlined. For unconstrained applications it is usually enough for the observer to be able to minimize the error. In this case the design of the observer has to explicitly consider the constraints. The optimization problem for the computation of the observer gain is mathematically developed. It is not possible to express the problem with LMIs, but with BMIs. So the procedure used for determining a solution is explained subsequently as a "LMI-based coordinate descendent method". Numerical evaluation of the found observer is given in conclusion of the chapter: quantities evaluated are the power performance and the constrained quantities of generator current, vertical stroke, and speed. A close look to the current-to-speed relationship is also given to assess its behavior in relation to limits imposed as well.

Chapter 6 concludes the thesis presenting the main findings and provides future research directions.

Chapter 2

Multi-Resolution LQ Control

In this Chapter, two competing novel LQ based multiresolution strategies are developed with the aim of power maximization, for a model of PA. Given the narrow-banded but irregular nature of sea phenomena the use of wavelet analysis is found to be attractive, for the design of the controller, able to incorporate the information of the local time varying frequency content of the signals. Hence, this can be used to target specifications that imply only certain frequency bands. Therefore, with LQ, the weightings of a conventional controller can be adjusted depending on the bands to be either suppressed or enhanced. Gains derived from frequency-localized optimization can be applied to the signals of the decomposed states and the control effort can be distributed strategically among the different bands.

The first variant of the proposed control strategy uses a reference velocity trajectory that can be computed offline and obtained with a sub-optimal approximation of the "complex-conjugate" control [9]. A reduction coefficient is needed to ensure that the displacement values don't exceed a chosen limit, to avoid driving the motion towards unrealistic and undesirable excursions, likely to cause damage to the floating body and overrun the generator capabilities. In fact, theoretical unconstrained optimization on WECs for maximum power harnessing, is known to result in dangerously high values of their states, needing reduction means for applicability and safety [109].

LQ controllers indeed, don't have the capability to include constraints in the problem formulation. Alternative maneuvers, such as manual adjustments of the control tuning, ought to be followed.

The second variant uses a modified objective function in order to maximize directly the power output. Wavelet analysis in this case is used to incorporate the information of the local time varying frequency content of the power signal in the design of the control law.

Numerical simulations are carried out to evaluate the performance of the two control algorithms. In both cases, the MRA controller has exhibited a clear superior performance compared

to its respective baseline. The use of a fast DWT based algorithm provides exact decomposition/reconstruction of signals and allows real-time implementation. By narrowing down the control effort to some chosen frequency distribution, versatility is enhanced, allowing the multiresolution strategy to outperform the baseline case, where the weighting matrices are uniformly distributed.

An important remark: the novelty of the proposed strategies lays on the control side of the formulation. Given that standard observers for linear kind of systems can be designed with ease, the controllers will be of full state feedback-type.

2.1 Point Absorber

As anticipated, frequency domain models describing the dynamics of WECs only work for regular waves, due to the nature of the radiation force. The integro-differential equation description (Cummins' equation) is [32] is to be applied for the successful application of control algorithms within this thesis. The model of the device where we are going to apply the strategy depicted in this Chapter, is described in the following section.

2.1.1 WEC dynamical model

The device employed in the studies of this Chapter is of cylindrical shape. Unlike the device in Chapters 4 and 5 its dimensions are of a reduced scale, which is meant to suitable for laboratory testing.

The details over the geometry and already the hydrodynamic coefficients typical of linear models (obtained by a BEM solver) are summarized in Table 2.1. The floating body, as it is common configuration, is linked through a linear PTO machinery to the seafloor. This machinery's dynamic behaviour is approximated and given in Section 2.2.1. This PTO, which performs the mechanical-to-electrical energy conversion, can be then either connected to the grid or to a storage unit. Details in this regard are left nonetheless, out of the this thesis.

The relative motion between the body and the seabed is responsible of the induced mechanical power. The device is supposed to be moving only in its vertical (heave) direction, so neglecting all the other Degrees-of-Freedom (DoF). We can call its vertical displacement by $z(t)$. A coordinate system is chosen for its description, as it appears in Fig. 2.1a. The origin is placed on the still water level when the floating body is in its static equilibrium following the vertical axis of the cylinder. The analysis assumes small amplitude oscillations and viscous effects are neglected. This is because linear theory is applied. One further assumption on the impacting waves implies them to be two dimensional (plane) waves propagating in the x-direction only. The motion of the body is subsequently defined in reference to the static equilibrium position, hence whereas the gravity

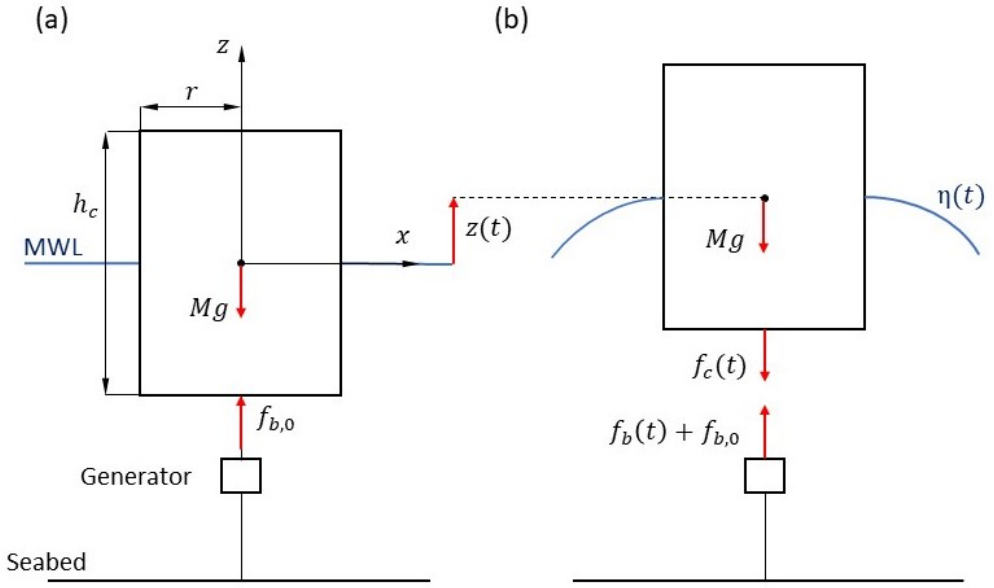

Figure 2.1: (a) The point absorber representation in static conditions, (b) in dynamic conditions

force Mg is balanced by the static buoyancy force $f_{b,0}$. Writing Newton's law gives the following equation of motion for the floating body

$$M\ddot{z}(t) = f_h(t) + f_c(t) \tag{2.1}$$

where M is the total mass, $\ddot{z}(t)$ is the heave acceleration and $f_c(t)$ is the control force exerted by the PTO. $f_h(t)$ is the hydrodynamic force, which can be decomposed as

$$f_h(t) = f_r(t) + f_e(t) + f_b(t) \tag{2.2}$$

where $f_r(t)$ is the reaction force due to radiation effects, $f_e(t)$ is the wave load and $f_b(t)$ is the increment of the buoyancy force relative to the static equilibrium.

Due to the cylindrical shape, the cross-sectional area cut by the still water plane is assumed to be constant and we can write

$$f_b(t) = -k_b z(t), \quad k_b = \rho S g \tag{2.3}$$

where k_b is the constant buoyancy coefficient, ρ is the density of sea water, S is the water-plane area and g is the acceleration of gravity.

Radiation Force

Let us spend now few more words describing the assumptions made over the approximation of the radiation force on the single body device employed in this chapter.

We can write that [32]

$$f_r(t) = -m_h \ddot{z}(t) - f_{r0}(t) \ , \tag{2.4}$$

where

$$f_{r0}(t) = \int_{-\infty}^{t} h_{r\dot{z}}(t-\tau)\dot{z}(\tau)d\tau \tag{2.5}$$

is known as *memory effect* of the fluid. $h_{r\dot{z}}$ appears as a causal Impulse Response Function (IRF- the integral is between $-\infty$ and the current time t) brought forward by the absorber velocity $\dot{z}(t)$; m_h is the added mass at infinitely high frequency. Due to linearity of the radiation problem, the kernel $h_{r\dot{z}}$ represents the IRF for the body radiating waves while oscillating in the absence of incident and diffracted waves. Since both radiation force and velocity are real values, $h_{r\dot{z}}$ is real and since the radiation force depends only on present and past oscillations, the kernel is causal, which means $h_{r\dot{z}} = 0$, $t < 0$. The causality of $h_{r\dot{z}}$ also implies that the Fourier transform is analytic in the upper half of the complex frequency plane.

Unfortunately, the formulation of the equation of motion based on the use of convolution terms (or also, on frequency-domain parameters as radiation damping or frequency dependent added mass) are not in agreement with the model implementation commonly used automatic control and the direct calculation of (2.5) is indeed computationally expensive. This motivates a problem reformulation.

As mentioned in the introductory Chapter, it is common practice to approximate the integral expression in (2.5) by a finite-order state-space system. This reduces dramatically the time needed for computation, without compromising the accuracy of the results. Typically orders between two and four suffice to reproduce first order wave effects.

The numerical approximation of Eq. (2.5) takes the form

$$\begin{aligned} \dot{x}_r(t) &= A_r x_r(t) + B_r \dot{z}(t) \\ f_{r0}(t) \approx y_r(t) &= C_r x_r(t) \end{aligned} \tag{2.6}$$

A_r, B_r and C_r are the state space matrices, $x_r(t)$ is the radiation state vector of dimension N_r, where N_r is the order of the system. Notice that $\dot{z}$ is the input and $y_r(t)$ is the output resembling $f_{r0}(t)$.

In order to determine the system above, the Frequency Domain Identification MATLAB Toolbox in [34] is employed. In particular, the hydrodynamic coefficients previously calculated with the BEM solver are first approximated by a transfer function and subsequently converted to time domain. This identification approach avoids transforming the data directly to time domain, which, if not handled properly, can result in errors due to the finite amount of data. The Nemoh [110] solver is chosen as BEM solver given its convenient MATLAB interface, and given its open source

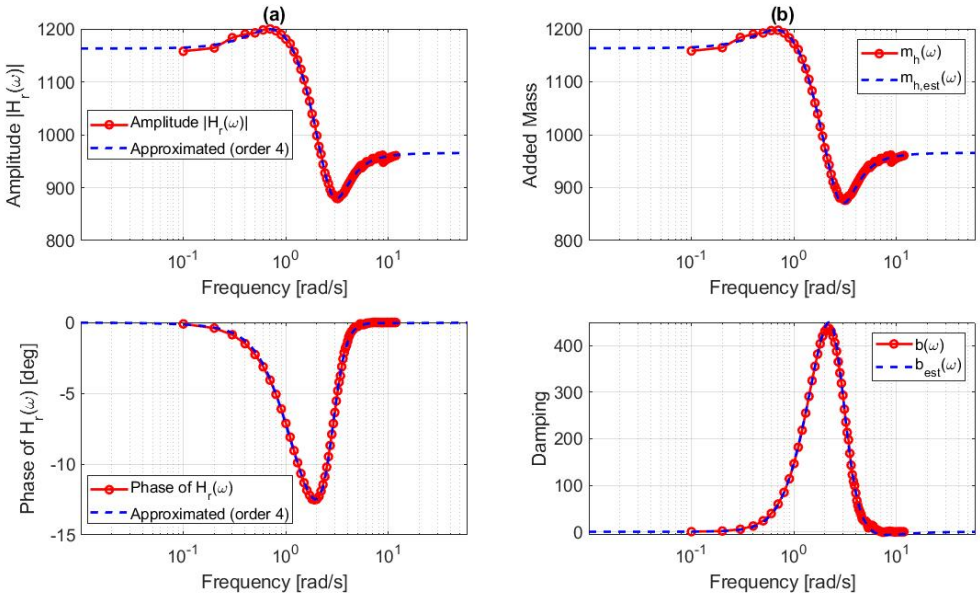

Figure 2.2: (a) FRF of the radiation force $H_r(\omega)$ with its amplitude (top) and phase (bottom); (b) related hydrodynamic coefficients, frequency dependent added mass (top) and damping (bottom)

distribution.

The results for $N_r = 4$ are presented in Fig. 2.2: the radiation Frequency Response Function $H_r(j\omega)$ is plotted in panel (a), while the estimate of the hydrodynamic coefficients $m_{h,est}(\omega)$ and $b_{est}(\omega)$ are plotted in panel (b). It can be seen that the chosen order leads to an acceptable approximation of the radiation force subsystem.

Excitation Force

Itis another aspect of the hydrodynamics of a WEC that complicates control in irregular waves. This is the approximation usually involved for what concerns the effect of the excitation force on the device. In frequency domain the relationship between the wave elevation $A(\omega)$ and the excitation force $F_e(\omega)$ can be expressed as [9]

$$F_e(\omega) = H_e(\omega)A(\omega) \tag{2.7}$$

where $H_e(\omega)$ is a frequency response function, which depends on the geometry of the device, and it is also obtained through the Nemoh BEM solver. Not directly reflected in this representation are the facts that (i) the force is a result of fluid pressure active over the entire wetted surface and (ii) the body experiences a force before the wave elevation actually arrives at the wetted surface, because the wave action is a continuum phenomenon.

Hence, when it comes to expressing Eq. (2.7) in time domain, we can write

$$f_e(t) = h_e(t) * \eta(t) \equiv \int_{-\infty}^{\infty} h_e(t-\tau)\eta(\tau)d\tau \tag{2.8}$$

where $f_e(t)$, $h_e(t)$, and $\eta(t)$ are the inverse Fourier transforms of $F_e(\omega)$, $H_e(\omega)$, and $A(\omega)$ respectively; "$*$" denotes the convolution operator.

We can observe that the integral in Eq. (2.8), entails non-causality. Knowledge of the future evolution of surface elevation is needed if the exciting force is to be known at the present instant. See [111] for a discussion of the physical implications that this involves.

The approach herein adopted to model this phenomenon, involves few assumptions, that are going to make the IRF $h_e(t)$ causal with a time-shift technique [112]. That causal IRF, if verified, can be then approximated by a finite order state space system as well. The fact that the function h_e can be truncated at finite lengths of time makes the process straightforward to execute. For instance, with h_e truncated at $\pm T$, the entire function can be shifted then to the right on the time axis (or equivalently shifting the origin to the left) by defining

$$h_{e,c}(t) = h_e(t-T).$$

In frequency domain , this procedure reflects as a new frequency-response function $H_{e,c}(i\omega)$, where

$$H_{e,c}(i\omega) = H_e(i\omega)e^{-i\omega T}$$

As described, it is easy to see how subsequently a surface elevation of the future is defined

$$\eta(i\omega) = \eta_{up}(i\omega)e^{-i\omega T}$$

so that in the time domain

$$\eta(t) = \eta_{up}(t-T).$$

The technique now considers this incident wave elevation $\eta_{up}(t)$, not in correspondence of the device exactly, but at a location, sufficiently "up-wave" (let us call it location A), to account for the propagation of the wave. This is based on the assumption of unidirectional, long crested waves: (i) the surface elevation η at a point B (being B a spatial point in correspondence of the device) and time t can be related to the up-wave elevations (in correspondence of A) at a previous time, (ii) η at point B that will occur at a future time $t+T$ will be the result of occurring up-wave

currently at time t. The agreement between the first equivalence in Eq. (2.8) and

$$f_e(t) = h_{e,c}(t) * \eta_{up}(t)$$

holds, with $h_{e,c}(t)$ as the time shifted IRF. In other words, the causalization implies the introduction of a frequency dependent delay $T(\omega)$, that entails

$$H_{e,c}(\omega) = H_e(\omega)e^{j\omega T(\omega)} \tag{2.9}$$

where $H_{e,c}(\omega)$ is the Fourier transform of $h_{e,c}(t)$. An appropriate value for T is chosen as a value that entirely translates any positive evolution of the $h_e(t)$ function to positive times t only.

Once a suitable "causalization" given these assumptions is obtained, a finite order approximation of $h_{e,c}(t)$ can be computed analogously to Eq.(2.6) as a state space formulation as well. Subsequently

$$\begin{aligned} \dot{x}_e(t) &= A_e x_e(t) + B_e \eta_{up}(t) \\ f_e(t) \approx y_e(t) &= C_e x_e(t) \end{aligned} . \tag{2.10}$$

In Fig. 2.3 the finite order six of a state space system is plotted to approximate the causal IRF $h_{e,c}$. This translates in a finite order linear causal sub-system between a wave elevation quantity η_{up}, and the wave force over the floating body.

Sea States

The values of the time series $\eta_{up}(t)$ in this Chapter (input of the system above (2.10)), and in the following ones are evaluated from JONSWAP spectra $S_\eta(\omega)$ [113], with the application of a random phase. The MATLAB Toolbox WAFO was conveniently employed to generate the spectra [52]. Analytical expression of the spectrum is given by

$$S_\eta(\omega) = \frac{\alpha g^2}{\omega^5} exp\Big(-\frac{5}{4}\big(\frac{\omega_p}{\omega}\big)^4\Big)\gamma_{js}^{\left(\frac{(-\omega/\omega_p-1)^2}{2\sigma^2}\right)} \tag{2.11}$$

where the parameters have the same definition as in the original formulation in [113]. In particular

$$\sigma = \begin{cases} 0.07 & \text{if } \omega < \omega_p \\ 0.09 & \text{if } \omega \geq \omega_p \end{cases}$$

$$\alpha \approx 5.061 \frac{H_s^2}{T_p^4}\{1 - 0.287\ln(\gamma_{js})\}$$

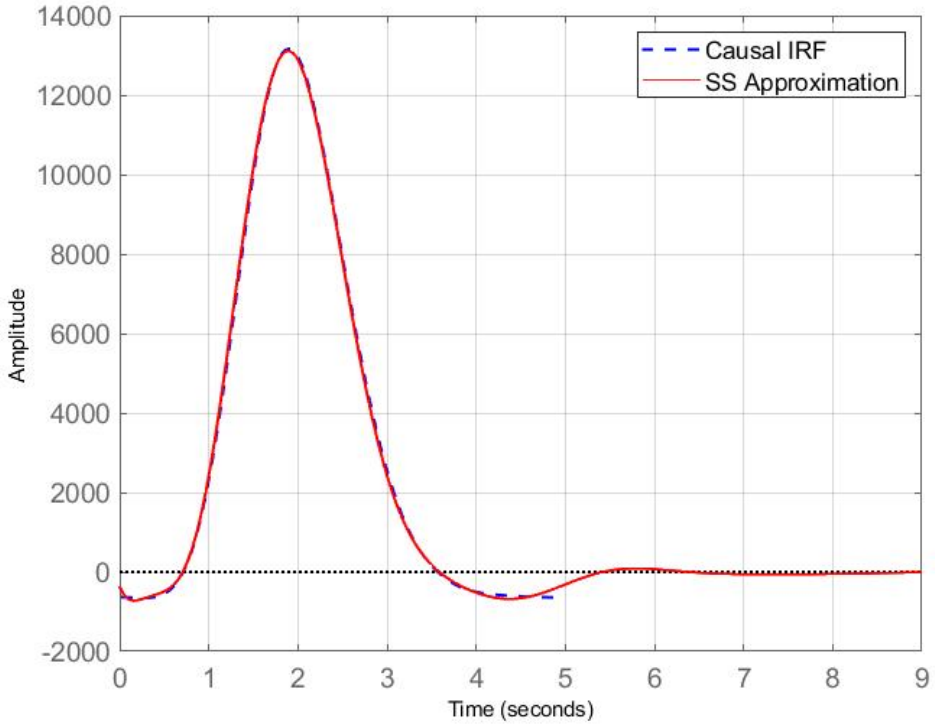

Figure 2.3: Causal excitation force IRF $h_{e,c}$ approximated by a sixth order state space system

In Fig. 2.4 the spectrum is plotted for a significant wave height of $H_s = 2m$ and a zero-crossing period of $T_p = 8s$ as an example. In the next subsection, details on the overall state-space system representation, needed for the control formulation, are given.

2.1.2 The WEC state-space system representation

As stated, in this Chapter we are presenting two different approaches in the use of LQ control with the application of multi-resolution analysis. Within the two techniques one involves a generated reference trajectory, while the second does not. The state space formulation developed in this section is convenient for the control development.

For both variants of the strategies the equation of motion introduced with Eq. (2.1) is expressed in state space form

$$\begin{aligned} \dot{x}(t) &= A_w x(t) + E_w f_e(t) + B_w f_c(t) \\ y(t) &= C_w x(t) \end{aligned} \tag{2.12}$$

where $f_e(t)$ and $f_c(t)$ represent the uncontrolled and controlled inputs respectively with E_w and B_w the corresponding matrices.

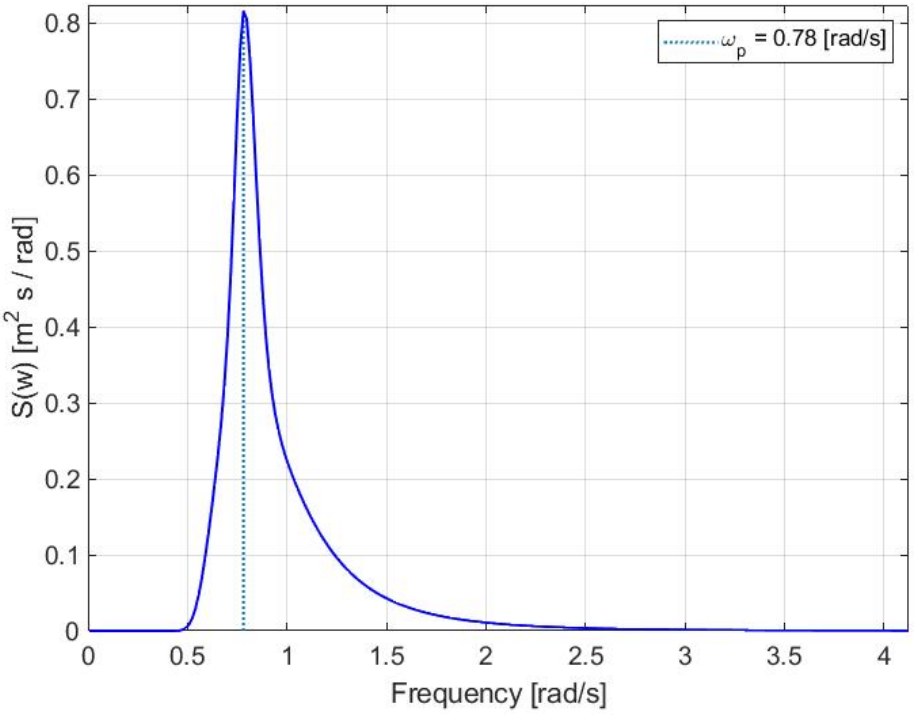

Figure 2.4: JONSWAP spectrum plotted for a significant wave height of $H_s = 2m$ and a zero crossing period $T_p = 8s$. Highlighted the peak frequency of the spectrum at $\omega_p = 0.78 rad/s$

With this representation, as it is commonly done, radiation terms can be incorporated in the main state-space equation (2.12) so the state vector $x(t)$ comprises the states of the linear system describing the heave dynamics and the radiation states $x_r(t)$

$$x(t) = \begin{bmatrix} x_r(t) & z(t) & \dot{z}(t) \end{bmatrix}^T$$

The system matrices are subsequently defined as

$$A_w = \begin{bmatrix} A_p & \mathbf{0}_{4\times 1} & B_p \\ \mathbf{0}_{1\times 4} & 0 & 1 \\ -\frac{C_p}{M+m_h} & -\frac{k_b}{M+m_h} & 0 \end{bmatrix}$$

$$E_w = \begin{bmatrix} \mathbf{0}_{5\times 1} \\ \frac{1}{M+m_h} \end{bmatrix}$$

$$B_w = \begin{bmatrix} \mathbf{0}_{5\times 1} \\ \frac{1}{M+m_h} \end{bmatrix}$$

$$C_w = \begin{bmatrix} \mathbf{0}_{1\times 5} & 1 \end{bmatrix}$$

2.2 The control design

It is possible now to describe the control architecture of both the novel methodologies introduced, relative to the augmented system just defined (2.12).

The general framework that leads to the development of the multi-resolution(scale) features of the present controller follows the principles of multi-resolution analysis MRA [114]. In this section the control architecture is formulated for power extraction on a Point Absorber Wave Energy Converter device. It is convenient to define the PTO machinery first.

2.2.1 The generator

The instantaneous mechanical power can be defined as

$$P_m(t) = f_c(t)\dot{z}(t). \tag{2.13}$$

The power conversion machinery is a component, whose dynamics can be all but trivial, and it can influence the behavior of the controller heavily. In the present methodologies though, the benefits of the strategies are better seen on, on a simplified model. In this regard, the behaviour of the PTO is resembled by a simple resistance $R_s = 0.01\Omega$.

The instantaneous electrical power is then

$$P_e(t) = \nu_{out} i = (\nu_{emf} - R_s i)i \tag{2.14}$$

where ν_{emf} is the back electromotive force, i is the generators current, ad ν_{out} the output voltage. The vertical velocity of the buoy $\dot{z}$ can be assumed equal to the relative velocity of the stator/rotor within the generator. The control force $f_c(t)$ and $\dot{z}$ are related to the current and voltage as

$$f_c = K_i i; \qquad \nu_{out} = K_v \dot{z} \tag{2.15}$$

with K_v and K_i as constants depending on the system. In Fig. 2.5 a schematic representation of the simplified generator is given. Values of $K_v = 938Vs/m$ and $K_i = 600N/A$ are implied.

Without loss of generality, the system input in (2.12) can be easily re-defined in terms of the current i as input and ν_{out} as output, by re-stating

$$B'_w = B_w K_i \qquad C'_w = K_v C_w. \tag{2.16}$$

in order to include the simplified generator dynamics.

The two multi-resolution methodologies are now introduced using wavelet analysis, being the

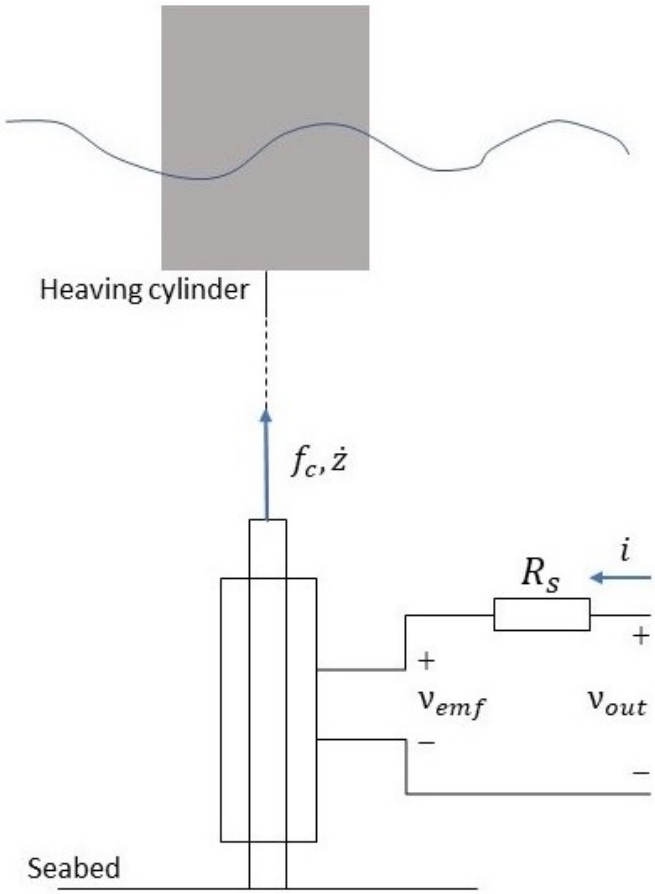

Figure 2.5: Augmented system schematic, with output ν_{out} and input i

implementation of the multi-controllers based on DWT of the state/output signals. The DWT is computed over a time interval from the initial time $t_0 = 0$ to the current time t_c and it is updated at each time step.

2.2.2 The velocity tracking method

The first method, which involves the computation of a reference velocity trajectory, and a time/frequency decomposition of the tracking error, is presented in this section. The first subsection describes the theory behind the computation of this trajectory.

The trajectory

The use of a velocity reference in wave energy is not a new idea [115], [66]. LQ control for tracking has been extensively used in different fields [116], [117]. An extensive description is found in [118].

In this development the output will be the heave velocity itself $y(t) = \dot{z}(t)$. Therefore, the second expression in both Eqs. (2.15)-(2.16) is not needed. From [9], the relationship between the optimal velocity and the wave load $F_e(\omega)$ in frequency domain is known

$$V_{opt}(\omega) = \frac{1}{2B(\omega)} F_e(\omega) \tag{2.17}$$

with $B(\omega)$ known as frequency dependent hydrodynamic damping coefficient. It is clear from this formula that the frequency dependency of the parameter $B(\omega)$ complicates the real time execution of a velocity trajectory computation, given that

$$v_{opt}(t) = \mathscr{F}^{-1}[V_{opt}(\omega)] \tag{2.18}$$

where $\mathscr{F}^{-1}$ is the inverse Fourier transform operator. Prediction techniques have to be used to benefit of (2.18) (see [119]).

To circumvent the non-causality of this relationship, it was shown in [120] that with a balanced realization of the state space system (2.12), the whole model of the PA dynamics could be reduced to second order and the relationship between the optimal velocity and the excitation force in Eq. (2.17) brought to a constant transfer function

$$\hat{H}(\omega) = \frac{1}{2\hat{K}} \approx \frac{1}{2B(\omega)} \tag{2.19}$$

so that a trajectory could be computed in real time

$$r_u(t) = \frac{1}{2\hat{K}} f_e(t). \tag{2.20}$$

This obviously implies a slight reduction on the performance given that this is a suboptimal condition, but as we will be able to observe in the results and the comparisons between the techniques, this is negligible when the device works close to resonance and for the majority of sea states (the ones with most probability of occurrence in a given location) this is usually true. The aim in this Chapter is to show the benefits of wavelet analysis on LQ control and a choice of a causal trajectory, simplifies this explanation.

The reduction factor

As mentioned in the introductory Chapter, it is in the intention of the author to develop control strategies that are applicable on real devices. So, one needs to observe that this methodology is not able to include physical constraint in its formulation. Trajectories computed with Eq. (2.20) then, are likely to drag to motions and forces to be exerted beyond generator capabilities, stroke lengths and safety limits imposed on the device. This is to be avoided, since the theoretical excursions implied by the vertical motions, the values of currents and voltages required in the PTO could be either unachievable or damaging for the device.

So, to keep the applicability on the method, the author chooses to apply a reduction factor α_r, so that the theory keeps its physical validity. These limits are fixed as

$$\begin{aligned} z_{lim} &= \pm 5 \quad \text{m} \\ \dot{z}_{lim} &= \pm 5 \quad \text{m/s} \\ i_{lim} &= \pm 1500 \quad \text{A} \end{aligned} \tag{2.21}$$

This turns the transfer function $\hat{H}$ in Eq. (2.19) into

$$\tilde{H}(\omega) = \frac{1}{2\alpha_r \hat{K}} \tag{2.22}$$

and the trajectory $r(t)$ is finally defined

$$r(t) = \frac{1}{2\alpha_r \hat{K}} f_e(t). \tag{2.23}$$

The value of α_r is chosen by the user, in order to keep the signals within the boundaries for both baseline and multi-resolution version of the controller.

The MRA Tracking

With a computable reference trajectory now available, a suitable tracking methodology is designed. As per Linear Quadratic Tracking (LQT) control theory, a quantity $w(t)$ is defined and added to

the state vector

$$x_g(t) = \begin{bmatrix} x(t) & w(t) \end{bmatrix}^T.$$

The system is redefined

$$\frac{d}{dt}\begin{bmatrix} x(t) \\ w(t) \end{bmatrix} = \begin{bmatrix} A_w x(t) + E_w f_e(t) + B'_w i(t) \\ y(t) - r(t) \end{bmatrix} \tag{2.24}$$
$$y(t) = C_w x(t)$$

where $y(t)$ is, as mentioned, the device velocity.

Now, the usual expression of the objective function in classic LQ control, expressed for the state x_g and the input i writes

$$J = \int_{t_0}^{t_c} (x_g^T Q x_g + x_g^T N i + i^T R i) dt \tag{2.25}$$

where $Q \geq 0$ and $R > 0$. The baseline controller is built on this cost function for the purpose of comparison.

In a wavelet transformed framework, given that the expressed system (2.24) is both linear and time invariant, the objective of the LQ problems to be formulated, is to find feedback matrices $[G]_a$ and $[H]_a$ on each frequency band such that the closed-loop system with feedback

$$\{W_{\psi_a} i\} = -[G]_a \{W_{\psi_a} x\} - [H]_a \{W_{\psi_a} w\} \tag{2.26}$$

minimizes the functional

$$J_a = \int_{t_0}^{t_c} [\{W_{\psi_a} x_g\}^T [Q]_a \{W_{\psi_a} x_g\} + \{W_{\psi_a} i\}^T [R]_a \{W_{\psi_a} i\} + \{W_{\psi_a} x_g\}^T [N]_a \{W_{\psi_a} i\}] db \tag{2.27}$$

where $\{W_{\psi a}[\cdot]\}$ is the continuous wavelet transform of $[\cdot]$ with respect to the basis function ψ; the parameter a determines the frequency content of each band (it is also known as the dilation parameter). The parameter b is a translation parameter and localizes information temporally around the time instant $t = b$.

Matrices $[G]_a$ and $[H]_a$ are the control gain matrices dependent on the dilation parameter a. Hence, these matrices, will be varying depending on the frequency bands over which the controller is desired to be acting.

As we can see in Eq. (2.27) also the weighting matrices $[Q]_a$, $[R]_a$ and $[N]_a$ are frequency band dependent. We can recognize Eq. (2.27) to be the quadratic functional as in (2.25), but written

for wavelet transformed states.

Matrices $[Q]_a$, $[R]_a$ and $[N]_a$ are associated with the transformed augmented state vector $\{W_\psi x_g\}$, the transformed control input $\{W_\psi i\}$ and their product, respectively. The quantity db denotes the differential respect to the translational parameter b.

For control related applications, a DWT framework is more appropriate for application due to its exact decomposition/reconstruction capabilities. An approximate relation between the DWT framework (for exact decomposition/reconstruction of signals over the finite interval $[t_0, t_c]$) and the continuous formulation was established [114]. Considering the state vector and using an appropriate wavelet with basis ψ and scaling function ϕ, so called scale equations are used to generate high and low pass filters. A low frequency signal approximation $\{x_g\}_L$ and band limited signal components $\{x_g\}_{d_j}$ can be computed, so that the (augmented) state vector is perfectly reconstructible

$$\{x_g(t)\} = \{x_g(t)\}_L + \sum_{j=L}^{n-1} \{x_g(t)\}_{d_j} \tag{2.28}$$

The value L corresponds to the subband lower than which such low frequency approximation is applicable. Subbands related to values between L and n correspond to the divisions of the signal in higher frequencies.

Using Eq.(2.28) given by the DWT, the application of Eq.(2.26) translates in

$$\{i(t)\} = -[G]_L\{x(t)\}_L - [H]_L\{w(t)\}_L - \sum_{j=L}^{n-1}[G]_{d_j}\{x(t)\}_{d_j} - \sum_{j=L}^{n-1}[H]_{d_j}\{w(t)\}_{d_j} \tag{2.29}$$

where we can observe the separate contribution of the original state vector $x(t)$ and the added error $w(t)$.

The frequency dependent control gain matrices $[G]_L$, $[G]_{d_j}$ and $[H]_L$, $[H]_{d_j}$ (with $j = L, ..., n-1$) are applied to the filtered time signals, based on the MRA decomposition and they are calculated by solving an optimal control problem for each frequency band, based on the system in Eq. (2.24).

Hence, the proposed control problem formulation, minimizes the weighted cost of the response, control effort and their combined effect together in the frequency band corresponding to the parameter a, which in a discretized form is represented by $[a]_j$ for DWT.

By choosing the weighing matrices $[Q]_{a_j}$, $[R]_{a_j}$ and $[N]_{a_j}$ accordingly it is possible to focus the attention on desired bands, depending on the frequency characteristics of the response signals.

In the present method, we will see that the described LQT combined with the MRA technique, is capable to outclass the baseline LQT, improving the tracking performance with comparable control effort.

2.2.3 The power maximizing method

Controller Architecture

We will start by depicting the non-MRA formulation, extending it to the MRA approach right after. The aim of this second controller is the maximization of the quantity

$$J = E\{P_e\} \tag{2.30}$$

compatibly with values of current $i(t)$, excursion $z(t)$ and velocity $\dot{z}(t)$ kept below prescribed limits (2.21). $E\{\cdot\}$ is the expected value under stationary conditions. To be converted into a suitable minimization problem we can say in general

$$\max_i J = \min_i -J \tag{2.31}$$

Referring to the general LQ formulation (2.25), given the system (2.12), rewritten with (2.16) and approximating the expectation operator by a temporal average, we can express the cost function in a general form as

$$\min_i \int_0^{t_c} [y^T N_{PM} i + i^T R_{PM} i] dt, \tag{2.32}$$

being N_{PM} the cross-coupled scalar weight assigned to the power generated, R_{PM} is a scalar weight assigned to the input effort (associated to the generator loss) and the scalar $Q_{PM} = 0$ in this context. Notice the formulation is written for the system output $y = \nu_{emf}$ as following (2.15) (defined for $y = \nu_{out}$) and adding the term $R_s i$ which effectively requires the output of the system dynamics in (2.12) to be re-stated by adding a term $D_w i$ contributed from the control input i, i.e. the generator current. Notice that in the case of minimising the temporal average of the electrical power generated P_e with a negative sign, the associated weights would be $N_{PM} = -1$ and $R_{PM} = R_s$ (i.e. equal to the generator resistance). Unfortunately, as it happens for the LQT case, minimizing this quantity for the specific case brings displacements, velocities and currents beyond prescribed limits so these weights are changed based on a series of trial and errors to ensure that limitations are not exceeded. Note that the multiplication of the weights with a positive scalar keeps the computed gains unchanged as the solution to the minimization problem remains unaffected. In the following sections the numerical values are stated.

Following the general formulation in wavelet domain (e.g. as given in (2.27)), with the analogy to (2.32), one can write the following

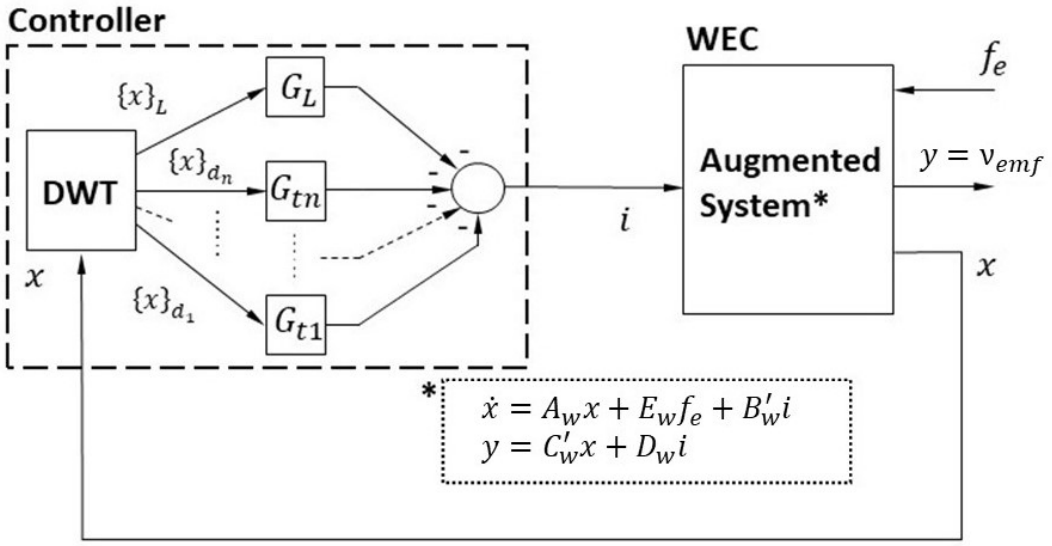

Figure 2.6: Overall scheme of the proposed power maximizing MRA-LQ controller

$$J_a = \int_{t_0}^{t_c} \{W_{\psi_a} y\}^T [N]_{PMa} \{W_{\psi_a} i\} + \{W_{\psi_a} i\}^T [R]_{PMa} \{W_{\psi_a} i\}] db \tag{2.33}$$

where the output weight matrices $[Q]_{PMa} = 0$. Eq.(2.33) allows us to solve the associated Algebraic Riccati Equations (in the asymptotic case) on each frequency band (accounting for the localized presence of the frequency bands) by a strategic choice of the matrices $[N]_a$ and $[R]_a$ for the respective bands. Again, we can assign appropriate weights N_{PMa} and R_{PMa} for different bands to minimize the weighted energy in each band corresponding to the two competing terms. This will generate band dependent gains, eventually leading to the generator control current. The control current can be calculated as

$$\{i(t)\} = -[G]_L \{x(t)\}_L - \sum_{j=L}^{n-1} [G]_{d_j} \{x(t)\}_{d_j} \tag{2.34}$$

.

Notice in (2.34) the lack of the affine terms, given the objective function directly aims to maximize the electrical power. Schematic of the present methodology is outlined in Fig. 2.6.

2.2.4 Determination of the Weighting Coefficients

In both methodologies, the matrices are chosen to suppress undesired subharmonic or superharmonic responses and, by contrast, to exalt band limited phenomena, given their occurrence. Outside of these preferred bands, weight on the control effort may be relaxed, as increased control

Table 2.1: Specifications of the Device (Multi-resolution LQ Control)

Variable	Parameter	Value	Units
r	Radius	0.8	m
h_c	Height	2	m
M	Mass	2030	kg
m_h	Added mass	970	kg
$\hat{K}$	Freq. Indep. Radiation damping	23,800	N/(m/s)
k_b	Buoyancy stiffness	19,700	N/m

effort may be required instead on those specific bands, so that no overall increase in cost will occur. More specifically, once a wavelet basis is chosen, and the time signals for the different states are decomposed in real time in the different approximation spaces containing frequencies of desired bands, attention on specific ones is driven by the energy content of the signal of interest over all bands.

For instance in the first method, for a good tracking of the trajectory, it is in the interest of the performance that the energy of $w(t)$ stays minimal, ideally brought to zero. It is good practice to plot the Fourier amplitude of these signals to progress with the determination of weighting coefficients. In the second method the choice of the matrices is driven instead by the frequency content of the signal P_e.

For both strategies is that the control weights configuration will be driven by the respect of limitations in (2.21) as well. Therefore, in both methodologies the choice is determined with a trial and error which insures maximum power absorption and respect of the imposed constraints.

2.3 Numerical Results

Table 2.1 reports the device characteristics used in the numerical study that follows. The hydrodynamic coefficients obtained with the BEM solver assume deep water conditions, hence the effect of the sea-bed is neglected. Time series $\eta_{up}(t)$ are generated from a JONSWAP spectrum of significant wave height $H_s = 2$ m, and peak period $T_p = 8$ s. A variable time step solver $ode45$ is used for integrating the equations over time. Simulation time is chosen as $T = 100s$. The length of the time window is deemed sufficient, given the zero crossing period of the defined waves.

2.3.1 Velocity tracking control

In reference to section 2.2.2, results obtained with a configured MRA controller are here shown and discussed, compared to the simple LQ case.

Weighting matrices of a baseline LQR used to benchmark the proposed solution, were chosen

as $Q = diag(1, 1, 1, 1, 1, 1, 10^5)$ and $R = 10^{-5}$, representing the emphasis relative to the state and control effort respectively. As expected, a much higher value of Q relative to the state $w(t)$ was assigned, for the purpose of good tracking. Combined weight matrix N is kept to zero.

The procedure used to choose the basis for the weights for the MRA controller is as follows. At first the simulation is run for the uncontrolled case, and the spectral distribution of $w(t)$ is observed (Fig. 2.8). From there, it is possible to evaluate the energy content of the signal. Based on this observation, the choice of a suitable wavelet basis for the MRA decomposition follows. Corresponding pseudo-frequencies for a specific wavelet family and order are calculated, and those correspond roughly to the desired bands. In the present case, it can be affirmed that the almost totality of the energy of the signal $w(t)$ lies on frequencies less than 1 Hz.

Therefore, an orthogonal Daubechies wavelet basis with four vanishing moments (*db4*), can be applied to decompose the time signals for the different states in the different approximation spaces. If four levels of decomposition are chosen, from each state four detail signals are generated, corresponding to bands with central frequencies ranging from 0.89 Hz to 7.14 Hz and an approximation signal at level 4. To put emphasis on the low frequency bands (where the energy of $w(t)$ lies), the LQ problems are solved with a relaxed weightage on the control effort $R = 10^{-7}$ and increased emphasis on the state $Q = diag(1, 1, 1, 1, 1, 1, 10^6)$ for the signals in the wavelet domain at the approximation spaces with dyadic frequency bands having central frequencies less than 0.89 Hz (approximation space for level 4). Notice, level five frequency band has a central frequency of 1.78 Hz. So it can be more or less stated that the approximation space covers from 0 Hz to 0.89 Hz. This means that most of the energy of $w(t)$ is included.

Control effort can be then limited on the remaining frequency bands, saving it where it is not needed. Hence, for those bands, a different tuning with $Q = diag(1, 1, 1, 1, 1, 1, 10^4$ and $R = 10^{-2}$ is used. The calculated gains are applied to the wavelet filtered signals of the states. The control input is constructed in time domain by a linear combination of the frequency dependent gain weighted filtered signals derived (Eq. (2.29)).

The MRA algorithm for wavelet decomposition is a fast algorithm with time complexity $\sim O(N)$, where N =length of data, faster than the fast Fourier transform (FFT) for which time complexity is $\sim O(NlogN)$, hence the synthesis is efficient and suitable for real time implementation.

The performance achieved with simple LQR is plotted in Fig. 2.9 in terms of velocity tracking (top), control force generated ($f_c(t) = K_i i(t)$ as $i(t)$ is the generators current), and electrical power output $P_e(t)$ (bottom). A close-up on the time window $10 - 30$ s is chosen to better distinguish the signals. A value of the reduction factor $\alpha_r = 5$ was given for the trajectory computation of Eq.(2.23). This allows the displacement $z(t)$, the velocity $\dot{z}(t)$ and the current $i(t)$ to be limited within the upper and lower limit. To observe the beneficial effect of the MRA controller over the

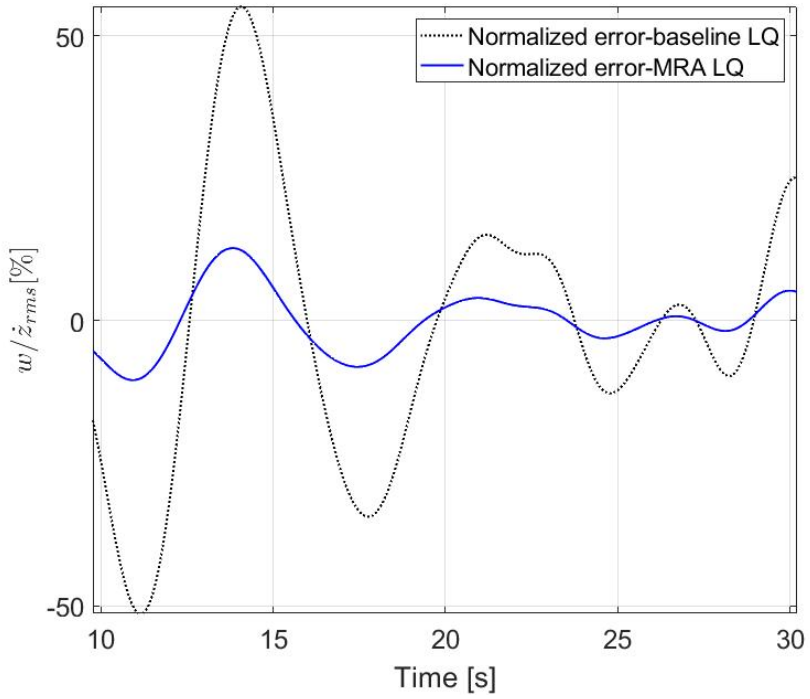

Figure 2.7: Time evolution of the error signal w normalized with respect to the *rms* value of the velocity and expressed in percentage

baseline LQT, the error signal $w(t)$ is plotted in Fig. 2.7 normalized respect to the root-mean-square value of the velocity $\dot{z}_{rms}$ and expressed in percentage. A dramatic reduction from peaks of over 50% to peaks of only 10% of $\dot{z}_{rms}$ can be appreciated. In Table 2.2, this is summarized. The MRA controller performance is eventually shown in Fig. 2.10.

2.3.2 The power maximizing method

For what concerns the power maximizing method in section 2.2.3, a baseline LQ controller (2.25) of weightage $R_{PM} = 5$, $N_{PM} = -600$ and $Q_{PM} = 0$ is chosen, after a series of trial and errors, in order to obtain a controller which response is contained within chosen limits. Following the logic and methodology expressed in the previous section, upon the spectral distribution of a signal of interest, a suitable choice of a wavelet basis can be made.

In this instance, the spectral density of the electrical power P_e is shown in Fig. 2.11. The behaviour exhibited in Fig. 2.11 suggests that, if the same orthogonal Daubechies family of wavelet is used, again with four levels of decomposition, a differentiation between the approximation space for level 4, and its complement (namely what covers all those bands with central frequencies higher than 0.89 Hz) could be repeated, in order to place increased attention on the approximation signal at level 4, and slack the weightings on its complement. In fact, on the frequency range $0 - 0.89$ Hz, a smaller value for $R_{PMa} = 3.5$, allows larger forces to be exerted, while $N_{PMa} = -600$

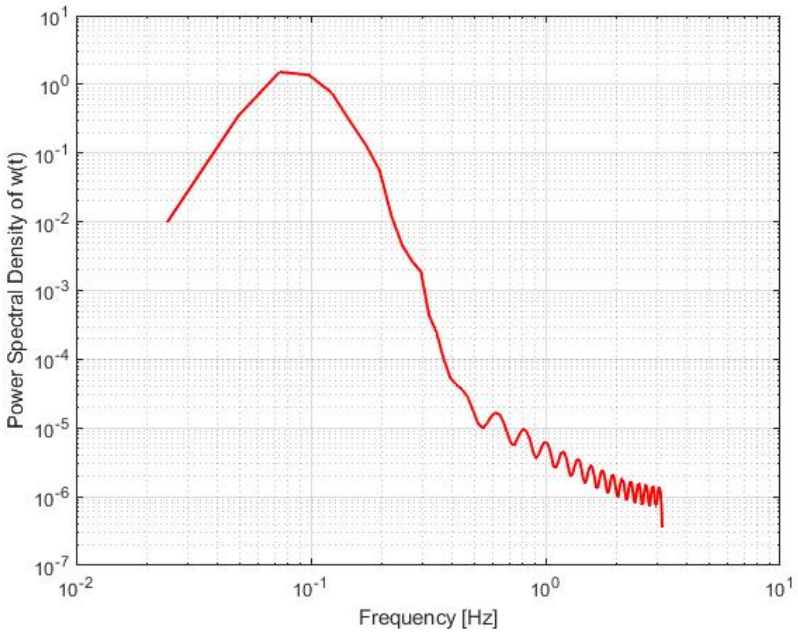

Figure 2.8: Power Spectral Distribution (PSD) of the error signal $w(t)$

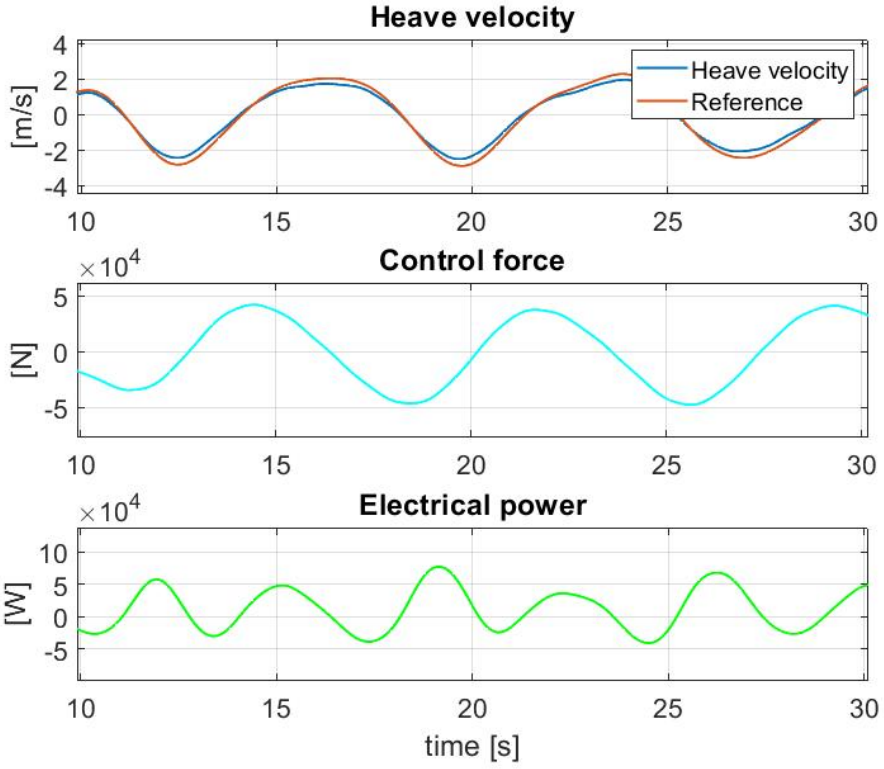

Figure 2.9: System response with simple LQT control: velocity tracking (top), control effort generated (middle) and electrical power (bottom)

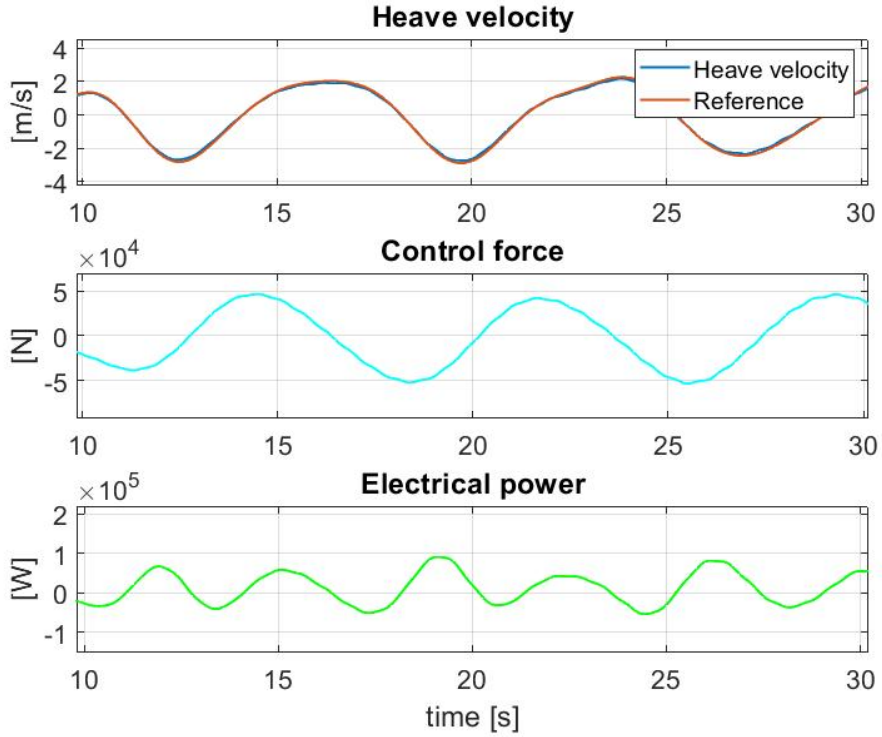

Figure 2.10: System response with MRA-LQT control: velocity tracking (top), control effort generated (middle) and electrical power (bottom)

can stay unchanged. On the complementary space covering the higher frequencies in the signals, $R_{PMa} = 20$ is increased, to limit the control effort keeping the value of N_{PMa} unchanged.

The fact that the choices are prudent are confirmed by the results. In Fig. 2.9 the performance of the simple LQ controller with given weights is plotted. It can be seen that, limiting the control effort on unnecessary bands, proves to be effective. See Fig. 2.10. Indeed, what appears to be overall a minor increase in control effort, gives a substantial power gain.

In Table 2.2 the performances of the two proposed controllers in comparison to their respective simple non-MRA case are presented. With the present tuning, the two methods have comparable performance, despite the differences in their implementation. With the only requirement of a limited displacement $z(t)$, velocity $\dot{z}(t)$ and generator current $i(t)$ values, the controllers accomplish similar generated power levels.

In particular, for the LQT controller, an essentially equivalent value in the control force translates in a severe reduction of the L_2-norm of the error $\|w(t)\|_2$ (in the rightmost column), and an appreciable rise in the mean power level, while for the MRA based power maximization method, a relatively small increase in the control effort, leads to a significant boost in power generated (compared to the non-MRA power maximizing algorithm).

Comparing the two methodologies to each other as they are, we can say that we notice a larger rms value on the output voltage ν_{out} in the second method, which means a generally larger

Table 2.2: Summary of Control Strategies

Strategy	$P_e(t)$ [kW]	f_c (*) [kN]	i [A] (*)	ν_{out} [kV] (*)	$\|\mathrm{w(t)}\|_2$
Baseline-LQT	15.9	39.9	42.5 / 118.90 / -91.51	0.80 / 2.88 / -2.72	9.45
MRA-LQT	18.1	40.8	43.49 / 131.12 / -99.40	0.88 / 3.02 / -2.79	1.66
Baseline LQ (power max.)	14.8	40.01	42.64 / 78.00 / -49.74	1.38 / 2.56 / -2.18	-
MRA-LQ (power max.)	18.5	41.3	44.02 / 88.12 / -89.92	1.49 / 3.05 / -2.99	-

(*) for the power P_e the value is an average, for the control force f_c root-mean-square, on the other quantities the values are respectively the root-mean-square / maximum / minimum value

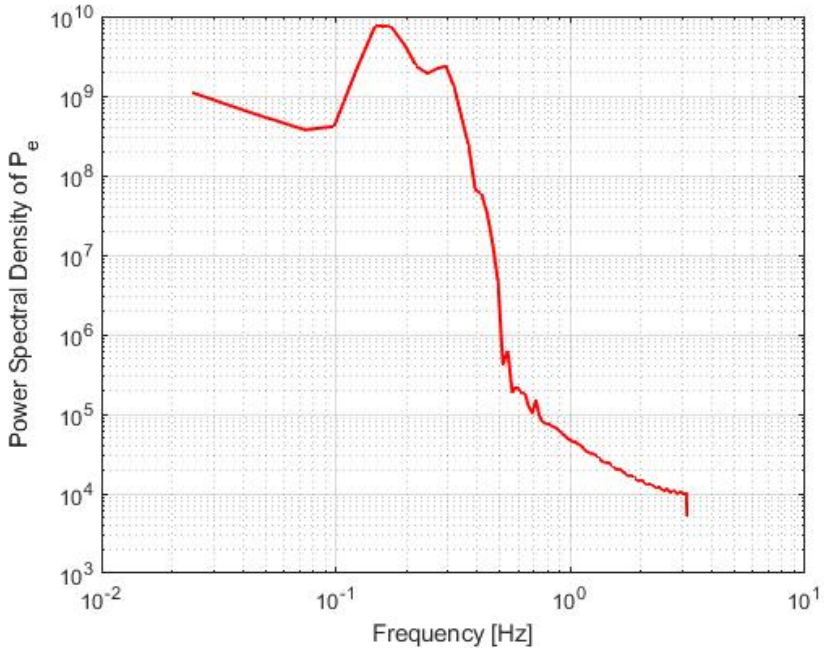

Figure 2.11: Power Spectral Distribution (PSD) of the electric power signal P_e

rms value of the heave velocity $\dot{z}(t)$, and a generally smaller control force and generators current. However this didn't seem to lead to an excessive increase in the displacement values $z(t)$ which are established within the prescribed limits.

2.4 Control vs Optimal

Before the concluding remarks on the Chapter, it is interesting to see the performance of the control next to the unconstrained optimal. As expected, the latter pushes the quantities beyond the allowed limits, while with MRA-LQT and power maximizing MRA-LQ, we can see how the quantities are indeed contained within the limits if a successful tuning id made. The optimal control is computed as described in Appendix A). Figs. 2.14-2.15-2.16-2.17 show the control force and vertical velocities

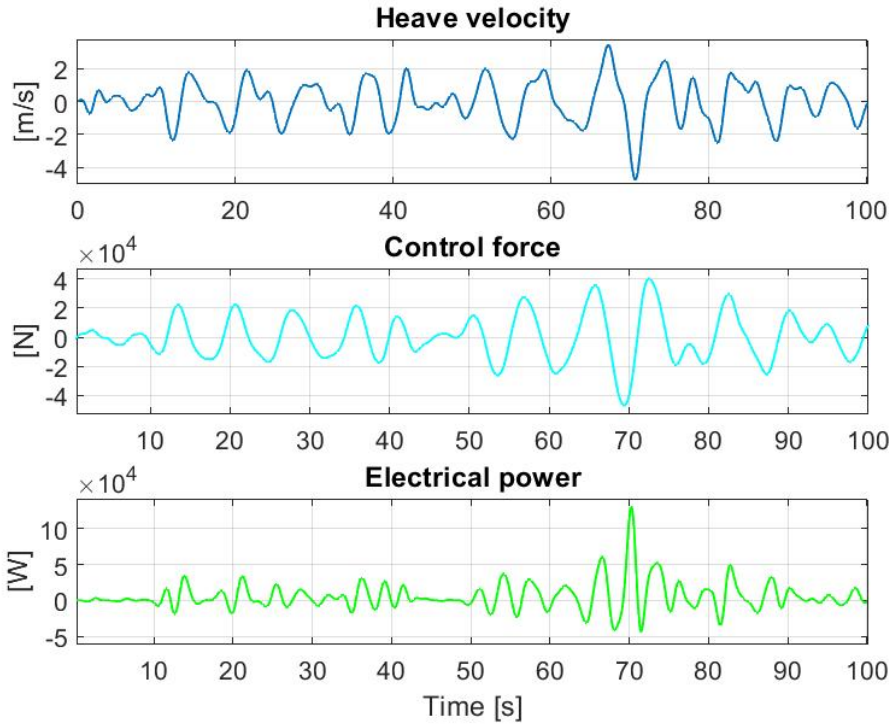

Figure 2.12: System response with simple power maximizing LQ control: velocity of the device (top), control effort generated (middle) and electrical power (bottom)

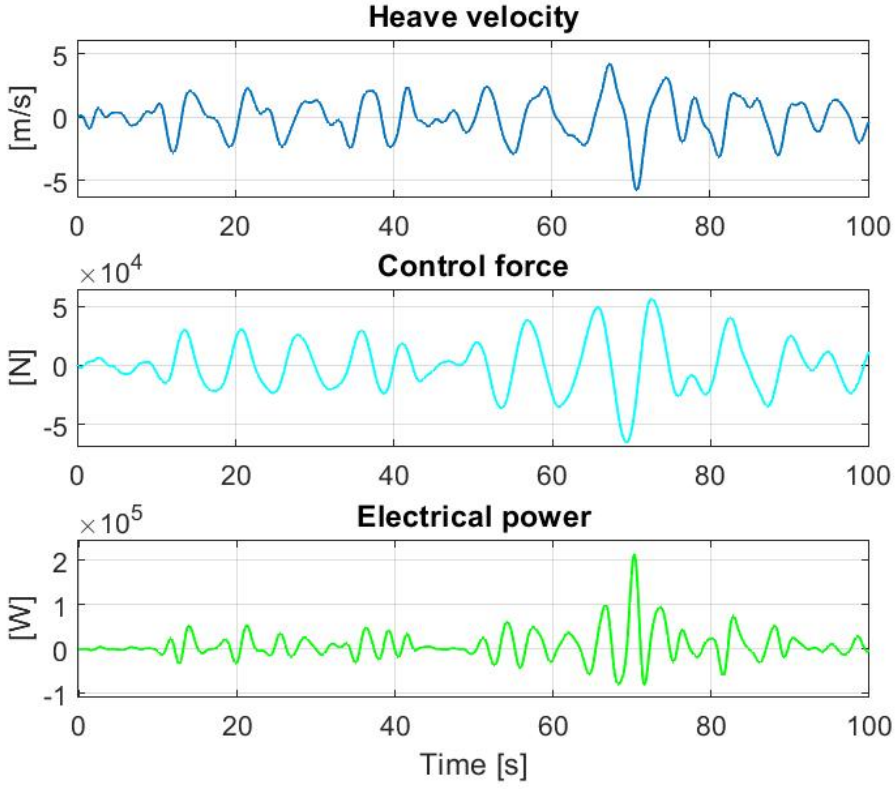

Figure 2.13: System response with power maximizing MRA-LQ control: velocity of the device (top) , control effort generated (middle) and electrical power (bottom)

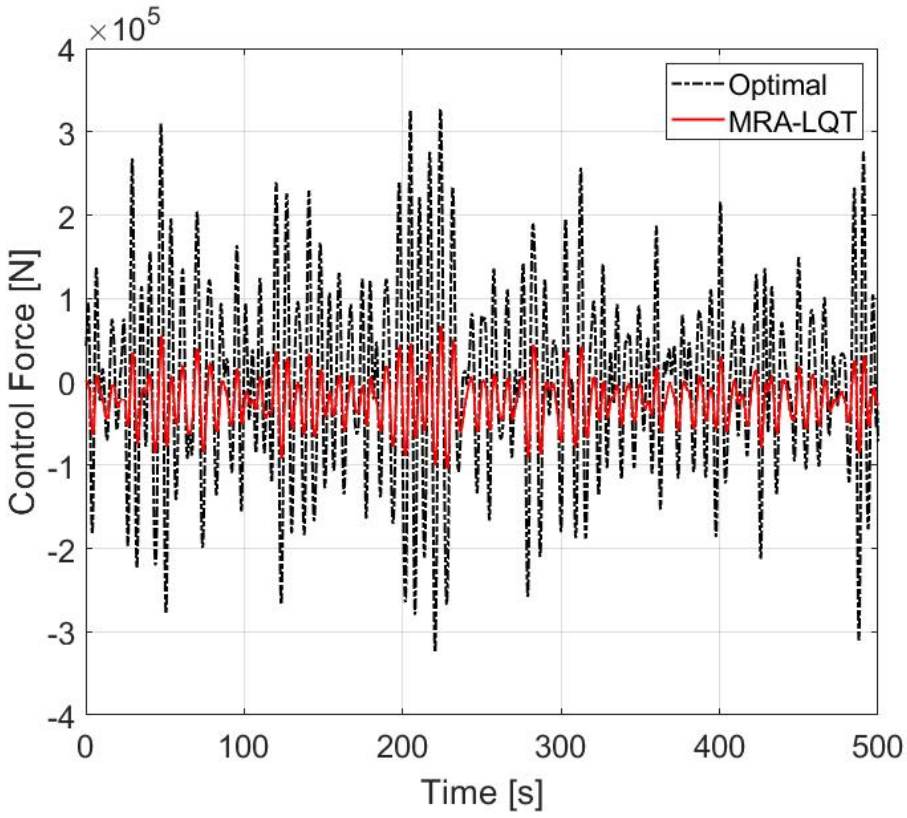

Figure 2.14: Control Force comparison between Optimal and MRA-LQT

over time. Simulation time is now set to $t_{sim} = 500s$ for a more comprehensive evaluation. Given the reduced tuning, it was not expected to see the controller anywhere near the unconstrained optimal performance, but this is just meant to highlight the importance of considering physical limitations in control.

2.5 Chapter conclusions

In this Chapter, two novel multiscale versions of LQ control are implemented on a model of a cylindrical Point Absorber. The strategies are fully causal and the frequency-dependent parameters of the controller can be computed offline, as the system is Linear Time Invariant (LTI). The formulations are developed for power maximization. With comparable control effort to the baseline non-multiscale case, the proposed techniques demonstrate a well improved performance. Indeed, by adjusting the parameters relative to one particular frequency band the overall control objective is tracked more effectively, with the result of boosting the power performance. This is true for both variants of the control. The power harnessed with the two methods seems to achieve similar levels, and the power fluctuation characteristics do not exhibit a difference between the first and second variant. The so called 'direct power maximizing' method appears to increase the device speed slightly, limiting the control effort; while the 'tracking method' seems to push the current to higher

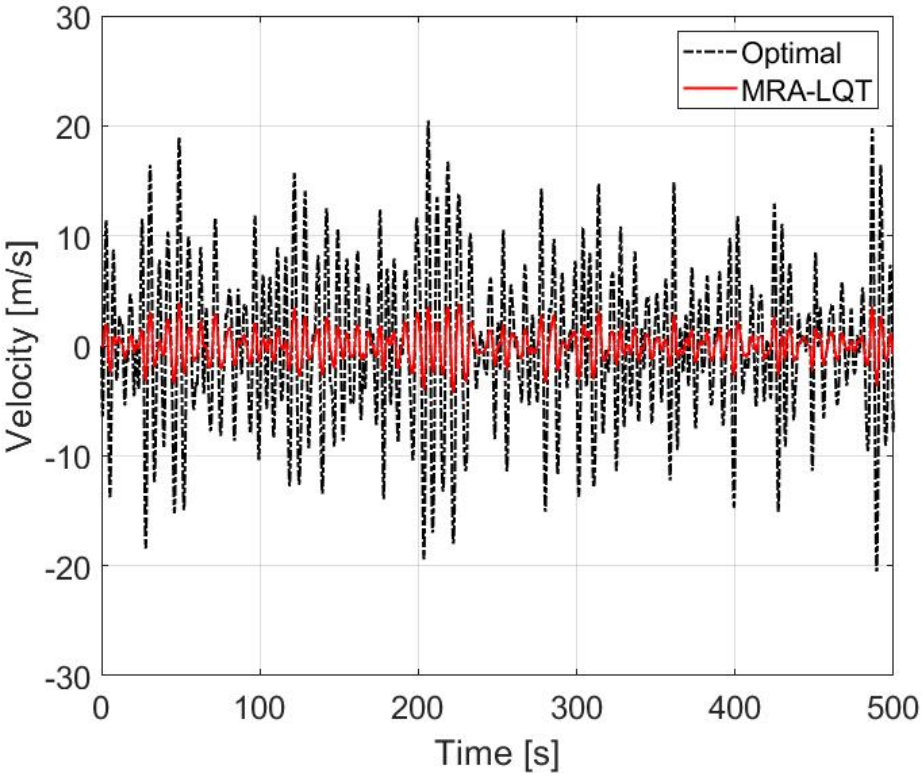

Figure 2.15: Velocity comparison between Optimal and MRA-LQT

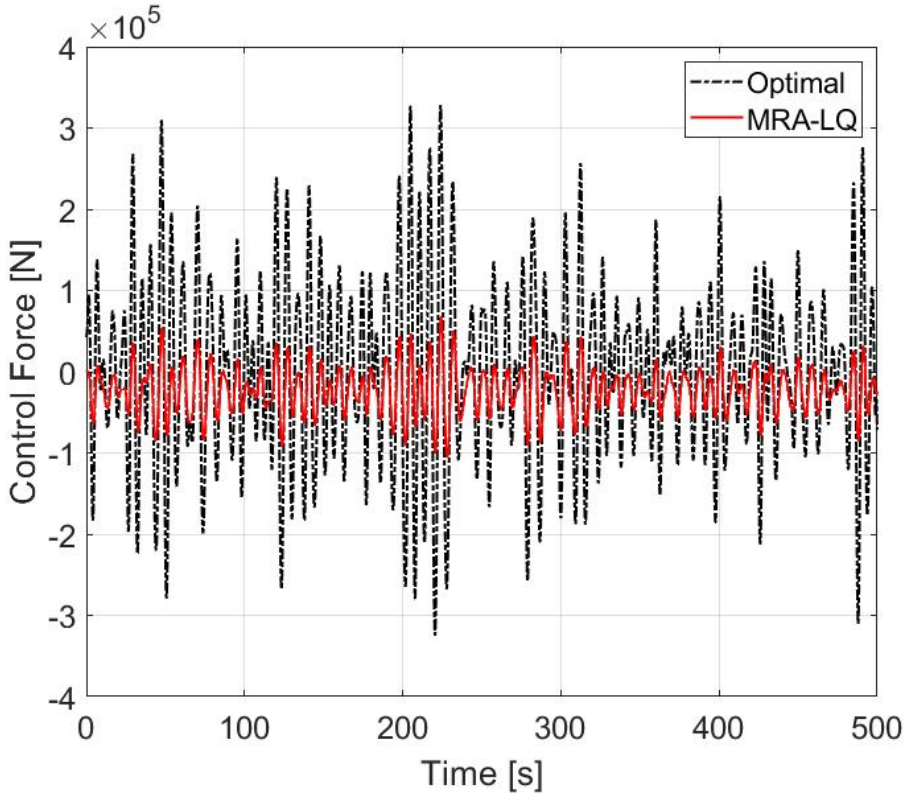

Figure 2.16: Control Force comparison between Optimal and MRA-LQ (max power)

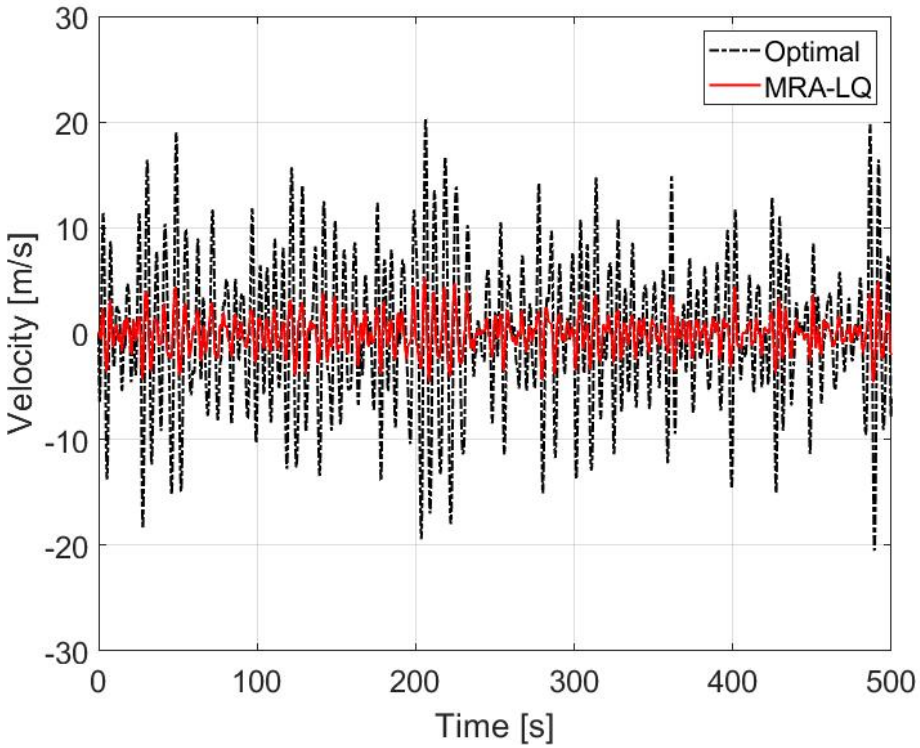

Figure 2.17: Velocity comparison between Optimal and MRA-LQ (max power)

values. Though, being unable to cast hard constraints explicitly, the tuning of the controllers has to be done with a series of trials and errors, to prevent quantities of interest surpass prescribed limits.

Chapter 3

Forward Propagating Riccati Equation Control in Wavelet Domain

In this Chapter a multiresolution strategy is developed for WEC power maximization, but unlike in Chapter 2, the dynamics of the Point Absorber for which it is implemented does not possess time invariant characteristics anymore. Given the spherical shape of the float, approximating the restoring coefficient as constant is not as accurate as for a cylinder, since the so called cut-water-plane area is varying. The presence of the varying term in the system dynamics makes the overall system nonlinear. So the assumption of LTI dynamics, present in the previous MRA control systems is invalid. Hence, in this Chapter the novel control method is developed for the non-linear WEC, representing it by a time-varying system.

Also, a difficulty linked to the deployment of controllers for time-varying or nonlinear systems is that future knowledge of system matrices is needed for the control implementation and this leads to a non-causal problem. Despite this, since it is in the very interest of this thesis to fully deploy control algorithms that do not depend on prediction techniques, the solution to this problem is sought in the basin of causal controllers.

It was found that control based on a Forward Riccati Equation is able to circumvent this issue, keep causal properties, and be suitable for TV and certain classes of nonlinear systems [121]. This is found true for both state feedback and output feedback kind of control. FRE control indeed uses dual differential Riccati equations that are solved forward in time.

As mentioned, in TV and nonlinear systems, the future system matrices are generally not known, and a standard backward Riccati formulation is not feasible in obtaining the optimal control gain.

The baseline FRE control was further extended into a multiresolution version applied to TV systems already in [122]. The wavelet domain formulation has again the advantage of incorporating

multiscale frequency dependent TV gains, which is suitable for nonlinear systems.

The model of spherical WEC herein, is developed in a weakly non-linear fashion and only the static contribution of the Froude-Krylov force is accounted. The strong nonlinear effects given by the restoring force are shown to be successfully addressed by the nonlinear controller, which takes them into account by converting the system to a TV-state space formulation. This is seen in close comparison with both the LTI based MRA control developed in Chapter 2, and the baseline FRE control. This means that both the nonlinear formulation of the novel MRA-FRE and the multiscale characteristics of the controllers are shown to be enhancing the performance.

3.1 Mathematical model

WECs are usually modelled using hydrodynamic coefficients determined using a BEM code such as WAMIT or NEMOH [123]. BEM assumes that all hydrodynamic forces on a floating body can be modelled using a set of linear hydrodynamic coefficients. In operational conditions, some WEC devices can be modelled using linear methods because the motions are small and the wetted surface area remains approximately constant.

Other WEC devices use a highly asymmetric float shape to maximize the power capture. This shape causes the wetted area with the movement of the float to change dramatically. This behavior does not allow the Froude-Krylov forces and the buoyancy force to be modelled by linear hydrodynamic coefficients. If the device is modelled with a , which means that it is constrained to move in the vertical direction only, considerations follow.

Under the assumption of an incompressible, inviscid and irrotational fluid flow, Newton's second law of dynamics can be written as

$$M\ddot{z}(t) = f_g - \iint_{S(t)} p(t)\mathbf{n}dS + f_{PTO}(t) \tag{3.1}$$

where z is the heave displacement with the overdot representing derivative with respect to time, M is the structural mass of the body, f_g is the gravity force, S is the submerged surface, $p(t)$ the time-dependent pressure of the fluid on the body surface and $\mathbf{n}$ the unit vector to the infinitesimal surface dS. The PTO applies a force f_{PTO} on the device and it is the object of our study for control as it will be seen later.

According to Bernoulli's equation [9], the fluid pressure acting on the surface of the body is

$$p(t) = -\rho g z(t) - \rho\frac{\partial\phi(t)}{\partial t} - \rho\frac{|\nabla\phi(t)|^2}{2} \tag{3.2}$$

where ρ is the density of the water, g the acceleration of gravity, $-\rho gz$ the hydrostatic pressure

(p_{st}) and ϕ the flow potential. The flow potential function based on linear wave theory can be written as

$$\phi(t) = \phi_I(t) + \phi_D(t) + \phi_R(t) \tag{3.3}$$

with $\phi_I(t)$ incident flow potential, $\phi_D(t)$ diffraction potential, and $\phi_R(t)$ radiation potential. This allows us to write

$$M\ddot{z}(t) = f_{FK_{st}}(t) + f_{FK_{dy}}(t) + f_D(t) + f_R(t) + f_{PTO}(t) \tag{3.4}$$

where the subscripts *FK*, *D*, *R*, *PTO* refer to Froude-Krylov, diffraction, radiation and PTO forces respectively. Note now that the FK force is composed of a static $f_{FK_{st}}(t)$ and dynamic part $f_{FK_{dy}}(t)$. The dynamic FK component and diffraction forces together are generally known as excitation forces. Given that the predominant component of the two forces is the static one, and also given the aim of the controller to show its performance superiority in a nonlinear environment, it is sufficient to limit the model to this non-linear static FK component only. Hence, the effect of the quadratic components in (3.2) is also neglected, as justified in [124] as well.

3.1.1 Nonlinear restoring force model

As written in (3.4) the FK force is divided in two parts: static, $f_{FK_{st}}$ and dynamic, $f_{FK_{dy}}$; where the static part is the balance between the gravity force f_g and the integral over the wetted surface of the static pressure p_{st}, and the dynamic refers to the integral over the wetted surface of the dynamic pressure $p_{dy} = -\rho\frac{\partial\phi_I}{\partial t}$. We can write

$$f_{FK} = f_{FK_{st}} + f_{FK_{dy}} = f_g - \iint_{S(t)} (p_{st} + p_{dy})\mathbf{n}dS. \tag{3.5}$$

Both the static and dynamic forces depend on the instantaneous wetted surface $S(t)$, which depends in turn on both the incident wave elevation and displacement of the body.

In the present work, the nonlinear model is limited to the static component of the FK force only. One additional reason for this is that an algebraic solution to the integral in (3.5) as in [125] would not be suitable for real time implementation given the numerous frequencies involved in an irregular sea state. A re-meshing routine technique for the calculation of the instantaneous wetted surface is also too computationally demanding and it goes beyond the scope of this work. So as it is commonly done for linear models, the dynamic component is computed together with the diffraction force f_D by means of the convolution product of the excitation IRF K_{ex} with the free surface elevation η, leading to

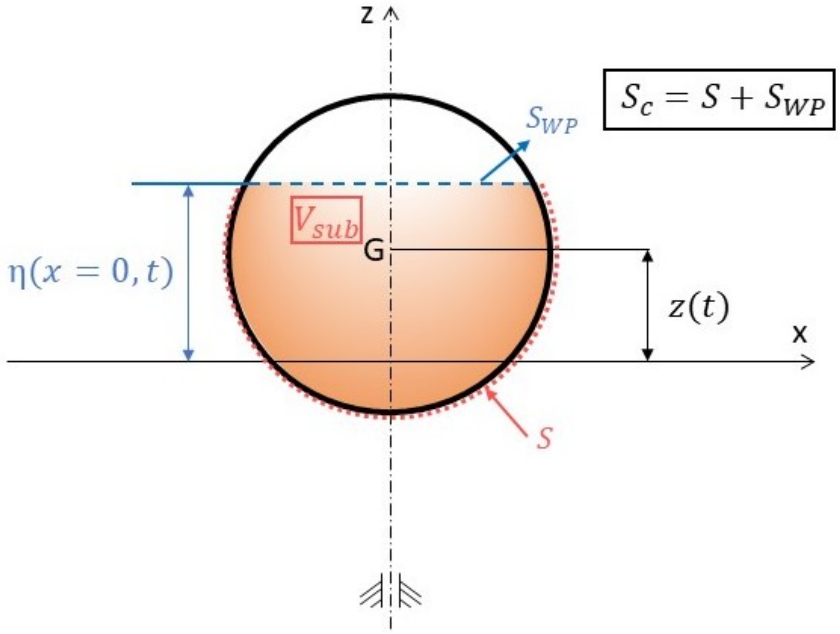

Figure 3.1: Sphere schematic in dynamic conditions (for a generic time t), highlighting the closed surface S_c surrounding the volume V_{sub}, and upper limited by the water plane surface S_{WP}.

$$f_e = f_D + f_{FK_{dy}} = -\int_{-\infty}^{\infty} K_{ex}(t-\tau)\eta(\tau)d\tau. \tag{3.6}$$

As already developed in Chapter 2 and with the same assumptions to obtain a causalized system, we will consider $\eta(t)$ not in correspondence of the device exactly but measured at some other location sufficiently "up-wave" from the unidirectional wave propagation, so that a finite order state-space formulation as in Eq. (2.10) can be written. Limited to this Chapter also, for convenience we will refer as $\eta_{up}(t)$ as $\eta(t)$. Refer to Chapter 2 for the explanation over this approximation.

In order to be able to express the static Froude-Krylov force, we notice that the wetted surface S in Eq.(3.5) can be described by the closed surface S_c which encloses the submerged volume V_{sub}, subtracting the horizontal surface S_{WP}. S_{WP} is defined as the intersection between the body and the horizontal plane at free surface elevation η. This can be appreciated in Fig. 3.1. It follows that

$$f_{FK_{st}} = f_g - \left(\iint_{S_c} p_{st}\mathbf{n}dS - \iint_{S_{WP}} p_{st}\mathbf{n}dS\right) \tag{3.7}$$

which, with applying Gauss's divergence theorem to the integral over the closed surface yields

$$f_{FK_{st}} = f_g + (\rho g V_{sub} - \rho g \eta A_{WP})\mathbf{k} \tag{3.8}$$

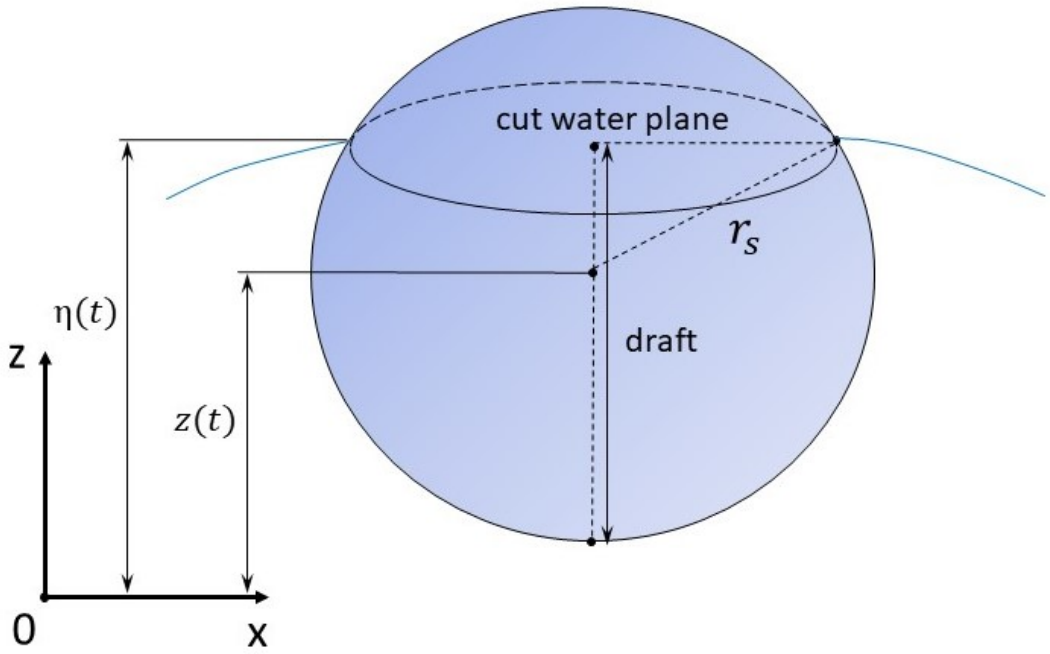

Figure 3.2: Sphere point-absorber geometry

where $\mathbf{k}$ is the vertical unit vector and A_{WP} is the area of S_{WP}.

For the particular case of a sphere of radius r_s (see Fig. 3.2), and with the assumption of the centre of mass G lying on the still water level in equilibrium ($Mg = \frac{2}{3}\rho g\pi r_s^3$) it is found that the nonlinear static FK force can be finally written in terms of the displacement z and wave elevation η as

$$f_{FK_{st}} = \rho g\pi\big(\frac{\eta^3}{3} - r_s^2\eta + z^2\eta - z\eta^2 + r_s^2 z - \frac{z^3}{3}\big). \tag{3.9}$$

The radiation force can be written using Cummins equation as

$$f_R(t) = -m_\infty \ddot{z}(t) - \int_{-\infty}^{\infty} K_R(t-\tau)\dot{z}(\tau)d\tau \tag{3.10}$$

where m_∞ is the added mass at infinite frequency and K_R is the radiation IRF. The computationally expensive convolution integral in (3.10) is also replaced by a state space formulation as in [34] and in Chapter 2, Eq. (2.6). See there for more details over this assumption. The same notation to Chapter 2 is used throughout this Chapter.

3.1.2 The TV state-space form

Given the nonlinear system described in Eq.(3.4), for the control development it is in the intention of the author to obtain, given the finite order state space approximations describing the excitation force and radiation force, an overall state space formulation

$$\begin{aligned}\dot{x}(t) &= A(x(t),\eta(t))x(t) + Bf_{PTO}(t) + E(\eta(t))\eta(t), \quad x(0) = x_0\\ y(t) &= Cx(t)\end{aligned} \tag{3.11}$$

where $x(t) \in \mathbb{R}^n$ denotes the augmented system state vector

$$x(t) = \begin{bmatrix} x_r(t) & z(t) & \dot{z}(t) & x_e(t) \end{bmatrix}.$$

$x_r(t)$ represent the vector of states approximating the radiation force subsystem in Eq. (3.10), $z(t)$ and $\dot{z}(t)$ are the vertical displacement and velocity of the device and $\mathbf{x}_e(t)$ is the vector of states representing the finite order approximation of the excitation force $f_e(t)$ in Eq. (3.6). $y(t) \in \mathbb{R}^p$ is the system output vector. $f_{PTO}(t) \in \mathbb{R}^m$ is the controlled input, $A(x(t),\eta(t)) \in \mathbb{R}^{n\times n}$ is the state-and-input dependent system matrix, $B \in \mathbb{R}^{n\times m}$ is the control influence matrix, $E(\eta(t)) \in \mathbb{R}^{n\times 1}$ is the input dependent exogenous signal matrix and $C \in \mathbb{R}^{p\times n}$ is the matrix relating the state to the output. This form might look unusual at first glance, given that the matrices $A(x(t),\eta(t))$ $E(\eta(t)$ not only are not constant but also they dependent on the current value of the state $x(t)$ the system they are trying to describe and of the input $\eta(t)$. This description though, given the online capability of the technique, is precisely what allows to handle the nonlinear effects, which instead are necessarily approximated by the control strategies in Chapter 2.

In particular, by casting the subsystems altogether, the matrices in Eq. (3.11) are

$$A(x(t),\eta(t)) = \begin{bmatrix} A_p & 0_{4\times 1} & B_p & 0_{4\times 6} \\ 0_{1\times 4} & 0 & 1 & 0_{1\times 6} \\ -\frac{C_p}{M+m_h} & -\frac{k_2(x(t),\eta(t))}{M+m_h} & 0 & \frac{C_e}{M+m_h} \\ 0_{6\times 4} & 0_{6\times 1} & 0_{6\times 1} & A_e \end{bmatrix}, \quad B = \begin{bmatrix} 0_{5\times 1} \\ \frac{1}{M+m_h} \\ 0_{6\times 1} \end{bmatrix},$$

$$E(\eta(t)) = \begin{bmatrix} 0_{5\times 1} \\ \frac{k_1(\eta(t))}{M+m_h} \\ B_e \end{bmatrix} \quad \text{and} \quad C = \begin{bmatrix} 0_{1\times 5} & 1 & 0_{1\times 6} \end{bmatrix}$$

with $k_1(\eta(t))$ and $k_2(x(t))$ input-dependent and state-dependent coefficients

$$k_1(\eta(t)) = \rho g \pi \Big(\frac{\eta(t)^2}{3} - r_s^2 \Big)$$

and

$$k_2(x(t),\eta(t)) = \rho g \pi \Big(z(t) - \eta(t)^2 + r_s^2 - \frac{z(t)^2}{3} \Big).$$

In the next section, the implementation of the controller follows.

3.2 Wavelet FRE Control Synthesis

The general multiscale features of the controller developed in this Chapter follow the framework described in [80]. The dynamics of the generator is reduced as in Chapter 2. It is assumed to be governed by a resistance $R_s = 5\Omega$, resulting in the expression for the mechanical and electrical power as

$$P_m(t) = f_{PTO}(t)\dot{z}(t) \tag{3.12}$$

$$P_e(t) = \nu_{out}(t)i(t) = \big(\nu_{emf}(t) - Ri(t)\big)i(t) \tag{3.13}$$

where the time dependency of variables is explicitly stated. Within the formulas

- $i(t)$ represents the generator's current (control variable);
- $\nu_{out}(t)$ is the output voltage (proportional to the output velocity);
- $\nu_{emf}(t)$ is the back electromotive force;
- $\dot{z}(t)$ is the compression rate (vertical speed of the actuator stroke), supposed equal to the vertical velocity of the device relative to the seabed.

Refer to Fig.2.5 for the schematic representation of the generator. In the same simplified manner, velocity $\dot{z}(t)$ and control force $f_{PTO}(t)$ can be related to the output voltage and current with

$$f_{PTO}(t) = K_i i(t) \quad \nu_{out}(t) = K_v \dot{z}(t). \tag{3.14}$$

and K_i, K_v are force constants determined by the generator's characteristics. This allows to rewrite the system (3.11) with the matrix substitutions

$$B' = BK_i \qquad C' = K_v C. \tag{3.15}$$

where needed.

3.2.1 The objective of the controller

Given the power quantities $P_m(t)$ and $P_e(t)$ interrelated with conversion efficiency ζ

$$P_e(t) = \zeta P_m(t) \tag{3.16}$$

recalling Chapter 2, the aim of the controller is the maximization of

$$J = E\{P_e\} \tag{3.17}$$

where $E\{\cdot\}$ is the expected value under stationary conditions. We can re-state it as a minimization problem as

$$\max_i J = \min_i -J. \tag{3.18}$$

This minimization problem can be solved using Algebraic Riccati equation only under a stationary assumption in an asymptotic case. Hence, the solution is strictly valid under a restrictive condition and is in fact not valid in the present case where we are dealing with non-stationary sea state excitations and responses. However, note that the power generation term is composed of two competing quantities, the first being the instantaneous power without losses and the other corresponding to the generator loss. Hence, we can set an optimization problem with appropriate sign defined weights assigned to these two quantities. Following a general framework, considering the weighted energy corresponding to a band associated with a scale 'a' in wavelet domain, one can conveniently define the objective functional for each individual frequency band as

$$J_a = \int_{t_0}^{t_c} \{W_{\psi_a}\nu_{out}\}^T[N]_a\{W_{\psi_a}i\} + \{W_{\psi_a}i\}^T[R]_a\{W_{\psi_a}i\}]db, \tag{3.19}$$

which is written extending the framework of the classic Linear Quadratic Regulator (LQR) objective function to a multi-resolution one, with output $y = \nu_{out}$, and where the output related weight terms (i.e., Q in the classical case, or by $[Q]_a$ in wavelet domain) are set to zero. Notice that the WEC dynamics was previously augmented with Eqs. (3.15). In fact, the control input is the current i. The convenience of including the voltage ν_{out} and the input i in Eq.(3.19) stands in the presence of their cross products $\{W_{\psi_a}\nu_{out}\}^T[N]_a\{W_{\psi_a}i\}$. The operator $\{W_{\psi a}[\cdot]\}$ is the continuous wavelet transform of $[\cdot]$ with respect to the basis function ψ and the parameter a determines the frequency content of the different bands. The matrices $[R]_a$ and $[N]_a$ are frequency dependent weights associated with the transformed control input $\{W_\psi i\}$ and the combined effect of the transformed control input and the transformed output $\{W_\psi \nu_{out}\}$. The parameter b denotes the translational parameter and signifies the localization of the energy corresponding to the band with scale 'a' temporally around $t = b$. db denotes the differential respect to b.

For design of the control input, it is convenient to use DWT owing to its exact decomposition/reconstructing capabilities. An exhaustive explanation on the relationship between the continuous transform expressed in Eq. (3.19) and the DWT (for perfect decomposition/reconstructions of the signals) used in the present work is found in [114].

3.2.2 Control Design

It is shown in [122] that by applying the continuous wavelet transform to the system (3.11), where the matrices B and C have been substituted for the new inputs and outputs with the matrices B' and C' (Eq. (3.15)) and using the slowly TV approximation, the first equation can be transformed to

$$\frac{\partial}{\partial b} W_{\psi_a} x(b) \approx A(b) W_{\psi_a} x(b) + B'(b) W_{\psi_a} i(b) + E(b) W_{\psi_a} \eta(b) \tag{3.20}$$

for a particular "a". Similarly we can write

$$W_{\psi_a} y(b) \approx C'(b) W_{\psi_a} x(b). \tag{3.21}$$

The aim is to find a wavelet domain (transformed) state feedback gain $K_a(b, x)$ such that

$$W_{\psi_a} u(b) = K_a(b, x) W_{\psi_a} x(b) \tag{3.22}$$

minimizes the objective function in Eq.(3.19). It is important to note that the gains are state and time dependent. Besides, they are also dependent on dilation scales, so on frequency bands. The goal is to find a feedback gain which only depends on past and present system matrices unlike other controllers where the backward Riccati solution requires the future knowledge of the nonlinear system.

To achieve the goal, a key step in the process is following the construction of the inversion transformation

$$\|W_{\psi_a} s(b)\| = \frac{1}{\|W_{\psi_a} x(b)\|}. \tag{3.23}$$

The transformation in Eq. (3.23) implies that a stabilization of the state of the system (3.20)-(3.21) results in a destabilization of the transformed state (see [122]). Effectively, in the present work it will simply translate into the minimization of the objective functional built in (3.19) with appropriate state transformations.

This also means that a transformed input $W_{\psi_a} v(b)$ can be found so that we have

$$\frac{\partial}{\partial b} W_{\psi_a} s(b) = \bar{A}(b) W_{\psi_a} s(b) + \bar{B}(b) W_{\psi_a} v(b) \tag{3.24}$$

where

$$\bar{A}(b) = -T(W_{\psi_a} x(b)) A(b) T^{-1}(W_{\psi_a} x(b)) \tag{3.25a}$$

$$\bar{B}(b) = -T(W_{\psi_a} x(b)) B'(b) \tag{3.25b}$$

and $T(W_{\psi_a}x(b))$ is a Householder transformation in wavelet domain [126]

$$T\big(W_{\psi_a}x(b)\big)= I - 2\frac{W_{\psi_a}x(b)W_{\psi_a}x^T(b)}{W_{\psi_a}x^T(b)W_{\psi_a}x(b)}. \tag{3.26}$$

It can be shown that such control input $W_{\psi_a}v(b)$ is found by solving for $P_a(b)$ the following forward Riccati differential equation

$$\frac{d}{db}P_a(b) = -\bar{A}^T(b)P_a(b) - P_a(b)\bar{A}^T(b) + Q_a(b) - \\ - \big(P_a(b)\times\bar{B}(b) + N_a(b)\big)R_a^{-1}(b)\big(\bar{B}^T(b)P_a(b) + N_a^T(b)\big) \tag{3.27}$$

$$P_a(b)\mid_{b=0}= P_{a0} > 0$$

resulting in control gains

$$K_a(b,x) = R_a^{-1}(b)\big(\bar{B}^T(b)P_a(b) + N_a^T(b)\big) \tag{3.28}$$

In Eqs.(3.27)-(3.28), $Q_a(b) > 0$, $R_a(b) > 0$, $N_a(b) > 0$ and $Q_a(b)$, $R_a(b)$, $N_a(b)$, $Q_a^{-1}(b)$, $R_a^{-1}(b)$ and $N_a^{-1}(b)$ are all uniformly bounded. Eq. (3.27) is integrated over the time interval $[0,t]$ for each scale. Through the transformation in Eqs.(3.25a)-(3.25b), the proposed controller implements a nonlinear dynamic state feedback which depends only on past and present states, removing the drawback of noncausality.

Now, the approximated relationship between continuous wavelet transform and the DWT, is well defined in [114]. Once the optimization is performed separately on the filtered signal with different bands, control current $i(t)$ can be found by adding together the components as

$$\{i(t)\} = -[K]_L\{x(t)\}_L - \sum_{j=L}^{n-1}[K]_{d_j}\{x(t)\}_{d_j} \tag{3.29}$$

and in turn, determine the control force $f_{PTO}(t)$ (Eq. (3.14)). The frequency dependent control gain matrices $[K]_L$ and $[K]_{d_j}$ (with $j = L,...,n-1$) are based on the MRA decomposition. On a generic signal (for example the state vector itself $x(t)$) using an appropriate wavelet with basis ψ and scaling function ϕ, so called scale equations are used to generate high and low pass filters, and then a low frequency signal approximation $\{x\}_L$ and band limited signal components $\{x\}_{d_j}$ is computed so that

$$\{x(t)\} = \{x(t)\}_L + \sum_{j=L}^{n-1}\{x(t)\}_{d_j}. \tag{3.30}$$

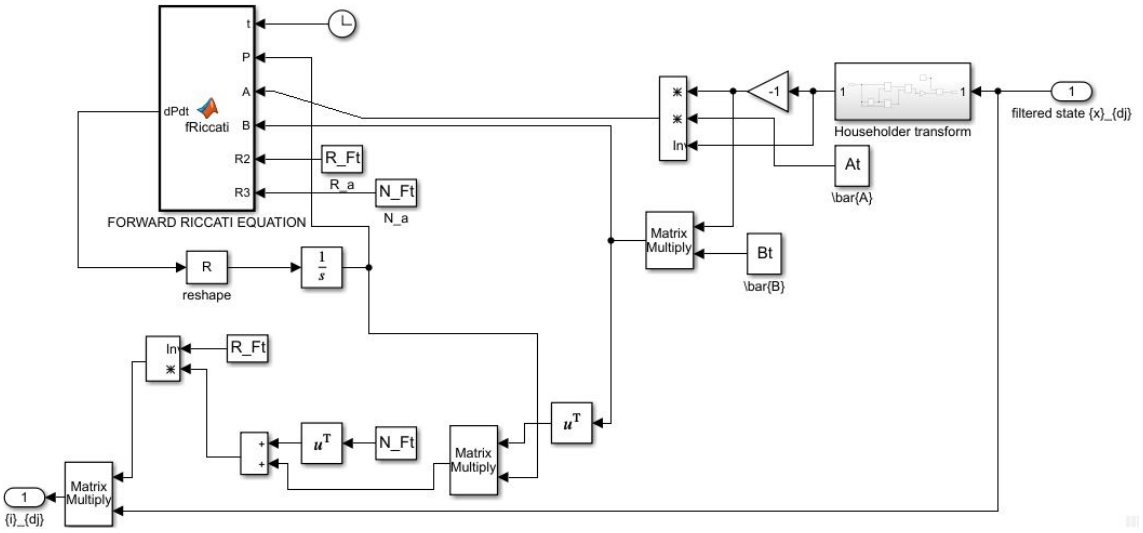

Figure 3.3: Signal processing of a single frequency sub-band, within the nonlinear controller: the decomposed signal $\{x\}_{d_j}$ is transformed to obtain $\{s\}_{d_j}$ and the feedback gain $[K]_{d_j}$ is computed online solving Eq. (3.27). It is then applied to the decomposed state vector $\{x\}_{d_j}$ to compute the component $\{i\}_{d_j} = [K]_{d_j}\{x(t)\}_{d_j}$ of the control current.

Table 3.1: Specifications of the Device (FRE Control)

Variable	Parameter	Value	Units
r_s	Radius	3	m
M	Mass	$5.75 \cdot 10^4$	kg
m_h	Added mass	$2.82 \cdot 10^4$	kg
k_b	Linearized Buoyancy	$2.77 \cdot 10^5$	N/m

In Fig. 3.3 a scheme of the signal processing on a single sub-band a is shown. The FRE (3.27) is computed based on the transformed filtered state $\{s\}_{dj}$ (which determines the transformed matrices $\bar{A}$ and $\bar{B}$). The feedback gain matrix is computed online and applied to the original filtered vector $\{x\}_{d_j}$.

3.3 Numerical Control Performance

In the present section, we illustrate the performance of the described strategy, compared to the previously developed Multiscale-LQR control from [122] and the simple version of the FRE control. Table 3.1 reports the device characteristics used in the numerical case study.

The hydrodynamic coefficients obtained with the BEM solver to calculate the state-space approximation of the radiation force, assume a deep water condition, meaning that the effect of sea bed is neglected. NEMOH was employed as solver, and the device meshing is shown in Fig. 3.4. The approximation of the radiation force was obtained with the Frequency Domain Identification MATLAB Toolbox, described in [127]. Results of the fourth order approximation are shown in Fig. 3.5: on the left-hand side, the radiation Frequency Response Function $H_r(\omega)$, on the right-

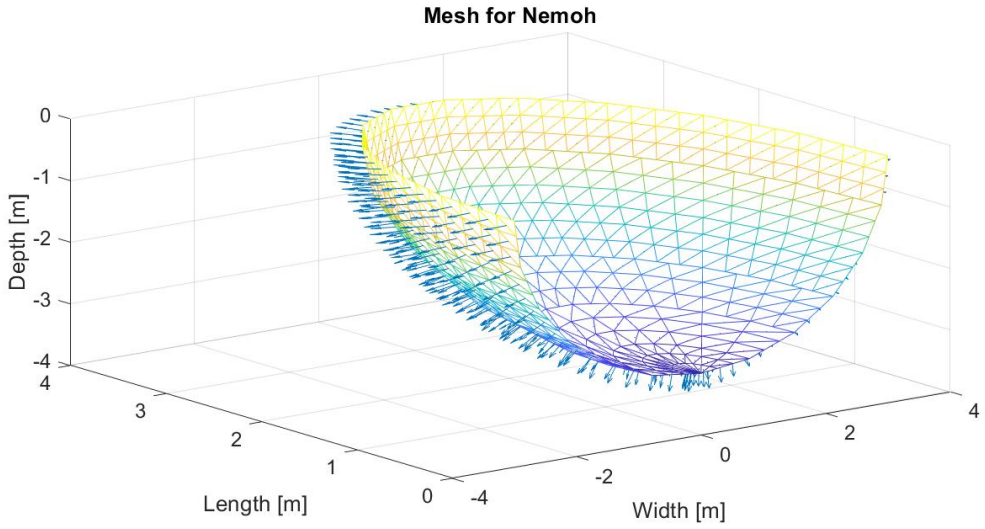

Figure 3.4: Mesh generated by Nemoh for the spherical PA, number of surface elements=500

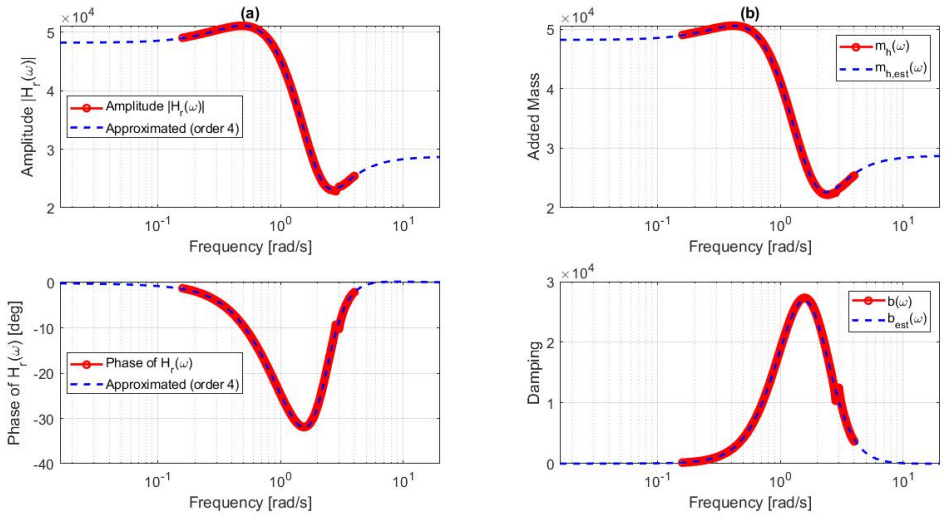

Figure 3.5: FRF of the radiation force with its amplitude (top-left) and phase (bottom-left) and related hydrodynamic coefficients: added mass (top-right) and damping (bottom-right)

hand side the hydrodynamic coefficients $m_h(\omega)$ and $b(\omega)$, approximated by $m_{h,est}(\omega)$ and $b_{est}(\omega)$ respectively.

Time series of the wave elevation $\eta(t)$ impacting the device are generated by a JONSWAP spectrum [113] of significant wave height $H_s = 2m$ and a zero-crossing period of $8s$ over a time window of duration $T_{sim} = 200s$. Simulations are carried out on a MATLAB-Simulink environment with a variable time step solver. The results are compared to the performances of the controllers described in [128] and Chapter 2.

Following the reasoning on the spectral distribution of the signal of interest, a suitable choice of wavelet basis is made. If the same orthogonal Daubechies family of wavelet used in Chapter 2 is chosen, based on the spectral distribution of the power signal P_e related to the present case

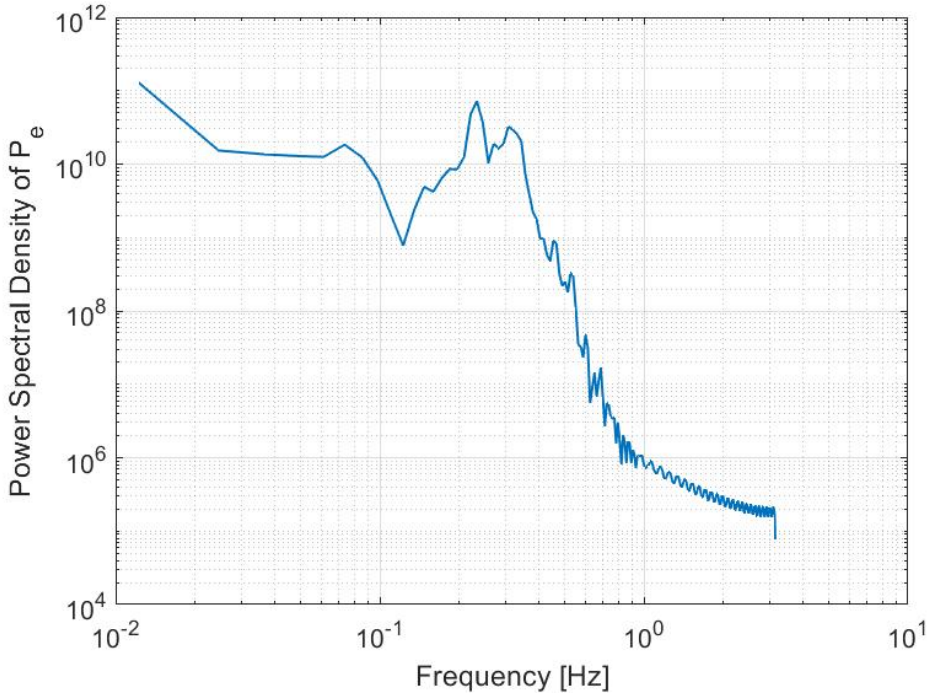

Figure 3.6: Power Spectral Distribution (PSD) of the electrical power P_e

(see Fig. 3.6), we notice that the same four level decomposition suffices to cover most of the spectrum. Attention can be placed on the approximation space for level 4, meaning that signals with central frequencies lower than $0.89Hz$ are covered, while weightings on its complement space can be relaxed, limiting the control effort.

Values of $R = 3.5$ and $N = -600$ are chosen for the approximation space at level 4, while on the complementary space $R = 20$ and $N = -600$ are used. The same wavelet decomposition and configuration is repeated as for the Multiscale-LQR controller, applied on the model of the sphere developed in this Chapter. For the non-MRA version of the FRE controller (see [128]), the objective function is expressed in the standard way, and there is no distinction between frequency bands. Weighting matrices have the value of $R_f = 5$ and $N_f = -600$. The subscript 'f' is used to distinguish the weights for the non-MRA FRE formulation.

The correct choice of the weights is immediately reflected in the results (Figs. 3.7-3.8). A clear gain in power is exhibited with the proposed controller. The performance of the multi-scale wavelet LQ is outperformed by the increased capabilities of the nonlinear FRE formulation. The control effort can be localized in one main frequency band, relaxing all the others. This gives rise to higher power generation with marginal increase in control force. The comparison is also summarized in Table 3.2.

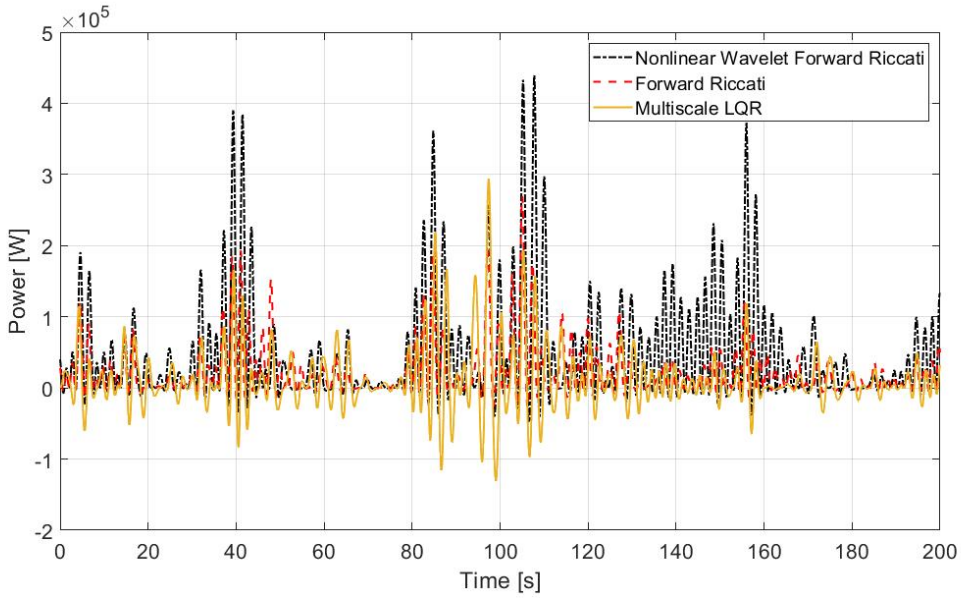

Figure 3.7: Power Performance of the proposed Nonlinear Wavelet FRE Control, compared to a simple FRE [128] and Multiscale-LQR

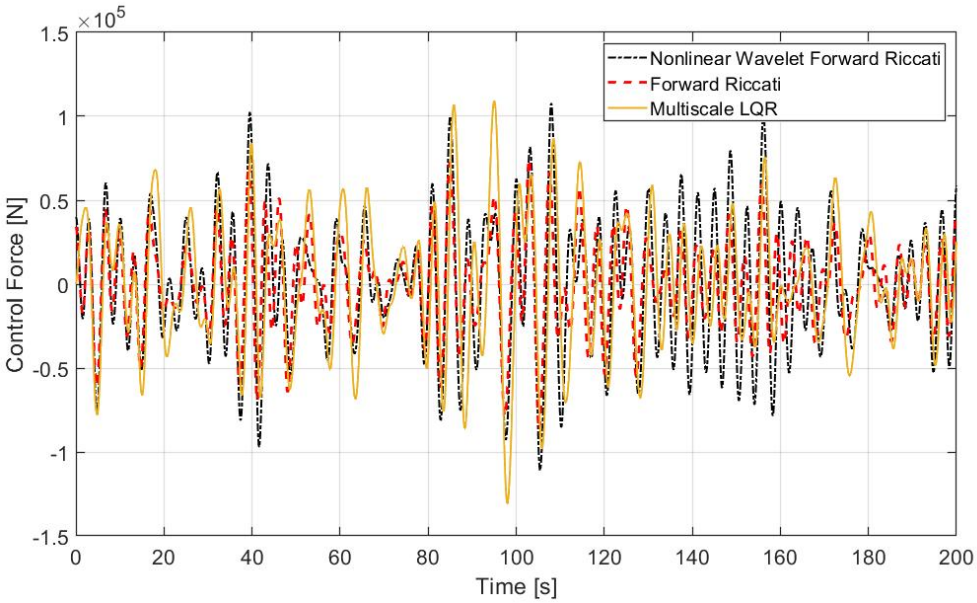

Figure 3.8: Control force in the proposed Nonlinear Wavelet FRE Control, compared to a simple FRE [128] and Multiscale-LQR

3.4 Chapter conclusions

In this Chapter, a multiresolution control based on a FRE formulation is proposed for the power maximization of a WEC modelled by nonlinear dynamics. The control design results in a TV nonlinear dynamic state feedback control law. Floating devices with varying cross sectional area are more accurately described by a nonlinear restoring force. The FRE formulation conveniently tackles this dynamics describing it by a TV state space system. By applying an inversion transformation of the state, the proposed formulation solves the associated differential Riccati equation forward

	Nonlinear FRE	**Baseline FRE**	**Multiscale-LQ**
Mean Power [W]	$4.75 \cdot 10^4$	$1.82 \cdot 10^4$	$1.19 \cdot 10^4$
$f_{PTO,RMS}$ [N]	$3.81 \cdot 10^4$	$2.72 \cdot 10^4$	$3.75 \cdot 10^4$

Table 3.2: Mean power and current rms value for the simulated sea state of $2m$ significant wave height and $8s$ zero crossing period

in time, so that future information about system matrices is no longer needed. By re-formulating this controller in wavelet domain, with a direct power maximizing objective in an LQ framework in Chapter 2, it is possible to target the frequency bands of interest and boost the performance further by saving the control effort on the non-active frequency intervals. This is highlighted in the numerical results, where a spherical device was modelled and simulated, against a baseline FRE formulation. The proposed control also shows a clearly higher performance as compared to the Multiscale-LQ control in Chapter 2.

Chapter 4

A Constrained H_2-H_∞ Maximum Induced Power State Feedback Control

The previous Chapters considered optimizing WEC performance without the presence of any explicit direct physical constraints or limits on the dynamics of the device or the actuators for controllers. A constrained H_2 and H_∞ MIPC control with full state feedback is formulated in this Chapter with application on a PA device. LTI dynamics is again assumed. The MIPC technique states that a performance index can be minimized as a vector, which enforces the energy harnessing requirement [95]. The LMI-based formulation is then potentially able to cast multiple objectives, even contrasting ones, in the same optimization framework. This is likely to be very beneficial since in wave energy, during the operation of a WEC, several considerations have to be taken into account simultaneously. One of the most important ones is given by the physical limitations imposed by the mechanical/electrical components. The best way to deal with them is to impose hard constraints on the system dynamics, which is considered in this Chapter. Without such constraints, there would no way to ensure that variables such as displacements, currents, voltages etc. would be within a safe and physically allowed range. In fact, alternatively one would have to consider the multi-objective optimization where each of the quantities is limited within specific domains, and then the minimization is performed on the overall vector of variables constituted by these quantities. This way though, there is still no assurance that boundaries would not be exceeded especially in varying sea conditions. In [96], hard-constrains are cast together with the LMI problem set, thanks to the concept of reachable sets in state space ellipsoids defined by a quadratic storage function. With this method, saturation effects are also avoided.

Table 4.1: Specifications of the Device and MIPC $S-H_2/S-H_\infty$ tuning

Variable	Parameter	Value	Units
r	Radius	3	m
h_c	Height	5	m
M	Mass	113097.33	kg
m_h	Added mass	51384	kg
$\hat{K}$	Freq. Indep. Radiation damping	298,132	N/(m/s)
k_b	Buoyancy stiffness	277,370	N/m
μ	MIPC coefficient	0.005	

Writing the MIPC condition for a heaving WEC was again facing the challenge of a noncausal relationship between the device optimal velocity and the excitation forces. The suboptimal assumption of a frequency independent relationship between these quantities, allows a real time implementation and allows for the MIPC requirement to be cast into the LMI formulation. The causal architecture herein is again within the spirit of the thesis, where we remind all control strategies are "forecasting-free". The performance of the described controller is best seen on a highly varying sea environment: on a sea state by sea state basis, the strategy is expected to harness a reduced amount of power compared to an optimal control, given the presence of constraints.

Here is the novelty. The included hard-constraints are conveniently tuned with a single scalar quantity, directly proportional to the energy of the input. This means that with such associated scalar value, power maximization can be validated on each changing sea scenario, with no required effort. To be expected is that compared with a standard LQ control formulation this would mean no constraint breach when LQ does, and higher performance when LQ is unable to be successfully tuned. This is seen in the results: a global outstanding increase in energy harnessed (up to 45% for the $S-H_2$ control), when a specific site off the west coast of Ireland is considered.

4.1 The Maximum Induced Power Control

As anticipated, this Chapter aims to develop a novel control strategy that will take advantage of the Maximum Induced Power Control applied to the model of PA described in section 2.1.1 and 2.1.2. In this Chapter, the device dimensions are different than Chapter 2, reported in Table 4.1. The dimensions relative to the device within this Chapter are referred to a full-scale floater, to be deployed for sea installations.

The goal of the control strategy is to prove that the simplicity of implementation and the ability to adapt easily to changing sea conditions is a winning skill for the controller: it is able to indeed outperform more standard control strategies as a baseline LQ.

Thanks to a convenient LMI formulation the optimization problem for the computation of the

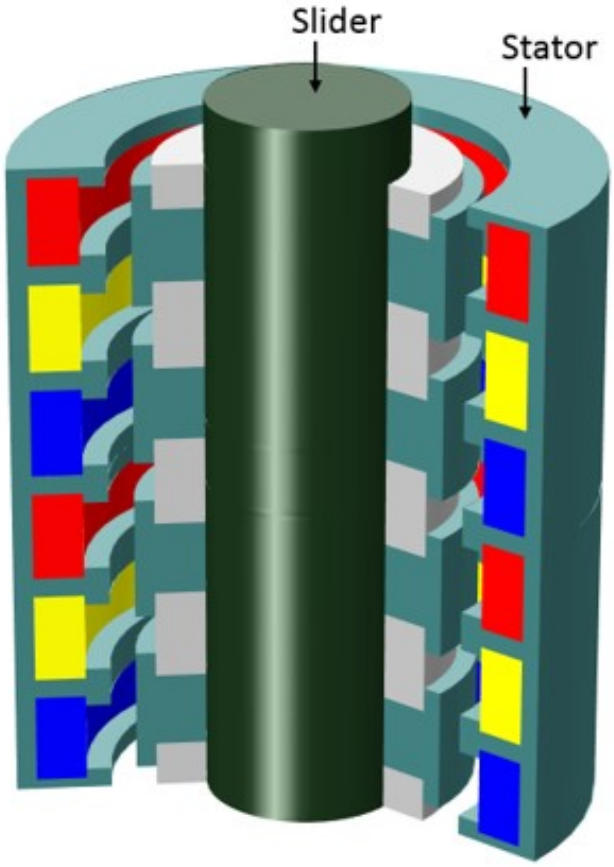

Figure 4.1: Linear Permanent Magnet Generator schematic, with the respective position of its stator and rotor highlighted

static gain is obtained as the result of a H_2- and H_∞- norm minimization of a suitable transfer function. The procedure in which the two proposed MIPC control strategies perform the power maximization is based on a causal assumption.

4.1.1 The Electromechanical Actuator

The control signal $f_c(t)$ consists of an electric current $i(t)$ produced by a power generator or Power-Take-Off, which must be carefully designed, in order to satisfy the constraints imposed by the controller.

For instance, if one wants to ensure a sufficiently long lifespan, it is crucial to prevent slamming and saturation. We consider a direct drive linear permanent magnet generator: it is simple and readily available. A schematic of the machine is given in Fig. 4.1. One of the main advantages of this kind of generators is that the use of magnets permits the avoidance of an excitation circuit.

Its governing equations are

$$\begin{aligned} \nu_a(t) &= R_a i(t) + L_a \frac{di(t)}{dt} + K_v \dot{z}(t) \\ f_c(t) &= K_v i(t) \end{aligned} \tag{4.1}$$

where $\nu_a(t)$ denotes the armature voltage, L_a, R_a and K_v are the inductance, resistance and force constant of the generator respectively. Following the notation in Chapter 2, $\dot{z}$ is the heave velocity, equal to the relative velocity between the stator and rotor.

A good choice is one that employs low currents and high voltages. Joule losses can be kept to a minimum and in turn good efficiency can be had. In other words an actuator with high force constant K_v and low resistance R_a is to be preferred. The generator's choice determines the control configuration. The constraints handling appears now very important.

4.1.2 Power Flow

The principles behind MIPC are found very attractive to the wave energy field. The idea behind MIPC is restated in this Chapter for the PA device, so that the control can be developed.

The electrical power P_e generated by the device is proportionally related to the mechanical power P_m as

$$P_e(t) = \nu_a(t) i(t) = \zeta P_m(t) \tag{4.2}$$

with ζ being the actuator efficiency. The mechanical power, is defined as

$$P_m(t) = f_c(t) \dot{z}(t). \tag{4.3}$$

When the motor acts as generator ($P_m > 0$), P_e is the useful power that can be harvested. On the contrary, when $P_m < 0$, P_e is the amount of power to be spent to produce P_m.

The power convention used throughout the Chapter is that $P_m > 0$ when it flows out of the system, while negative if it is flowing into the system. The same convention applies to all power quantities. Finally, the power dissipated for Joule effect is

$$P_d(t) = R_a i^2(t) \tag{4.4}$$

and this is the main contribution to the losses. It appears clearly now why it is important to keep the current low. Other contributions to the losses are neglected for simplicity.

The idea of MIPC is to consider the term P_s given by

$$P_s(t) = -f_e(t)\dot{z}(t) \tag{4.5}$$

(which is basically the power that the device exchanges with the impacting waves). Being $f_e(t)$ the wave excitation force, it follows that it is the only exogenous signal in the system (2.12). Hence, it is the only source of power to be harvested. Subsequently, in the above scenario, no power can be harvested if $f_e(t) = 0$. This is intuitive.

The following power balance holds

$$\dot{E}(t) = P_s(t) + P_m(t) \tag{4.6}$$

where $\dot{E}(t)$ represents the instantaneous power stored into or dissipated by the system.

One arrives with simplicity to

$$\dot{E}(t) = -f_e(t)\dot{z}(t) + f_c(t)\dot{z}(t). \tag{4.7}$$

This finally allows to draw out some conclusions that lead to the main principles behind MIPC:

- given that in the system there is no mechanical dissipative device such as a damper, and the signal $f_e(t)$ is bounded (and the system is asymptotically stable), if obtaining an ideal controller would be possible, both quantities $P_m(t)$ and $P_s(t)$ would be sign defined at all times. In particular

  $$P_m(t) >> 0, \quad P_s(t) << 0 \quad \text{and} \quad P_m(t) = -P_s(t).$$

  This would ensure that P_s is always large and flowing from the waves to the device whereas P_m is large as well and flowing from the actuator to the grid/battery. In other words, all the power induced would be harvested. This would also mean $\dot{E}(t) = P_s(t) + P_m(t) = 0$ so there is a perfect transfer of energy. In real situations, only approximations of the above situation are obviously possible.

- since $f_c(t)$ is a directly manipulable variable it is theoretically easy to make $P_m(t)$ sign-defined and as large as we desire, but this does not take into account the role of $P_s(t)$ and one arrives very quickly to the conclusion that, when we are working in the favorable situation of $P_m(t) > 0$ and $P_s(t) < 0$

  $$\int_0^T P_m(t)dt \leq \int_0^T \mid P_s(t) \mid dt \tag{4.8}$$

  and that (4.8) cannot be violated. Thus, this establishes a bound on the amount of electrical

energy $P_e(t) = \zeta P_m(t)$ that can be harvested and suggests that it might make no sense to synthesize control strategies that try to maximize $P_m(t)$ if $P_s(t)$ is small and there is no way to increase its amount any further.

4.1.3 The aim

Now, based on the considerations just made on the power flow, it could be convenient to optimize P_s as sign defined and large as desired regardless of P_m as $P_s(t) > 0$ at all times would provide a barrier for the internal potential energy from flowing back towards the waves. It would be enough to enforce the following ideal condition, which develops considering Eq. (4.5). We could state that if

$$\dot{z}(t) = -\mu f_e(t) \tag{4.9}$$

remained true at all time instants, then $P_s(t)$ would be negative sign-defined. That would lead to

$$P_s(t) = -\mu f_e(t)^2. \tag{4.10}$$

Therefore, the power coming from the waves would be flowing into the system at all times and it could be made as large as required by choosing suitable values for μ. In practice, this is obviously not possible as the current $i(t)$ would increase as well and this would make the Joule losses too large over a certain threshold, where the harvested energy would be reduced instead of increased further.

The parameter μ is indeed a key parameter that has to be tuned for the most convenient setup. We are going to show that, starting from zero, the electrical power output increases for increasing values of μ, but then as expected, the impact of the current in the losses becomes too large when μ goes over a threshold. The value for μ that maximizes the electrical power output P_e is found with the help of a bisection algorithm. Details on this choice will be given at the end of the Chapter. It is important for now just to qualify μ as a constant. This allows the implementation of the controller to be causal, and the control optimization expressible as a LMI combination. The constant nature of μ results in a sub-optimal approximation of the known optimality condition for maximum power extraction, as fully later justified. But the benefits gained by this approximation in the control implementation are largely counterbalancing the marginal power reduction resulting from the approximation.

4.2 The Multiobjective H_2 and H_∞ Control Design

Now, we are able to show how an H_2 and H_∞ control design approach is able to cast into a (possibly) multi-objective framework, this energy harvesting objective discussed this far. We introduce the following performance output

$$z_o(t) = \dot{z}(t) + \mu f_e(t). \tag{4.11}$$

given that it is simply not possible to find a dynamics for z such as Eq.(4.9) is perfectly satisfied.

The energy harvesting goal is precisely that of minimizing z_o. This objective is pursued as a H_2 and H_∞ norm minimization of the transfer function (with s as Laplace variable) built between the output $z_o(t)$ and the input $f_e(t)$. It can be stated that, by minimizing the H_2 and H_∞ norms of such transfer function, the energy/power of $z_o(t)$ is minimized as well, provided that $f_e(t)$ has finite energy.

4.2.1 The Augmented System

To express the control requirements as LMIs, needed for the optimization, the system (2.12) is first reformulated by the input $f_c(t)$ with $i(t)$ as control variable

$$\begin{aligned} \dot{x}(t) &= Ax(t) + Bi(t) + Ef_e(t) \\ y(t) &= Cx(t). \end{aligned} \tag{4.12}$$

With the definitions given in Chapter 2, the matrices in Eq. (4.12) are redefined as $A = A_w$, $B = B_w$, $E = E_w$, $C = C_w$.

The objective in (4.11) also can be re-stated in matrix form as

$$z_o(t) = Cx(t) + Di(t) + Ff_e(t) \tag{4.13}$$

where

$$C = \begin{bmatrix} \mathbf{0}_{1\times 5} & 1 \end{bmatrix}, \quad D = 0, \quad F = \mu \ . \tag{4.14}$$

The present matrix formulation, as it could be observed now, would make it very easy to add parallel objectives in the vector z_o, which now includes only the one which implies power maximization, following the guidelines of MIPC. The multi-objective capabilities of the controller are yet to be fully explored.

The inclusion of hard constraints is done with considerations that are clarified in the following sections.

In the development of this kind of controllers (H_2 and H_∞ norm minimization based), it is good practice to add a filter for the input f_e with the aim of localizing the energy of the disturbance on specific frequency bands. Adding such filters helps to localize the effort of the actuator in the optimization process. Such filter W_d is usually chosen as a low-pass filter, to damp out any undesired high frequency component, most likely originated by system/optimization inaccuracies. Mathematically this is done by augmenting the state space, i.e. extending x_o to

$$x_g = \begin{bmatrix} x & x_d \end{bmatrix} \tag{4.15}$$

where $x_g(t) \in \mathbb{R}^{n_g}$ is the redefined WEC state, which includes the state x_d of the filter W_d.

With the addition of the filter to the state-space formulation, the plant P results as

$$P : \begin{cases} \dot{x}_g(t) &= A_g x_g(t) + B_{g2} i(t) + B_{g1} f_e(t) \\ z_o(t) &= C_{g1} x_g(t) + D_{g12} i(t) + D_{g11} f_e(t) \\ z_C(t) &= C_{gC} x_g(t) + D_{gC2} i(t) \end{cases} \tag{4.16}$$

This brings in the need to redefine the system matrices accordingly, given below. In addition, the vector of constrained outputs is added.

- $\{i(t), z_o(t)\} \in \mathbb{R}^{n_{p1}}$ are the port variables of the PTO. The current $i(t)$ is the variable that can be controlled directly, while $z_o(t)$ is the variable that responds to that control action. n_{p1} is the number of ports.
- $z_C(t) \in \mathbb{R}^{n_{p2}}$ is the vector of constrained outputs, i.e.

$$|z_i(t)| \leq z_{i,max}, i = 1, 2, ..., p_2 - 1, t \geq 0, \tag{4.17a}$$

$$|i(t)| \leq i_{max}, \quad t \geq 0 \tag{4.17b}$$

with $z_{i,max}$ and i_{max} imposed limits on state and input current.

In particular,

$$\begin{gathered} A_g = \begin{bmatrix} A & EC_d \\ \mathbf{0}_{1\times 6} & A_d \end{bmatrix}, \quad B_{g1} = \begin{bmatrix} ED_d \\ B_d \end{bmatrix}, \\ B_{g2} = \begin{bmatrix} B \\ 0 \end{bmatrix}, \quad C_{g1} = \begin{bmatrix} C & FC_d \end{bmatrix}, \\ D_{g11} = FD_d, \quad D_{g12} = D \end{gathered} \tag{4.18}$$

with A_d, B_d, C_d, D_d being the minimal state-space realization of the filter W_d. Also, from Eq.

(4.17), matrices D_{gC2} and C_{gC} are

$$D_{gC2} = \begin{bmatrix} 0 \\ 0 \\ 1 \end{bmatrix}, C_{gC} = \begin{bmatrix} \mathbf{0}_{1\times 4} & 1 & 0 & 0 & 0 \\ \mathbf{0}_{1\times 4} & 0 & 1 & 0 & 0 \\ \mathbf{0}_{1\times 4} & 0 & 0 & 0 & 0 \end{bmatrix}$$

Their application is clarified within the next section, where the optimization routine is formulated for the computation of the controller gain.

The next section clarifies the procedure for the inclusion of the hard constraints in the H_2 case and H_∞ case.

4.2.2 Constrained State H_2 $(S - H_\infty)$ Control

Based on the overall plant P, now it follows the procedure for the full-state H_2 controller design. This means that it is assumed that all the state variables are available for feedback. In other words, the law

$$i(t) = K_2 x_g(t) \tag{4.19}$$

is to be enforced, where $K_2 \in \mathbb{R}^{n_{p1}\times n_g}$ is the H_2 optimal state feedback controller gain.

By substituting the state feedback control law (4.19) in the open loop plant P we obtain

$$\begin{cases} \dot{x}_g(t) &= (A_g + B_{g2}K_2)x_g(t) + B_{g1}f_e(t) \\ z_o(t) &= (C_{g1} + D_{g12}K_2)x_g(t) + D_{g11}f_e(t) \\ z_C(t) &= (C_{gC} + D_{gC2}K_2)x_g(t)\ . \end{cases} \tag{4.20}$$

Based on the plant, the control design consists in the minimization of the H_2 norm of the following transfer function (between the performance output z_o and the uncontrolled input f_e)

$$W_{z_o f_e}(s) = (C_{g1} + D_{g12}K_2)(sI - A_g - B_{g2}K_2)^{-1}B_{g1} + D_{g11}. \tag{4.21}$$

This means that, for a given $\gamma > 0$, the necessary and sufficient conditions for the existence of such a feedback law Eq. (4.19), which guarantees internal stability and the H_2 norm from the disturbance f_e to the performance output z_o less than γ, are equivalent to the conditions for existence of matrices $X = X^T > 0$, Y and W that satisfy the following LMIs

$$\begin{bmatrix} A_c + A_c^T & B_{g1} \\ B_{g1}^T & -I \end{bmatrix} < 0, \quad \begin{bmatrix} X & (C_{g1}X + D_{g12}Y)^T \\ C_{g1}X + D_{g12}Y & W \end{bmatrix} > 0, \quad Tr(W) \leq \gamma \tag{4.22}$$

with $A_c = A_g X + B_{g2} Y$. If solvable, the state feedback will be given by $K_2 = Y X^{-1}$.

Now, for the inclusion of constraints, defining the matrix $Q = X^{-1}$, with a quadratic storage function as $V(x_g) = x_g^T Q x_g$ we can show that the feasibility of (4.22) guarantees that the closed-loop system (4.20) is asymptotically stable and that $\frac{d}{dt}V(x_g(t)) - \|f_e(t)\|^2 < 0$ which after integration [129] leads to

$$V(x_g(t)) - V(x_g(0)) < \int_0^t \|f_e(t)\|^2 d\tau. \tag{4.23}$$

In addition, the assumption of bounded disturbance energy gives

$$V(x_g(t)) \leq V(x_g(0)) + \int_0^t \|f_e(t)\|^2 d\tau \leq V(x_g(0)) + f_{e,max} \tag{4.24}$$

for any $t > 0$. This implies that the closed loop trajectory stays in an ellipsoid defined by

$$\Omega(Q, \kappa) := \{x_g \in \mathbb{R}^{n_g} | V(x_g) \leq \kappa\} \tag{4.25}$$

with $\kappa := f_{e,max} + V(x_g(0))$. In order to cast the time-domain constraints in (4.17) as LMIs, we can say that the ellipsoid $\Omega(Q, \kappa)$ contains the set of all reachable states for the closed-loop system with disturbances whose energy is bounded by $f_{e,max} := \kappa$ ($V(x_g(0)) = 0$ is assumed). We can recall the result from [94] and state that

$$\begin{aligned}
\max_{t\geq 0} |i(t)|^2 &= \max_{t\geq 0} |(Y X^{-1}) x_g(t)|^2 \\
&\leq \max_{x_g \in \Omega} |(Y X^{-1}) x_g|^2 \leq \kappa \left\| (Y X^{-\frac{1}{2}}) \right\|_2^2, \\
\max_{t\geq 0} |z_{Ci}(t)|^2 &= \max_{t\geq 0} |(C_{gC} + D_{gC2} Y X^{-1})_i x_g(t)|^2 \\
&\leq \max_{x_g \in \Omega} |(C_{gC} + D_{gC2} Y X^{1})_i x_g|^2 \\
&\leq \kappa \left\| ((C_{gC} X + D_{gC2} Y) X^{-\frac{1}{2}})_i \right\|_2^2,
\end{aligned} \tag{4.26}$$

where the Cauchy-Schwarz inequality is used. Then, if the matrices X and Y furthermore satisfy that

$$\begin{aligned}
\begin{bmatrix} \frac{1}{\kappa} Z & Y \\ Y^T & X \end{bmatrix} \geq 0, \text{with} \quad Z \leq i_{max}^2 \\
\begin{bmatrix} \frac{1}{\kappa} N & C_{gC} + D_{gC2} Y \\ \star & X \end{bmatrix} \geq 0, \text{with} \quad N_{ii} \leq z_{i,max}^2
\end{aligned} \tag{4.27}$$

for some symmetric matrices Z and N, then the constraints are satisfied. Ultimately, the solution of the following semi-definite programming

$$\min_{X=X^T, Y, Z=Z^T, N=N^T, \gamma} \gamma \quad \text{s.t. LMIs in (4.27) and (4.22)} \tag{4.28}$$

guarantees all the previous assumptions. By using the YALMIP parser [130] and the SeDuMi [131] solver, the full state-feedback control gain K_2 is computed offline.

4.2.3 Constrained State H_∞ $(S - H_\infty)$ Control

When it concerns the development of the H_∞ controller, the procedure follows the same logical steps in the previous section, but the LMIs specified will be different.

So, still referring to plant P, the feedback law will be equivalent

$$i(t) = K_\infty x_g(t) \tag{4.29}$$

where again, $K_\infty \in \mathbb{R}^{n_{p1} \times n_g}$ is the H_∞ optimal state feedback gain. The minimization of the transfer function in (4.21) will now refer to its H_∞ norm. For a given $\gamma > 0$, the necessary and sufficient conditions for the existence of such feedback law, guaranteeing hence internal stability and indeed the H_∞ norm from the disturbance f_e to the performance output z_o less than γ are equivalent to the existence of matrices $Q^T = Q > 0$ and Y satisfying

$$\begin{bmatrix} A_c + A_c^T & B_{g1} & (C_{g1}X + D_{g12}Y)^T \\ \star & -\gamma I & D_{g11}^T \\ \star & \star & -\gamma I \end{bmatrix} < 0 \tag{4.30}$$

where $\star$ represents the transpose of the element across the diagonal. See Appendix C for more information on the LMIs specific of these norms. The feedback gain is defined by $K_\infty := YP$ with P of analogous meaning to the previous section. The LMIs referred to the inclusion of hard constraints repeat from paragraph 4.2.2.

So eventually the solution will be given by the following semi-definite programming minimization

$$\min_{X=X^T, Y, Z=Z^T, N=N^T, \gamma} \gamma \quad \text{s.t LMIs in (4.30) and (4.27)} \tag{4.31}$$

given that it is convex and numerically tractable. If solvable, the state feedback gain is given by $K_\infty = YX^{-1}$.

Now, before discussing the numerical results of the Chapter, in the next section the details over

the implementation of the LQ control are given, so that the comparison is fully defined, and the meaning of the numerical results is clarified.

4.3 Linear Quadratic Control

As stated, given its popularity in many different engineering fields and being perhaps the closest relative to H_2 control, one of the most logical comparisons as an optimal strategy written in state-feedback form is the LQ control.

As the name suggests, Linear Quadratic control is applied to linear systems or to systems that can be approximated as linear under some assumptions. The quadratic objective function can be re-formulated to accommodate different needs, but it is not suitable neither for multi-objective optimization nor to accommodate hard constraints. So, besides being optimal, a cautious tuning has to be considered in real applications given that there is no guarantee that the variables will operate in delimited region.

The LQ control is going to directly maximize the power in its objective function, as in [132] and as previously seen in Chapter 2. The work by [133] applies the function to a single generator configuration as in the present case. This is taken as reference for the present development. The only difference is that here no observer is used to allow the comparison with the proposed state feedback controller.

The strategy is sea state dependent (its optimal tuning will change when the sea condition change), if the system in (2.12) describing the heave dynamics, is augmented with (2.10) which describes the wave elevation-to-excitation force causal model. This means that when the sea state changes the configuration chosen for the controller will no longer be optimal and a new configuration should be find and studied for the controller to work at its best. This is not very convenient in an environment where every few hours or sometimes shorter, new sea conditions occur and a re-computation is needed.

From a practical development, the overall system (4.12) and the excitation force subsystem (2.10) are cast together so that LQ optimizes on the sea properties as well.

The two systems are cast together as

$$A_a = \begin{bmatrix} A & BC_e \\ \mathbf{0} & A_e \end{bmatrix} \quad B_a = \begin{bmatrix} B \\ \mathbf{0} \end{bmatrix} \quad E_a = \begin{bmatrix} \mathbf{0} \\ B_e \end{bmatrix} \tag{4.32}$$

which results in

$$\dot{x}_a(t) = A_a x_a(t) + B_a i(t) + E_a \eta(t) \tag{4.33}$$

where $x_a(t)$ is the augmented state including the excitation substates. The controlled input vector

is once again the current $i(t)$.

The control input $i(t)$ is determined by finding a feedback matrix K_{LQ} such that

$$i(t) = K_{LQ} x_a(t), \tag{4.34}$$

in a form analogous to Eq. (4.19). K_{LQ} is determined by solving the Algebraic Riccati Equation (expressed later in (4.38)) associated with the problem.

We must now recall the role the electrical power P_e, to subsequently identify our objective function

$$J = \varepsilon\{-P_e\} \tag{4.35}$$

where $\varepsilon\{\cdot\}$ is the expected value under stationary conditions.

To qualify as a LQ type of controller Eq. (4.35) must be written as quadratic function. Given the linear generator, the instantaneous electrical power $P_e(t)$ can be simplified as

$$-\nu_a i = -(\nu_{emf} + R_a i)i = -\nu_{emf} i - R_a i^2, \tag{4.36}$$

where ν_{emf} is the back electromotive force and ν_a is the output voltage.

The minimization problem can be then expressed

$$\min_i -\varepsilon[\nu_{emf}^T N_a i + i^T R_a i], \tag{4.37}$$

N_a being the cross coupled weighting matrix and R_a once again the generator resistance. State matrix $Q_a = 0$. We can observe the first term being obviously a power quantity, and the second directly related to the control input $i(t)$. The resistance R_a quantifies the weight on the current, and it is the only tool of this LQ formulation, in relation with the N_a quantity, that can limit or suppress the output. Unfortunately this does not directly guarantee that any state trajectory will be contained in any given limited variable space.

The quadratic formulation of the objective function and the linear model, implies that the symmetric matrix solution P_{LQ} to the algebraic Riccati equation associated with the infinite horizon problem

$$P_{LQ} A_a + A_a^T P_{LQ} - (P_{LQ} B_a + N_a) R_a^{-1} (B_a^T P_{LQ} + N_a^T) = 0 \tag{4.38}$$

and the gain $K_{LQ} = R_a^{-1} B_a^T P_{LQ}$, with P_{LQ} and K_{LQ} are both constant values.

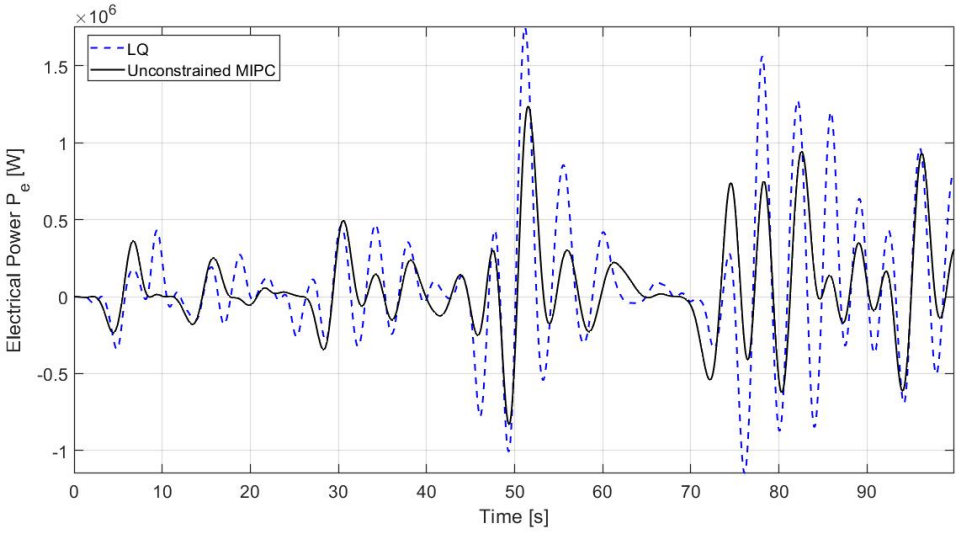

Figure 4.2: Intermediate sea state simulation with $H_s = 1.76$m and $T_o = 7.99$s (corresponding to LQ tuning). Comparison of electrical power output between unconstrained MIPC and LQ on 100s length simulation

4.4 Numerical Results

4.4.1 Comparison between $S - H_2$ and LQ

First, the results are given with the application of the $S - H_2$ control. An actual site was chosen to collect the data of the sea states simulated.

Unconstrained $S - H_2$ to LQ

Before going to fully assess the power performance of the constrained controller on the given scenario, since the present formulation of MIPC implies a suboptimal assumption, it is interesting to evaluate quantitatively the gap between the technique in absence of constraints and LQ, described in section 4.3. Mathematically, this corresponds to solving the LMI problem in Eq. (4.28) without the conditions in Eqs. (4.27). This comparison is limited to the controller $S - H_2$. For LQ, this means choosing the set of parameters which will maximize P_e compatibly with the physical limits, applying a trial and error approach, to identify the most convenient setup.

Simulations are run on a single sea-state of significant-wave height $H_s = 1.79$m and zero-crossing period $T_o = 7.99$s. The electrical instantaneous power comparison is plotted in Fig. 4.2.

As expected, LQ being optimal slightly exceeds $S - H_2$ in terms of power generated. The gap is indeed not found to be significant, given the mean power of 77.4 kW for $S - H_2$ and 89.3 kW for LQ, so just 13% larger.

For higher sea states, if considering the full constrained controller, the ability of $S - H_2$ (and $S - H_\infty$), by the tuning of κ (proportional to the energy of the input signal) the state trajectories are easily adjusted inside the prescribed limits, still aiming for the power maximization objsective,

while LQ fails to stay within the limits in such sea-states. For lower seas instead the tuning of κ leads to push the lowered performance towards higher energy, indirectly adjusting the tuning to the different states, which also LQ is incapable of doing.

Constrained Control Performance

In this section, we are going to evaluate and compare the performance of $S - H_2$ and LQ control. The theoretical development of the control is presented in Section 3.3 and it is applied to the device modelled in Chapter 2, section 2.1.1. The specific site conditions considered for power generation are introduced in subsection 4.4.1. Where limits are applied, the PTO force is bounded to $3MN$ (and subsequently the current limit is $\approx 3kA$), the PTO excursion is limited to $5m$ and the PTO velocity is limited to $5m/s$. The limits are based on typical estimates of PTO capabilities [134]. PTO efficiency is not considered in this work but it would be an interesting future addition.

A time span of $1000s$ is chosen for each simulation using irregular waves on wave period ranging between $5s-16s$ binned in six different classes, while wave heights range between $1m-6m$ classified in six classes as well. This makes up to a total of thirty-six sea state combinations for investigation.

An average power output with both the $S - H_2$ controller and the LQ controller is calculated for each wave height and period combination, and then given the probability distribution characteristics of the site, shown in Fig. 4.3, the total energy capture is determined as well. A comparison between the novel *state-feedback H_2 MIPC controller* with the LQ control described in subsection 4.3 is presented. We see from the results, how with the addition of the LMIs in Eq.(4.17) to the optimization problem, hard constraints are accounted for, and the power is maximized in a highly varying sea state scenario. With the proposed control, saturation is also fully avoided, given that the trajectories of the states are meant to be contained within the defined ellipsoid (Eq. 4.25). Only in case of unpredictable extreme events, the states might reach such conditions, which will however, be rare. With an appropriate tuning, it is possible to push the operational region of the device to harness the highest power feasible, outperforming the unconstrained controller LQ, guaranteeing that all the variables are within the acceptable range at all times.

Site conditions

When designing a controller for a WEC it is fundamental to consider the site conditions where the device is going to be operational. In the present case, the site chosen is an area of the sea to the North West of Ireland. Data is collected over a period of six months between May and November 2020. The data is taken from official measurements [135]. Among all sea conditions, an operational region has been highlighted. Only within that region (shown in Fig. 4.3 with a black rectangle), the device is supposed to be harnessing power. Therefore, those will be the sea state combinations

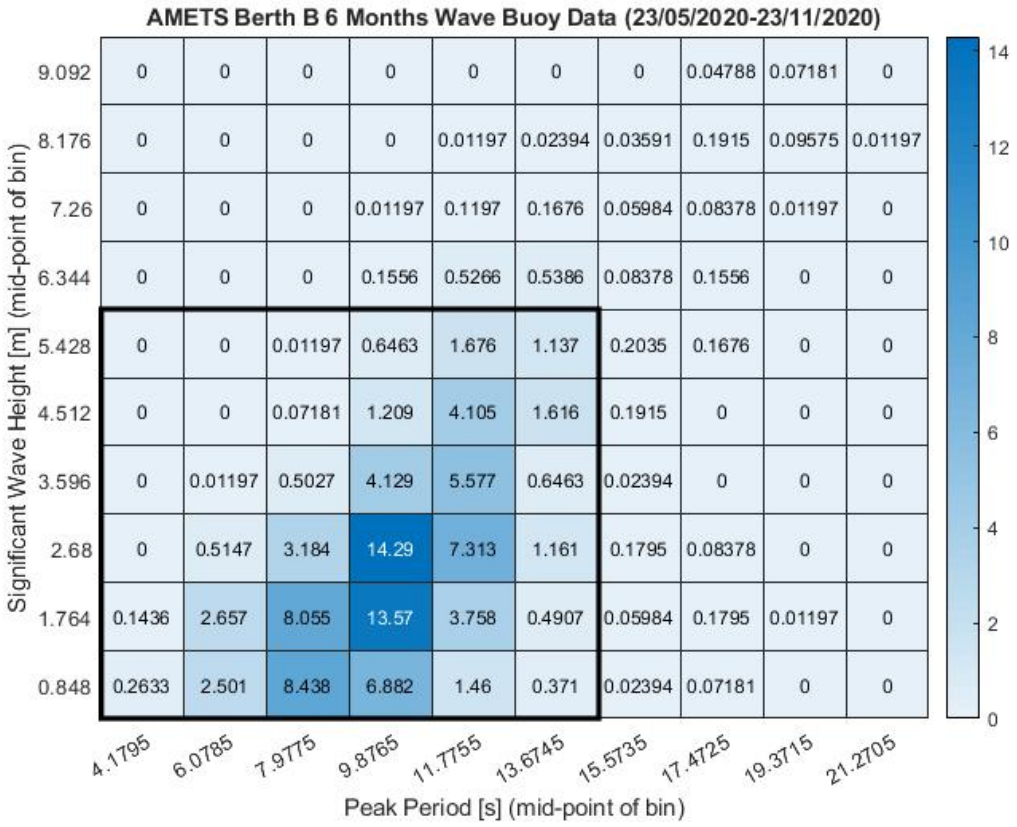

Figure 4.3: Probability (%) of sea conditions for the chosen site. The operational conditions are highlighted in the black box and encompass 90.24% of the conditions (data from AMETS Berth B Wave Buoy offshore north west coast of Ireland).

that are simulated.

Comparison of Average Power Capture

The average power harnessed (energy divided by simulation time) is shown in Fig. 4.4. The first thing that we can observe is that the LQ controller slightly outperforms the novel $S - H_2$ control in some cases relative to low-to-medium sea states. This is due to the fact that LQ does not rely on a suboptimal assumption, and it is exactly tuned for an intermediate (nominal) sea state ($H_s = 1.76m$ and $T_p = 7.99s$). The simulations are then repeated for LQ with the same tuning for all the other sea states. This results in an under-performance for the sea state combinations lower than the nominal, and it leads also to possibly too large excursions for sea state combinations which are higher then the nominal one. Highlighted in black, we can already observe where the LQ control fails to keep the variables within boundaries, and this is for a substantial portion of the simulations.

With the $S - H_2$ control instead, when the sea states become larger, constraints get activated and prevent the quantities of interest to go out of the boundaries. Associated to each of the sea-states, the value of κ also guarantees that while the constraints get activated, the problem is still

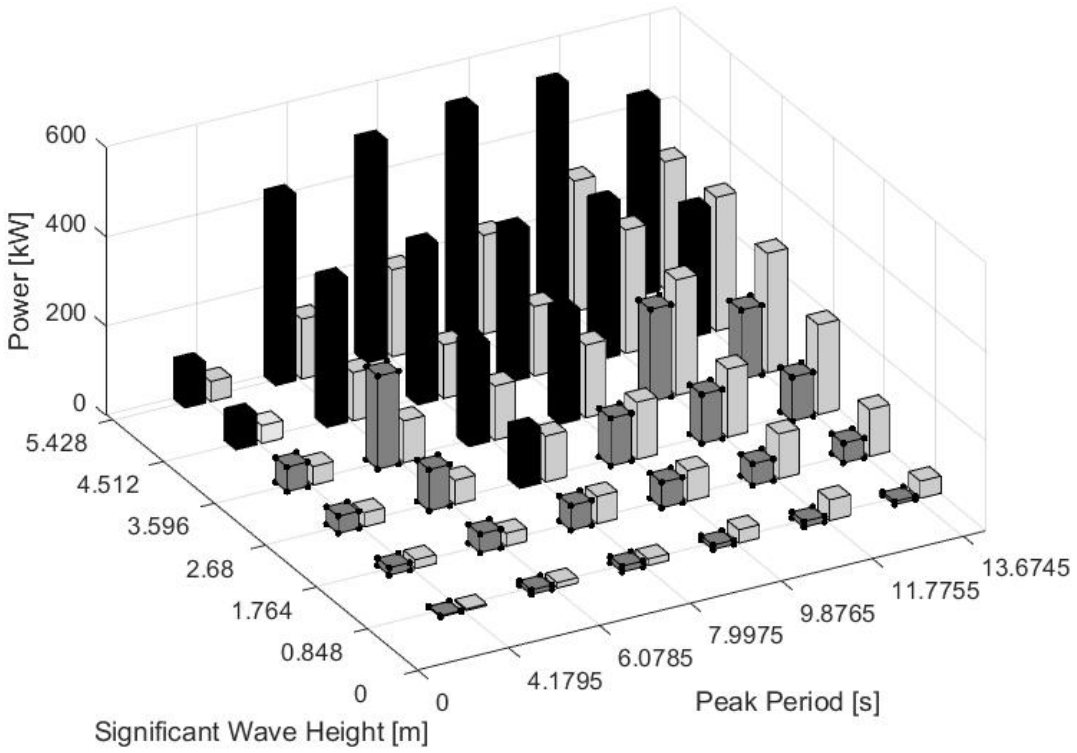

Figure 4.4: Average Power for each wave height and period combination given the two strategies: in dark grey (LQ), in light grey (Constrained $S-H_2$). Highlighted in black the sea state combinations where LQ fails to be applicable because of a constraint breach.

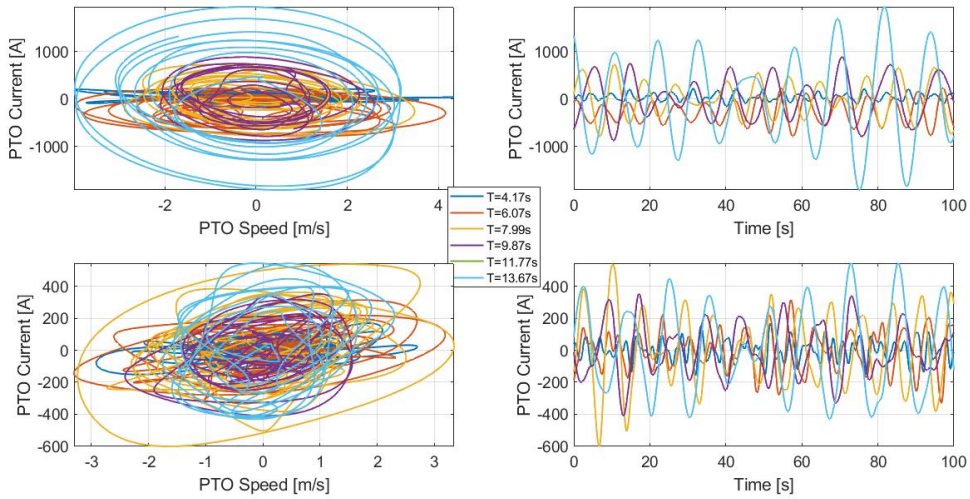

Figure 4.5: PTO current in 1.76m waves

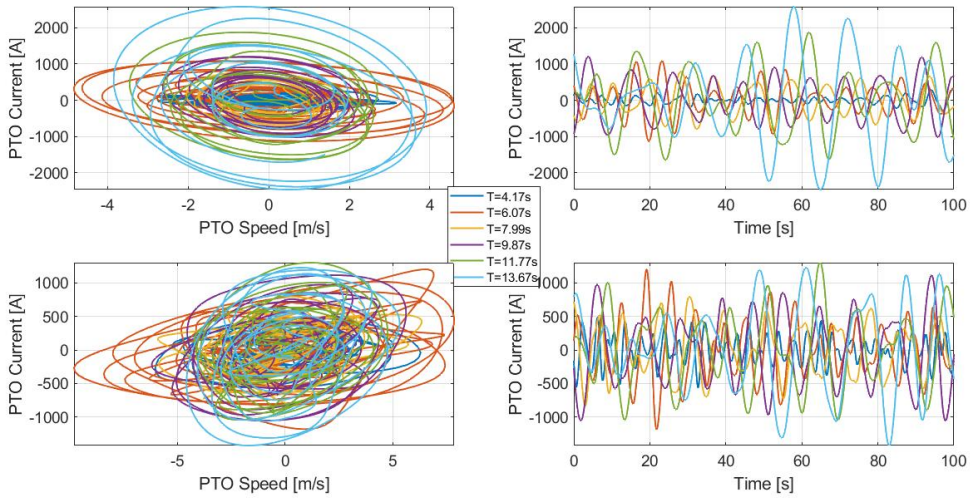

Figure 4.6: PTO current in 4.51m waves

Figure 4.7: PTO current and PTO speed. In each sub-figure the left hand side shows the PTO force against the PTO speed for the constrained $S - H_2$ (top plot) control and the LQ control (bottom plot). The right hand side shows the time series for the PTO current. Sampled at intervals of 0.1s, between simulation time $t_1 = 900s$ to $t_2 = 1000s$.

solved for maximizing power performance. In Table 4.2 all values of κ are listed with each of the sea states simulated. If no constraints are built-in within the formulation, all variables are virtually allowed to fluctuate with no restrictions; and as we can see with LQ this can result in infeasible conditions for the real case scenarios, and it is subsequently not applicable. The cases where the limits are exceeded cannot be taken into account for the calculation of the total harnessed energy.

In Fig. 4.4 the combinations where the LQ control fails to keep the device within boundaries are highlighted in black - as observed, in almost half of the cases with the LQ control, at least one constraint is breached, may that be the current, the velocity, the vertical excursion or all of

	Zero Crossing Period [s]					
SWH* [m]	4.179	6.078	7.997	9.876	11.775	13.674
0.848	1	1	1	1	1	1
1.764	1	1	1	1	1	1
2.68	1	$1.2 \cdot 10^4$	$2.0 \cdot 10^4$	$2.5 \cdot 10^4$	$2.5 \cdot 10^4$	$3.0 \cdot 10^4$
3.596	1	$2.5 \cdot 10^4$	$3.0 \cdot 10^4$	$3 \cdot 10^4$	$3 \cdot 10^4$	$3.0 \cdot 10^4$
4.512	$1.0 \cdot 10^4$	$3.0 \cdot 10^4$	$3.5 \cdot 10^4$	$4.2 \cdot 10^4$	$4.0 \cdot 10^4$	$4.0 \cdot 10^4$
5.428	$1.2 \cdot 10^4$	$3.5 \cdot 10^4$	$4.0 \cdot 10^4$	$4.2 \cdot 10^4$	$4.25 \cdot 10^4$	$4.25 \cdot 10^4$

Table 4.2: Values of κ relative to the simulated sea states. *SWH=Significant Wave Height

them together. On the contrary, the proposed $S-H_2$ controller is able to maintain the trajectories within the given boundaries, for all of the cases.

Assuming that the wave climate is like it appears on the scatter diagram of Fig. 4.3 and the WEC is operated in the outlined region (in black border), the $S-H_2$ shows a 45% increase in harnessed energy as compared to what is available using LQ control, and this is due to the non-negligible portion of cases where the power is not accountable for LQ. The LQ control tuning is chosen with $N_a = \begin{bmatrix} 0 & 0 & 0 & 0 & -K_v & 0 \end{bmatrix}$ and $R_a = 0.05\Omega$, with $K_v = 938N/A$ (see [133]). A different tuning of N_a could have been evaluated, but it is likely that it would have shown less violation of the limits in high seas but with at the same time a decreased power capture in lower seas, hence not justifying the choice and still largely under-performing compared to the proposed constrained $S-H_2$. Also, a broader distribution of wave periods would probably see an even greater benefit in the use of the $S-H_2$ controller as the performance would be guaranteed independently of how close to the resonance the device operates.

Comparison of Currents

Plots of the PTO currents against PTO speed, and PTO current against time with a wave height of $1.76m$ are shown in Fig. 4.5; and with a wave height of $4.51m$ in Fig. 4.6. It is clear that the limits are never reached with the constrained controller, whereas the LQ control fails to keep the PTO speed within the limit for large waves, as anticipated. For both the controllers, we can see that the relationship between the current and the velocity is far from linear, as it would be expected. Saturation conditions are shown to be fully avoided with $S-H_2$, given a correct tuning of κ. We can observe that the magnitudes of the currents are slightly higher when larger waves occur, but the PTO forces are still contained within the $3kN$ limit.

4.4.2 Comparison between $S-H_\infty$ and LQ

With the same approach as the comparison between $S-H_2$ and LQ was made in the previous paragraphs, we are hereby going to illustrate the numerical results of the comparison on the $S-H_\infty$ control instead.

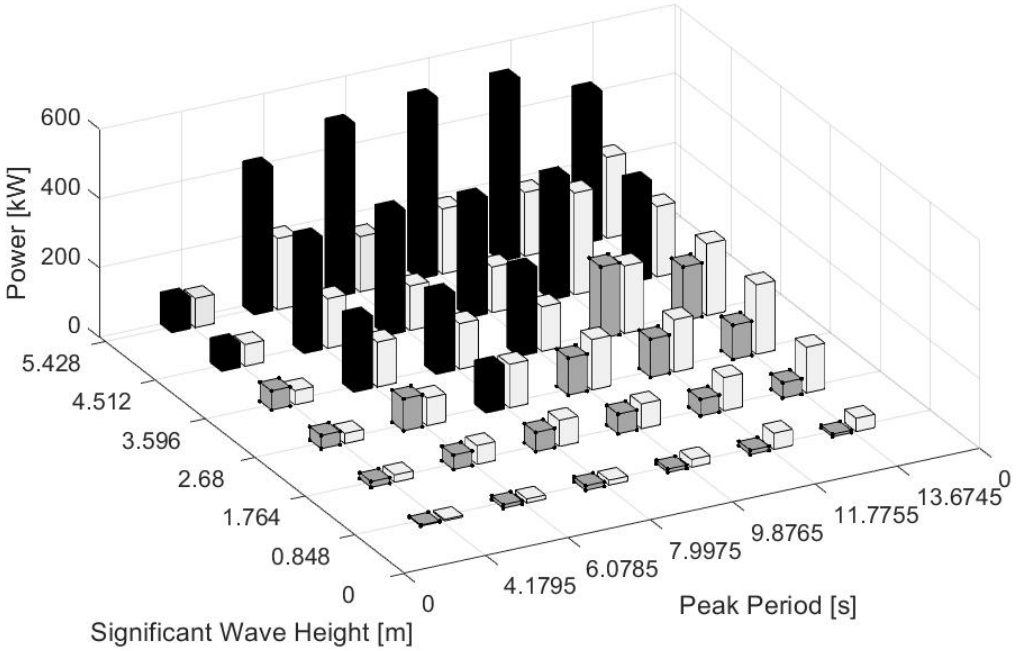

Figure 4.8: Average Power for each wave height and period combination given the two strategies: in dark grey (LQ), in light grey (Constrained $S-H_\infty$). Highlighted in black the sea state combinations where LQ fails to be applicable because of a constraint breach.

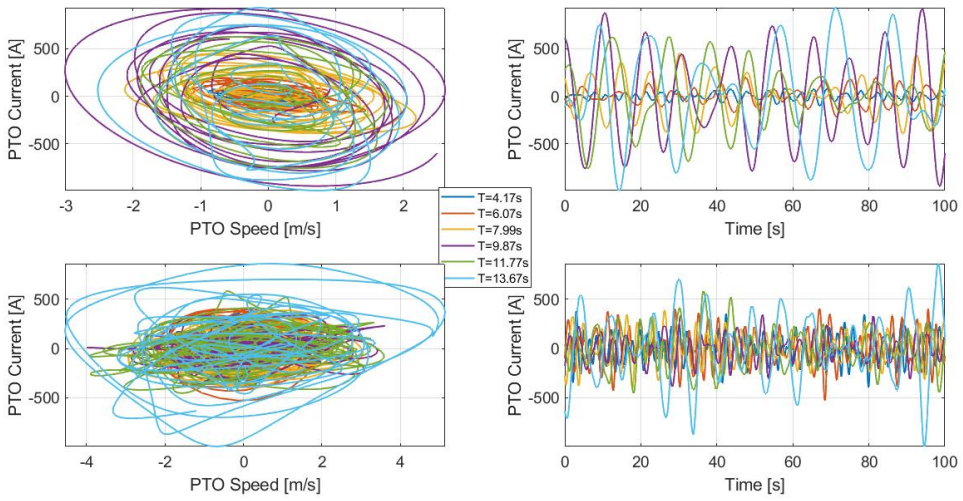

Figure 4.9: On the left-hand side: PTO current vs PTO speed. On the right hand side: PTO current over simulation time. $S - H_\infty$ control (top) vs LQ control (bottom). Significant wave height $1.5m$.

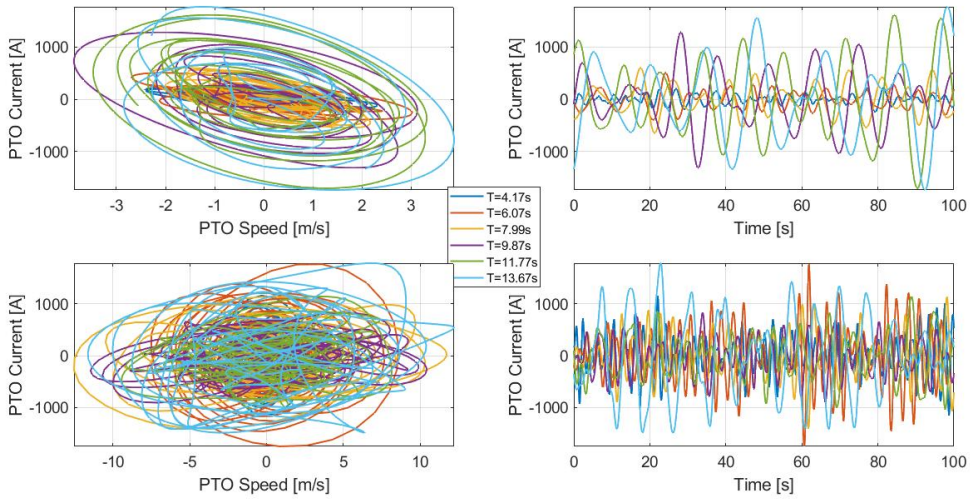

Figure 4.10: On the left-hand side: PTO current vs PTO speed. On the right hand side: PTO current over simulation time. $S - H_\infty$ control (top) vs LQ control (bottom). Significant wave height $4.5m$.

The theoretical approach linked to the results that follow is explained in section 4.2.3. Once again, the site conditions are the same of section 4.4.1 and the same are the operational sea states. Applied limits hold with the same values described, and once again a 1000 s time window for each simulation is chosen given the irregular waves ranging between $5s - 16s$ period and wave heights between $1m - 6m$.

So the average power for each sea state combination is calculated and plotted in Fig. 4.8. The probability distribution of each state characterizing the site (Fig. 4.3) allows to determine uniquely the average energy capture. Thanks to the added LMIs which account for the hard constraints (Eq. (4.27)), the power is maximized on a highly varying sea scenario and saturation is avoided. Table 4.2 summarizes the values of κ. The resulting states are fully contained in the defined ellipsoid with this method as well, as shown in the next paragraph.

Average Power Capture

For the controller just discussed, analogously to the $S-H_2$ the average power harnessed is computed for each sea state combination simulated. What is expected is that, given that LQ control is tuned for a particular sea state, the strategy is optimal for that sea state only and it would underperform on a wide portion of scenarios. As stated, this is due to the difficulty in tuning effectively LQ control for changing sea states. Moreover, the inability of LQ to consider constraints, does not guarantee that variables comply with the physical limitations. This results in a number of breaches which are already highlighted in the previous sections. So the power harnessed in those cases cannot be considered in the overall energy calculation. In Fig. 4.8 the comparison between $S - H_\infty$ and LQ is shown for each sea-state combination.

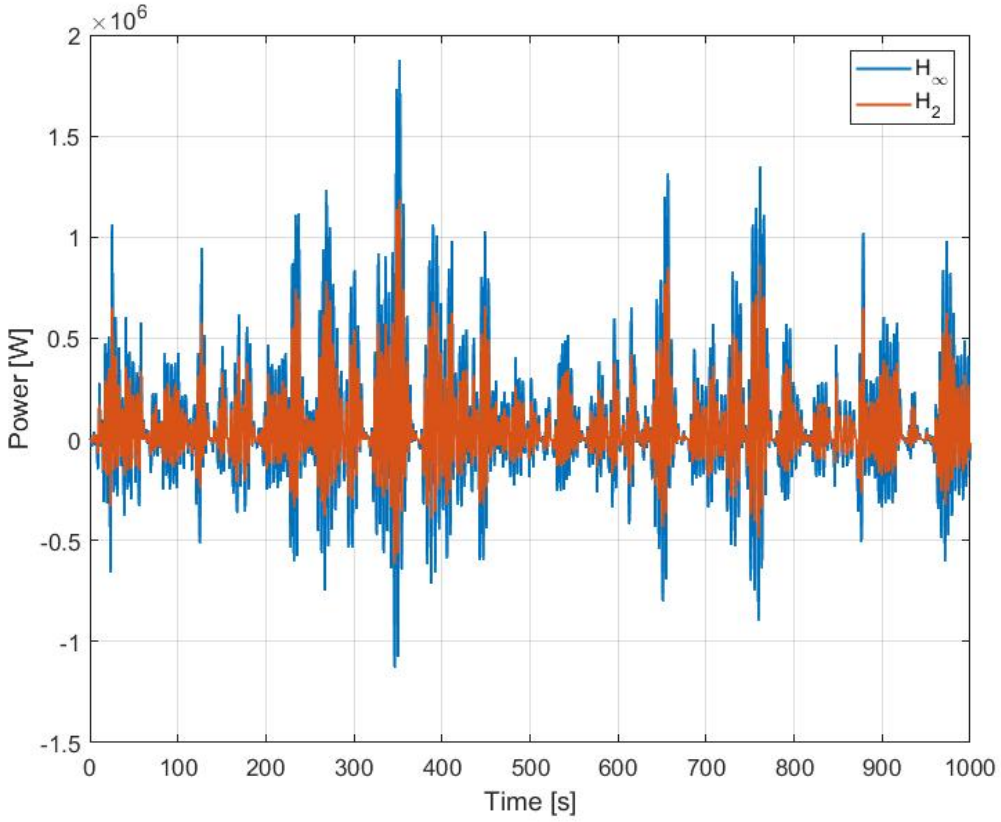

Figure 4.11: Electrical power P_e over time with the application of the two strategies $S-MIPC\ H_2$ and $S-MIPC\ H_\infty$ in an intermediate sea state defined by a significant wave height of $H_s = 1.76m$ and zero crossing period of $T_p = 7.99s$

Comparison of Currents

In this paragraph, comparisons between $S - H_\infty$ and LQ is given for what concerns the generator current $i(t)$. The relationship between $i(t)$ and the PTO speed $\dot{z}(t)$ is shown for two significant wave heights ($1.76m$ and $4.51m$). The time evolution of the current $i(t)$ is shown for the same range of cases as well. Once again, it is clear that the limits are never reached with the constrained controller and saturation is also avoided. We can also observe that currents are slightly reduced for $S - H_\infty$ compared to $S - H_2$. This could appear as counter-intuitive given that the power output sees larger excursions in H_∞. The reason is though that velocities are slightly higher (which is observed), still compatibly with constraints. What mentioned appears in Figs. 4.9 and 4.10

Comparison between H_2 and H_∞

$S - H_2$ or $S - H_\infty$ controllers merely differ on their LMI norm computation. How this effects the results is less predictable. It is observed that no substantial gain in the use of one or the other appears in power production, resulting in no outstanding gain of energy with either choice as well. A 42% energy gain is computed with $S - H_\infty$ with respect to LQ while $S - H_2$ registers a 45%.

When it comes to the instantaneous power over time (as for example the sea state simulated in Fig. 4.11), it appears that H_∞ has higher spikes and both the maximum and minimum peaks are further from the average than the $S - H_2$ case. This perhaps makes the strategy less attractive given that the generator is meant to handle the power excursions in both directions. Complications in finding suitable machinery is added, which is likely to drive costs up. The tuning of LQ control and the choices for κ are as described in subsection 4.4.1. In the author's opinion, $S - H_\infty$ does not present advantages over $S - H_2$

4.4.3 The choice of μ

We are going to conclude by explaining how the choice of μ as constant was made, and which physical consequences and meaning this has.

By looking at Eq. (4.9) and the overall plant in Eq. (4.12), it is clear how a constant expression for μ allows a neat LMI optimization. In [120], with a second order model reduction, it was found that the relationship obtained in optimal control theory, between the vertical velocity of a SDoF PA and the excitation force could be approximated with a frequency independent one, or namely a constant, for a relatively broad set of input frequencies, with little gap to optimal performance. With this in mind, an approach for a constant causal approximation to the "wave force-to-device velocity" relation, looked desirable. The electrical powert is indeed just a fraction of the harvested mechanical power P_m

$$P_e = P_m - P_d. \tag{4.39}$$

This means, that the losses P_d play a critical role. When μ increases, so does the mechanical power P_m but also the control current i. Given the quadratic dependency of P_d on the current, the electrical power results necessary reduced after a threshold (optimal value), as the losses will be grown way more than P_m does. Mathematically, on order to compute the optimal value of μ which maximizes the net electrical power P_e, on the assumption that one maximum in terms of average electrical power $\bar{P}_e$ does exist when varying μ from zero to infinity, it is found convenient to employ the bisection method. The bisection algorithm is known to be able to find the roots of a continuous function for which one knows two values with opposite sign.

The function under investigation is the derivative $\frac{\partial P_e}{\partial \mu}$. So, starting from two limit cases with $\mu_1 = 0$ and $\mu_2 = 10$ (where the latter is found to be a reasonable upper limit given the physics of the problem), the following values of μ and $\frac{\partial P_e}{\partial \mu}$ are computed according to the signs of the derivative functions.

In Fig. 4.12, the quantity $\bar{P}_e$, or average electrical power, is plotted for increasing values of μ as a parameter. It is clear that a maximum value is found for $\mu \approx 0.005$. The harnessed energy

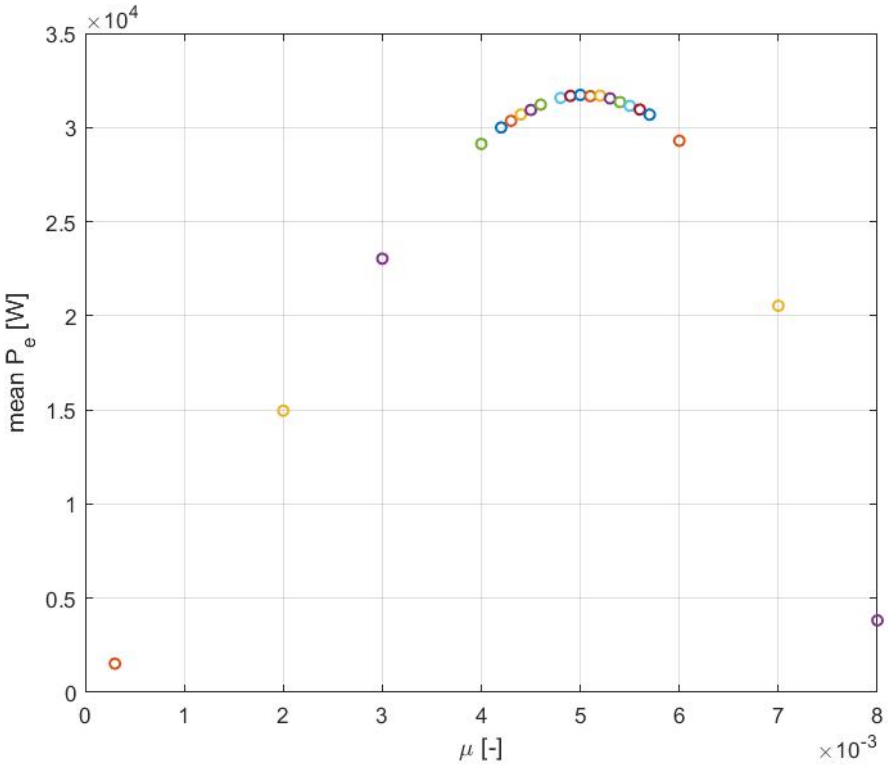

Figure 4.12: Electrical mean power for an intermediate sea state of Significant Wave Height $H_s = 1.76m$ and Zero Crossing Period $T_o = 7.99s$ with increasing values of μ. The problem reaches an optimum at about $\mu = 0.005$.

(Fig. 4.13) as μ increases, subsequently increases, but starts to be more and more bidirectional also, till the maximum is reached.

In fact, the choice of μ as constant is an approximation of a more complex condition, but the benefits given by this approximation leading to the simplicity of the formulation, fully justify it.

Alternative expressions for μ could logically then have been evaluated, but the added benefit when weighted against the complexity may not be worth the effort involved. A more rigorous proof to justify this statement is left out of the scope of the present work. However, as already pointed out, the choice of μ is motivated by the real time capabilities of the control technique, and it is chosen in such a way so as to keep the computational burden associated with the optimization algorithm to a minimum. The non-causalities resulting from more complicated expressions for μ also might result in an infeasible solution in terms of expressing the problem in a Linear Matrix Inequalities formulation, which is indeed crucial in the successful development of the controller.

4.5 Unconstrained $S - H_2$ vs Optimal

Before the concluding remarks, the comparison between unconstrained $S - H_2$ and the noncausal optimal controller in Appendix A is also given. $S - H_\infty$ is left out as similar conclusions can be

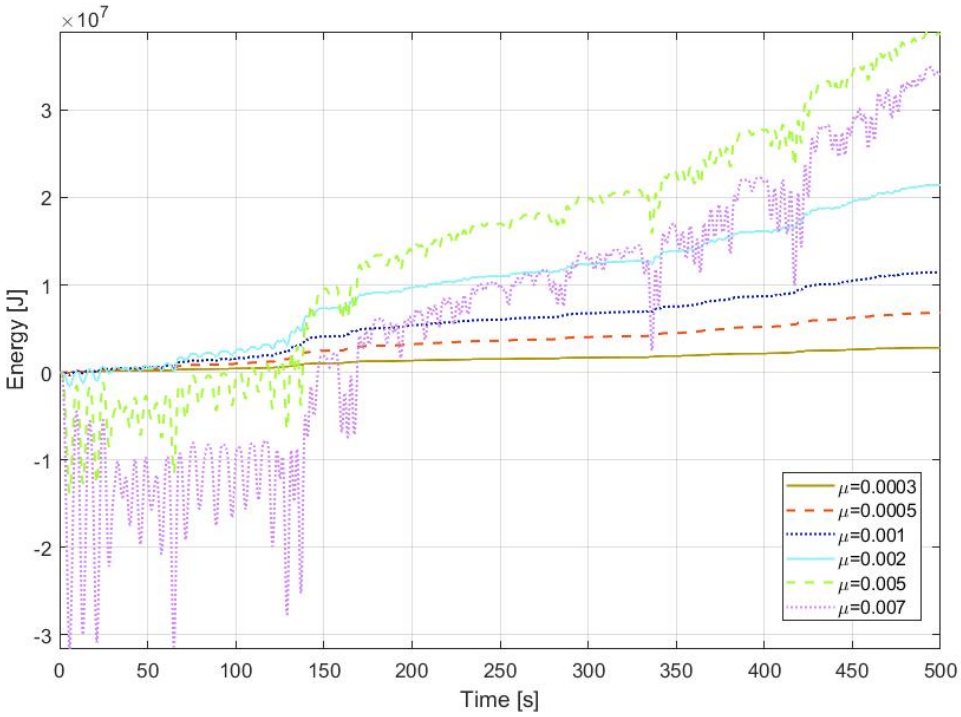

Figure 4.13: Electrical energy capture for an intermediate sea state of Significant Wave Height $H_s = 1.76m$ and Zero Crossing Period $T_o = 7.99s$ with increasing values of μ. The first $500s$ of the simulation are shown. The problem reaches an optimum at about $\mu = 0.005$.

drawn. This comparison is found of interest in order to evaluate the magnitude of the gap induced by the causal approximation in $S - H_2$.

The observed gap is more significant than the one observed in Section 4.4.1 as expected, given the causal nature of LQ. (see Fig. 4.14). Since a high sea is here simulated ($H_s = 4.51m$) the velocity excursion and generator's current are dragged to very high values and the need for constraints is apparent (Fig. 4.15).

4.6 Chapter conclusions

This Chapter tackles the problem of constrained power maximization on a WEC with two novel control strategies applied on a linear PA WEC. The control strategies are built, in order to optimize the performance on a highly varying sea environment while facing physical constraints. The controls are H_2-based and H_∞-based full state feedback schemes. The power objective is inspired by the MIPC concepts. Hard constraints are incorporated in the control formulation and solved by transforming the problem into a LMI setting. One first advantage is immediately seen, as the control architecture is causal and fully implementable offline. The second and most relevant advantage is seen when running the simulations: the strategies are always capable of maximizing the power while the physical limitations are respected, despite the changing sea conditions. This

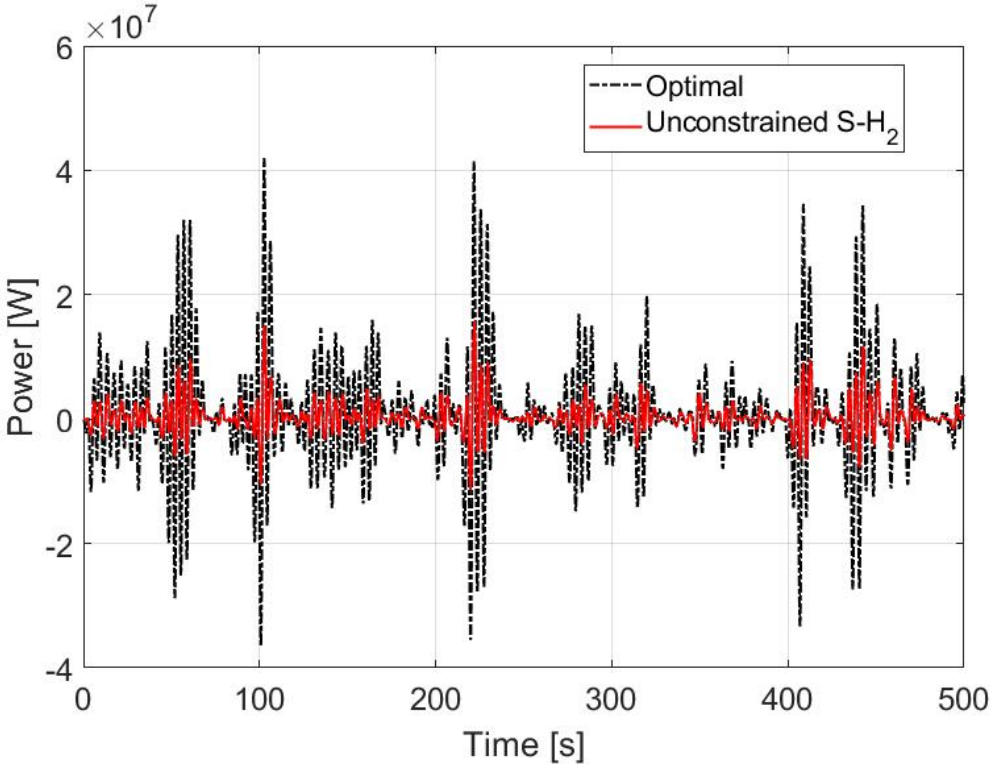

Figure 4.14: Unconstrained $S - H_2$ vs Optimal (power)

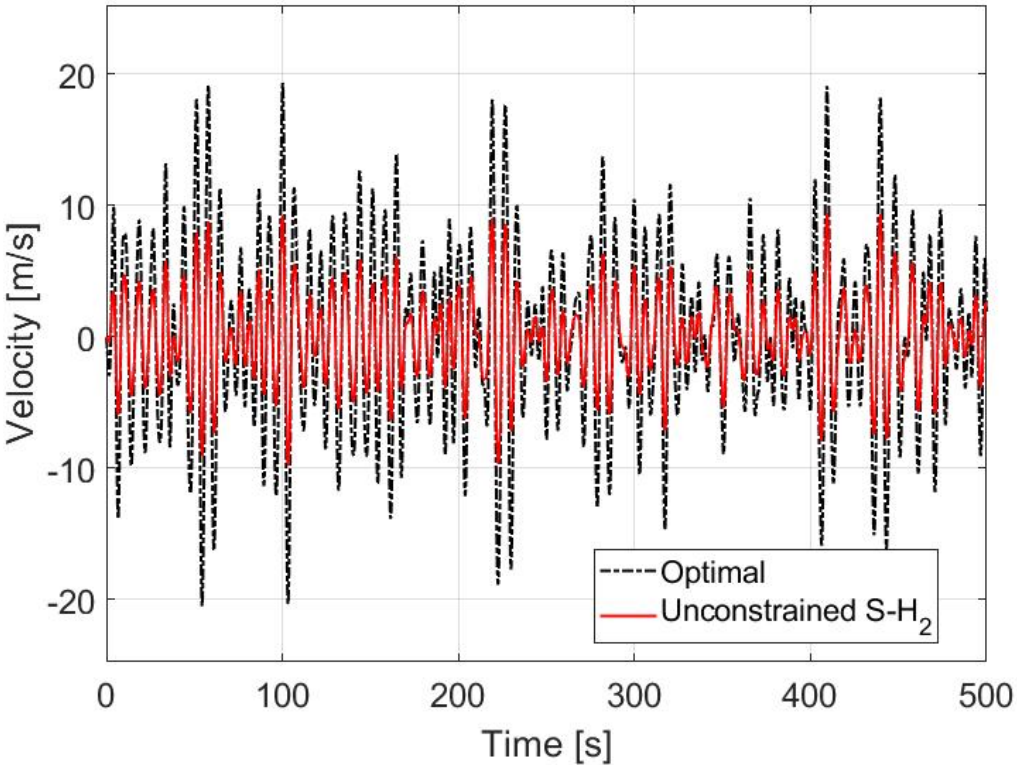

Figure 4.15: Unconstrained $S - H_2$ vs Optimal (velocities)

is done simply by adjusting a tuning parameter proportional to the energy of the input. The result is a dramatic boost of energy if a comparison is made with a strategy that does not take constraints into account. An immediate comparison was done with LQ control: its inability to be tuned efficiently and to tackle hard constraints brought the proposed $S - H_2$ and $S - H_\infty$ schemes to harness up to 45% more energy. The $S - H_2$ and $S - H_\infty$ controls are also able to cast multiple objectives in their formulation, given the LMI representation, without significant added computational burden. The numerical evaluation of this statement is left for future work. Differences between the performance $S - H_2$ and $S - H_\infty$ are not seen to be particularly relevant. To be noticed though, power variation with $S - H_\infty$ control appears poorer given a higher ratio between peak power and average power output. On the other hand, it generates a slightly higher mean power. So, the one to be preferred for applications, will depend on the actual PTO machinery in use.

Chapter 5

Observer-based Constrained Maximum Induced Power H_2- H_∞ Control

The state feedback nature of controllers in this thesis so far relies on the assumption of fully known state vectors. This assumption applies to all the formulation in the previous Chapters (from Chapter 2 to Chapter 4). In this Chapter an iterative LMI-based procedure, is used to find solutions to the BMI formulations with an appropriate algorithm. The results are verified on the same model of WEC in Chapter 4. Results are shown both for the H_2 and H_∞ case.

5.1 Observer-based Control

The general procedure is developed for the purpose of illustration on the H_2 control case. But the procedure remains unchanged if the observer is applied on the H_∞ controller.

The substantial difference of observer based control with state feedback control is that the assumption of a fully known system state is eliminated. The feedback gain is not applied anymore on the state itself as in Eq. (4.19) but it will be multiplied to a state estimate $\hat{x}_g$ instead, which is the subject of the investigation here. The state estimate $\hat{x}_g$ will be computed from real time measurements, for which the overall augmented system (4.16) is rewritten for convenience, with the addition of the measurement equation

$$P: \begin{cases} \dot{x}_g(t) &= A_g x_g(t) + B_{g2} i(t) + B_{g1} f_e(t) \\ z_o(t) &= C_{g1} x_g(t) + D_{g12} i(t) + D_{g11} f_e(t) \\ y(t) &= C_{g2} x_g(t) + D_{g22} i(t) \\ z_C(t) &= C_{gC} x_g(t) + D_{gC2} i(t) \end{cases}. \tag{5.1}$$

where $y(t)$ is the vector of feedback measurements. We can also observe that the current $i(t)$ (control variable) is supposed to be known with certainty and its contribution in the measurement vector is determined by D_{g22}. In particular,

$$C_{g2} = \begin{bmatrix} -\frac{C_r}{M+m_h} & -\frac{K_b}{M+m_h} & 0 & 0 \end{bmatrix} \quad \text{and} \quad D_{g22} = \frac{1}{M+m_h}.$$

The design of the observer is based on the measurement vector $y(t)$. So attention has been given on this quantity. Its expression will directly result from the measuring equipment available. Light and cheap accelerometers are the most available type of sensors in marine energy field. This determines the outline of C_{g2} and D_{g22} above. A review of measuring devices in ocean energy field can be find in [98]. The use of accelerometers can be appreciated in an evaluation between an experimental setup and a linear model. In [136] notice also in $y(t)$, the measurement of the excitation signal $f_e(t)$, which is usually more complicated, can be fully avoided. Different choices in measuring equipment could have been made, leading to perhaps more accurate results. Costs of such choices would probably be higher and in our opinion not justifiable given the accuracy of the results found in this research.

The observer-based control law, can be written in the form

$$\begin{cases} \dot{\hat{x}}_g &= A_g \hat{x}_g + B_{g2} i - L_2 (y - \hat{y}) \\ \hat{y} &= C_{g2} \hat{x}_g + D_{g22} i \\ i &= K_2 \hat{x}_g \end{cases} \tag{5.2}$$

where L_2 is the observer gain to be computed and K_2 the state feedback controller gain. The role of the estimated states $\hat{x}_g$ is central to the controller, and it is clear that the computation of an accurate $\hat{x}_g$ is decisive for its successful implementation.

We can now write the error dynamics related to plant P

$$\begin{cases} \dot{e} &= (A_g + L_2 C_{g2}) e + (B_{g1} + L_2 D_{g21}) \\ z_e &= C_3 e \end{cases} \tag{5.3}$$

where $e = x_g - \hat{x}_g$ is the error variable and z_e is a vector output that can be weighted and can be tuned in order to target the observation error less affected by disturbances. Substituting plant P (Eq. (5.1)) in Eq. (5.3) the closed loop system is obtained as

$$\begin{aligned} \begin{bmatrix} \dot{\hat{x}}_g \\ \dot{e} \end{bmatrix} &= \begin{bmatrix} A_g + B_{g2}K_2 & -B_{g2}K_2 \\ \mathbf{0} & A_g + L_2 C_{g2} \end{bmatrix} \begin{bmatrix} x_g \\ e \end{bmatrix} + \begin{bmatrix} B_{g1} \\ B_{g1} + L_2 D_{g21} \end{bmatrix} f_e \\ \tilde{z} &= \begin{bmatrix} C_{g1} + D_{g12}K_2 & -D_{g12}K_2 \end{bmatrix} \begin{bmatrix} x_g \\ e \end{bmatrix} + D_{g11} f_e \end{aligned} \tag{5.4}$$

The objective is now to design an observer-based control law so that the closed-loop Eq. (5.4) is stable and respects hard constraints, or in other words, the plant in (5.1) is stable and the error dynamics in (5.3) is simultaneously satisfied, while the constraints are not breached.

The approach to this is to design the control law as follows. First, the stabilizing state feedback is designed without an estimator (as in previous Chapter 4). Subsequently, the observer is computed based on the controller designed. It was chosen to follow the reasoning behind [102] to deal with the observer design in a constrained environment. The concepts described in the reference to input constraints are extended to formulate constraints on the state vector in the same optimization process. The invariant ellipsoid theory is mapped out onto a second problem set. The overall result though appears to be inevitably a bilinear non-convex optimization. It will be tackled in the next section.

5.2 Observer Design

The linear control law in (5.2) is behind the design of the observer gain L_2. The state feedback controller gain K_2 is found first, independently from the computation of the observer. The procedure for its computation is outlined in Chapter 4.

If no hard constraints (4.17) were to be applied on the system (5.1), an estimator capable of minimizing the error dynamics in (5.3) would suffice, as the performance of interest would be limited to the power.

Prior to further computations it is useful to determine the so called "observability" of the system (5.1), defined in control literature as the measure of how well internal states can be inferred from knowledge of external outputs. In Linear Time Invariant systems like the present, one can determine if a systems is or not observable by looking at the pair (A_g, C_{g2}). If the system is observable, the matrix

$$W_o = \int_0^t e^{A_g^T \tau} C_{g2}^T C_{g2} e^{A_g \tau} d\tau \tag{5.5}$$

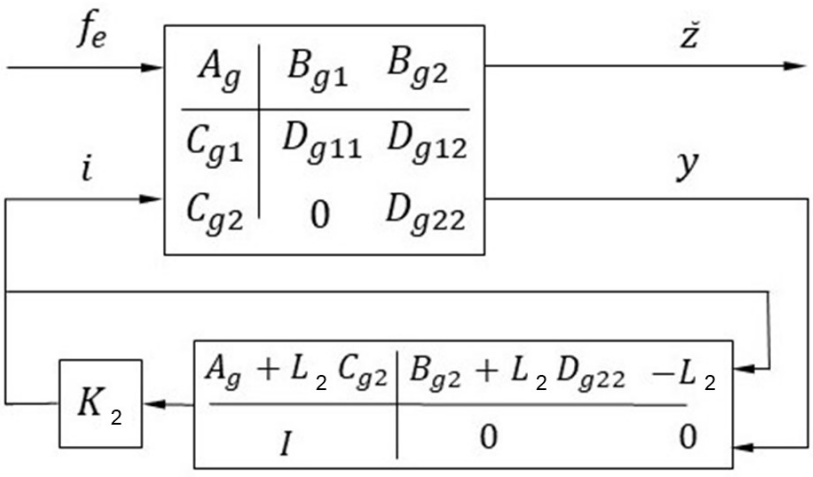

Figure 5.1: Observer-based control architecture

is nonsingular for any $t > 0$. This can be easily verified. Now, for the design of the observer further steps are necessary.

In the present circumstance, it is not sufficient to establish the observability of the system by the property just shown, as the basin of attraction of the problem for the computation of the observer gain L_2, is substantially different, given the presence of constraints in the control problem. Additional considerations are present. As in [102], in order to include input constraints, it is first useful to define a "linear region" for a given observer gain, meaning the region where the variables of interest do not reach the problem boundary, and hence they do not saturate. We remind that one of the advantages of the constrained MIPC controller is its ability to both handle constraints and also keep the values of the constrained variables away from saturation.

The first condition to be met by the observer is by defining a Lyapunov function $V_e(x_g, e)$ as

$$\Omega_e = \left\{ \begin{bmatrix} x_g \\ e \end{bmatrix} \middle| V_e(x_g, e) = \begin{bmatrix} x_g \\ e \end{bmatrix}^T R \begin{bmatrix} x_g \\ e \end{bmatrix} \leq \kappa \right\} \tag{5.6}$$

where $R > 0$, $R \in \mathbb{R}^{2n \times 2n}$. To be a correct estimate of Ω, Ω_e must be positively invariant and both the states and the input must be unsaturated over Ω_e. Translated in LMI formulation this means

$$R > 0, \quad \hat{A}^T R + R\hat{A} < 0, \tag{5.7}$$

with

$$\hat{A} = \begin{bmatrix} A_g + B_{g2}K_2 & -B_{g2}K_2 \\ \mathbf{0} & A_g + L_2C_{g2} \end{bmatrix} \tag{5.8}$$

which have to be met by the matrix variable R. Now, the input i can be written as function of x_g and e

$$i = -K_2\hat{x}_g = -\begin{bmatrix} K_2 & -K_2 \end{bmatrix} \begin{bmatrix} x_g \\ e \end{bmatrix} \tag{5.9}$$

resulting in, and analogously to Eq. (4.27) given by

$$\begin{bmatrix} R & \begin{bmatrix} K_2^T \\ K_2^T \end{bmatrix} \\ \begin{bmatrix} K_2 & K_2 \end{bmatrix} & \frac{1}{\kappa}Z_o \end{bmatrix} \geq 0, \quad Z_o \leq i_{max}^2. \tag{5.10}$$

Equivalently, for the state vector condition we obtain

$$\begin{bmatrix} R & \begin{bmatrix} C_{gC} \\ \mathbf{0}_{n\times p_2} \end{bmatrix} \\ \begin{bmatrix} C_{gC} & \mathbf{0}_{p_2\times n} \end{bmatrix} & \frac{1}{\kappa}N_o \end{bmatrix} \geq 0, \quad N_{o,ii} \leq z_{i,max}^2. \tag{5.11}$$

Eq. (5.7) contains terms that are products of matrix variables. As we can see, it is not an LMI but a BMI. Generally, these problems are non-convex, and not straightforward to solve. This is mainly due to the fact that non-convex optimization problems can possess local optima. Unfortunately, this equation cannot be written as an LMI, even with substitutions. So, in our particular problem, it is found the most straightforward to operate iteratively. Still, there is no guarantee that the found solution is indeed the global optimum.

In order to write the optimization problem, from Eq. (5.7) an extended upper limit σ can be defined on the output energy leading the expression to

$$\begin{bmatrix} \hat{A}^T R + R\hat{A} & \begin{bmatrix} I_{n\times n} \\ \mathbf{0}_{n\times n} \end{bmatrix} \\ \begin{bmatrix} I_{n\times n} & \mathbf{0}_{n\times n} \end{bmatrix} & -\sigma I_{n\times n} \end{bmatrix} < 0 \tag{5.12}$$

Now, the optimization problem is written combining the previous equations as

$$\min \sigma \tag{5.13a}$$

such that

$$R > 0, (5.10), (5.11), (5.12) \tag{5.13b}$$

in the matrix variables R and L_2. By using again the YALMIP parser [130] and the SeDuMi solver [131], also the observer gain L_2 can be computed offline. Now, let us see more in details the procedure employed for the solution of Eq. (5.13).

5.3 LMI-based Coordinate Descendent Method

In this section, we show how a so called "LMI-based Coordinate Descendent Method", succeeds in giving an acceptable solution to Eq. (5.13), despite not being able to prove that such solution is an optimum in any sense. Given the cost function decreasing at each iteration, the solution seems to converge: the performance simulated with the observer computed at the end seems to satisfy the constraints while keeping the error e within an acceptable range. It is with these criteria that the solution is deemed admissible. In [103], a so called sequential LMI-based coordinate descent method for solving BMIs is proposed with some improvements given a change of variables, where in [137] the considerations are extended to multi-objective optimizations. The basic method, so called $V - K$, is found to be enough for our purposes.

5.3.1 The algorithm

In this section, we illustrate the steps of the iterative process which lead to a solution to (5.13). The procedure in this Chapter sees initiating the matrix variable $R = I_{2n\times 2n}$ to compute a first observer gain L_2. By substituting the values found for L_2 in the optimization problem (5.13), the iteration process can advance with the computation of a new R matrix. The value of the cost function is suppose to decrease at every iteration, if the algorithm is meant to converge. In other words, starting from an initiated fixed variable R, the problem is brought to LMI form and at each step the optimization is convex and it can be solved with standard techniques. Then sequentially, with the optimized variable L_2 just found and fixing it for the coming step, R is recalculated as a result of a the LMI optimization. Sequentially step by step, the objective function is supposed to decrease. At this point, with a pre-defined level of accuracy, if the problem converges, a solution will be deemed as acceptable when the objective reaches a value below the one agreed in advance.

The proposed algorithm allows one to further explore the non-convex space of all solutions using successive convex subspaces. In our case, the initial choice of R already brings to an acceptable solution on Eq. (5.13), so the discussion on the impact of a different initial R is left out of this work.

In general, trying to illustrate graphically the algorithm, we can think of a Cartesian plane

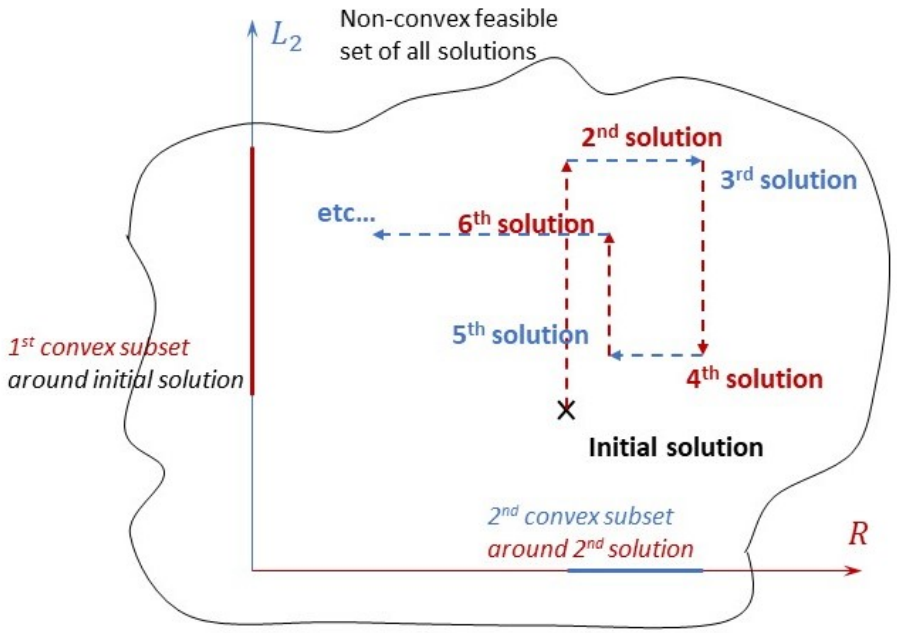

Figure 5.2: First few steps of the algorithm on a general set of grouped variables x_α, x_β.

which axes are one the matrix L_2 and one the matrix variable R. As shown in Fig. 5.2, the optimization in general does not follow necessarily one path, nor is intended to converge. But it can be visualized as a sequence of convex, LMI optimizations, within the space of all non-convex feasible set of all solutions. Now some more comments are given in relation with the convergence property of the known sequential methods used to approach BMI problems.

5.3.2 Discussion on convergence

In [104], the so called method "alternating LMI for BMI" shows how not to converge to a local optimum. In general, as mentioned, the local convergence of LMI-based coordinate descent methods cannot be proved. It is reminded that this kind of algorithms critically depends on the choice of coordinates (grouped variables), and not only on the initial choice for the solution. In [138], it is shown that local optima are found, but proof of convergence is still missing. The simple method proposed describes more in details what is implemented in this Chapter: since the BMI design is due to products between two sets of decision variables, the Lyapunov matrix(ces) V and the controller state space matrices K, starting from an initial solution the objective is iteratively optimized alternating each step between the two sets of variables, the so called $V - K$ iteration.

The intrinsic weakness of this method, which often leads to poor or no convergence at all, is that the nature of optimal control design is to find through an optimization of a mathematical criterion or properties of the system, a configuration which changes the properties of the system in a desired way; when a controller K is completely fixed, or as in our case the observer gain L_2, the

entire representation is fixed and properties don't change. Therefore, during this step of the $V-K$ iteration no closed loop improvement is made and the actual objective remains the same as after the previous K (or L_2) updated step. This method, can only work if, during the $V-$update step (R in our case), the matrix is modified so that is "oriented" in a way that, at the following $K-$ update step, the new Lyapunov matrix is fit for a better gain. Nothing ensures such a property in this algorithm. Considering this, convergence in this method cannot be guaranteed in general. That said, if the objective cost is seen to descrease at every iteration, convergence is shown in that particular case.

Consequence of this fact though is that in general, potentially the procedure can lead to infeasible solutions, due to the fact that the controller is designed first without taking into account that an observer will be added afterwards. If a certain accuracy value is pre-agreed though, it can be shown that if an appropriate descent sequence is found with right grouped variables and/or initial solution, with decreasing values for the objective, eventually leading to a cost lesser than the imposed accuracy, then this can be deemed as acceptable even with no guarantee that the solution is optimal.

The intention in this Chapter indeed is to prove that if an observer is found (leaving ample margin to investigate upon more effective procedures on the solution of its associated problem), that observer is able to fulfil the requirements of not decreasing substantially the power harvested by the WEC compared to the full state feedback case and of not violating the hard constraints. Observers found with proven properties of convergence, or which are easier to obtain, remain highly desirable though, and will be the focus of future research.

5.4 Numerical Results

Now, in this section the performance of the H_2 and H_∞ observer-based controller is tested on two different sea states, computed from a JONSWAP spectrum: a low-to-medium sea state of significant wave height $H_s = 1.76m$ and zero-crossing period of $T_p = 7.99s$ and a high sea state with $H_s = 4.51m$ and same zero-crossing period $T_p = 7.99s$. See in Fig. 5.3 the time evolution of the wave elevation $\eta(t)$ described the two mentioned sea states.

The intention is primarily to numerically determine whether the observed state is not going to drag the power performance down excessively and/or is violating constraints on the original trajectories. Obviously, it is in the intention of the present observer design to guarantee this, so we are going to show that this is satisfying the conditions. This intends to serve as a proof that an actual implementation of the constrained MIPC H_2 and H_∞ control is possible. The lack of literature though, on observer-based control with application of hard constraints and on the

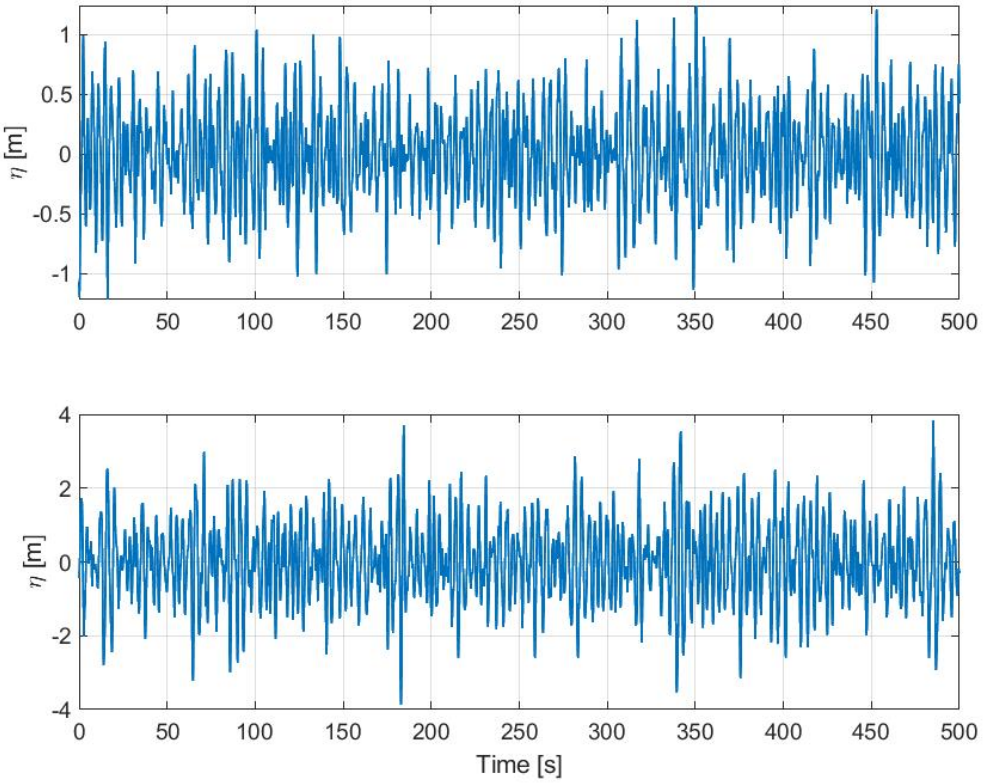

Figure 5.3: Wave elevation $\eta(t)$ of the two sea states simulated: $H_s = 1.76m$ (top), $H_w = 4.51m$ (bottom).

general solution of BMI problems is seen still as a very open quest, and it does make the present problematic nontrivial. The intention is to introduce the reader to it, and to raise the interest of ita applications on wave energy devices. Table 5.1 reports again the device specifications and geometrical parameters of the device where the strategy is applied, repeated from Chapter 4. The equations of motion (fully explained in Chapter 2, with the control optimization in Chapter 4, are solved again in a MATLAB/Simulink environment with a variable step solver option. The simulation time window is set this time on a 500s length, considered enough given the intermediate wave period ($= 7.99s$) of the waves simulated, and given the results observed on the full-state feedback case in Chapter 4.

Variable	**Parameter**	**Value**	**Unit**
r	Radius	3	m
h	Height	5	m
M	Mass	$1.13 \cdot 10^5$	kg
m_h	Added Mass	$5.13 \cdot 10^4$	kg
μ	MIPC Gain	0.005	-

Table 5.1: Device and MIPC filter specifications (Observer Based Control)

5.4.1 Observer based H_2 Control

The comparison of the performance against the full state feedback control, is made by keeping the tuning characteristics (namely κ and the MIPC parameter μ) unchanged. Values of κ in Eqs. (5.10)-(5.11) for the LMI relative to the hard constraints, as explained in [96] are tuned with the energy content of the input and they still follow Table 4.2. To insure that no constraints are violated, the choice could have been taken slightly different, ensuring with an additional reasonable safety margin, that no violation occurs. The larger the margin though, likely the poorer the power performance. From post-simulation hindsight, it is seen that values of κ show not to originate any constraint breach with the observer based strategy, so it was not necessary to adapt them.

The generator characteristics are now recalled [134] as

$$\begin{aligned} L_a &= 0.005 \quad \text{H} \\ K_v &= 938 \quad \text{N/A} \\ R_a &= 0.05 \quad \Omega \end{aligned} \tag{5.14}$$

and this is what determines the physical limits. $\pm 3MN$ for the PTO force (resulting in $\approx \pm 3kA$ for the PTO current), $\pm 5m$ displacement excursion z_{max} and $\pm 5m/s$ velocity limit $\dot{z}_{max}$. PTO efficiency is not considered.

Results for the H_2 controller are observed in Figs. 5.4-5.5, where the time evolution of the electrical power, PTO current, velocity and displacement are drawn for two sea states of significant wave height $H_s = 1.76m$ and zero-crossing period $T_p = 7.99s$ (the first), and $H_s = 4.51m$, $T_p = 7.99s$ (the second) on controllers with and without the observer. Performances on mean power output, root-mean square values of the currents and the values of κ are summarized in Table 5.2.

	State Feedback	**Observer Based**
Mean Power [W]	$6.41 \cdot 10^4$	$6.08 \cdot 10^4$
i_{RMS} [A]	337.2	318
κ	1	1
Mean Power [W]	$1.68 \cdot 10^5$	$1.54 \cdot 10^5$
i_{RMS} [A]	408	323
κ	10^4	10^4

Table 5.2: Mean power and current rms value for sea state of $1.76m$ (top) and $4.51m$ (bottom) significant wave height (H_2 Control)

A very marginal reduction in power performance is observed, with no constraint breach. This is very encouraging given the limited studies on the observer design and the complications given by its bilinear non-convex optimization. This fully proves the interest of MIPC and its applicability in the real world is proven. Further studies will bring more straightforward techniques to ensure an

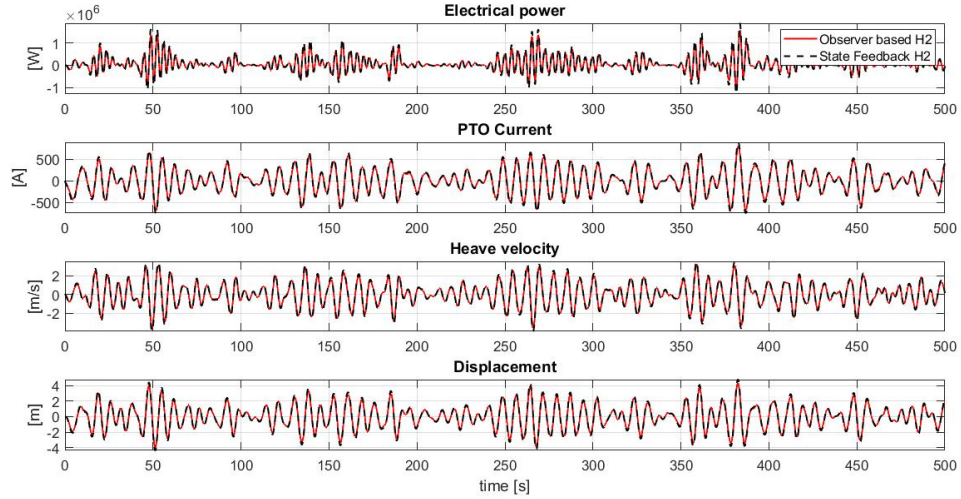

Figure 5.4: From top to bottom: time evolution of the electrical power output, PTO current, heave velocity and displacement in a sea state with significant wave height $H_s = 1.76m$ and zero-crossing period $T_p = 7.99s$ (H_2)

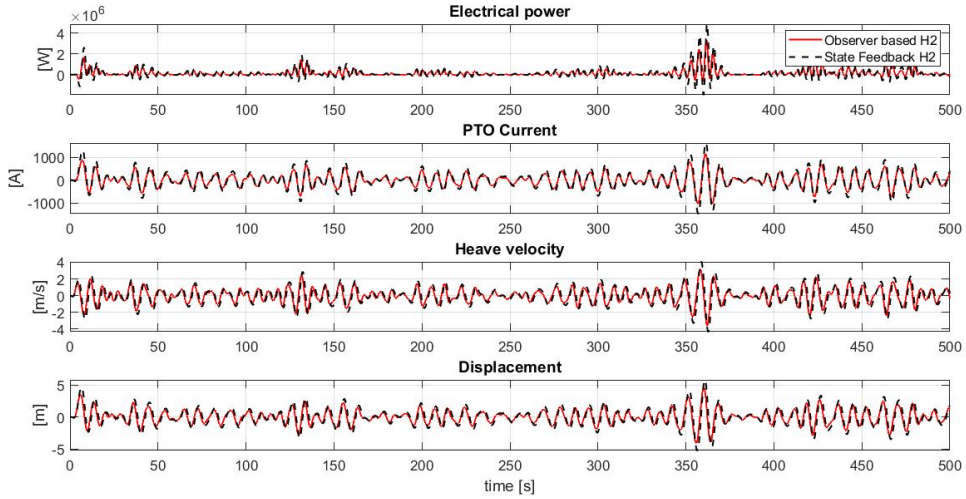

Figure 5.5: From top to bottom: time evolution of the electrical power output, PTO current, heave velocity and displacement in a sea state with significant wave height $H_s = 4.51m$ and zero-crossing period $T_p = 7.99s$ (H_2)

easy deployment of the observer, given the little scarcely tackled problem, but with huge applicative perspectives, in the author's opinion.

5.4.2 Observer based H_∞ control

In the case of H_∞ control, the procedure developing the observer stays the same. The difference is only the description of the controller formulation and relative optimization, developed in Chapter 4. As seen, with the same MIPC and κ configuration, H_∞ was showing a very marginal power gain on a single sea state for the full state feedback case, at the expense of larger spikes in the

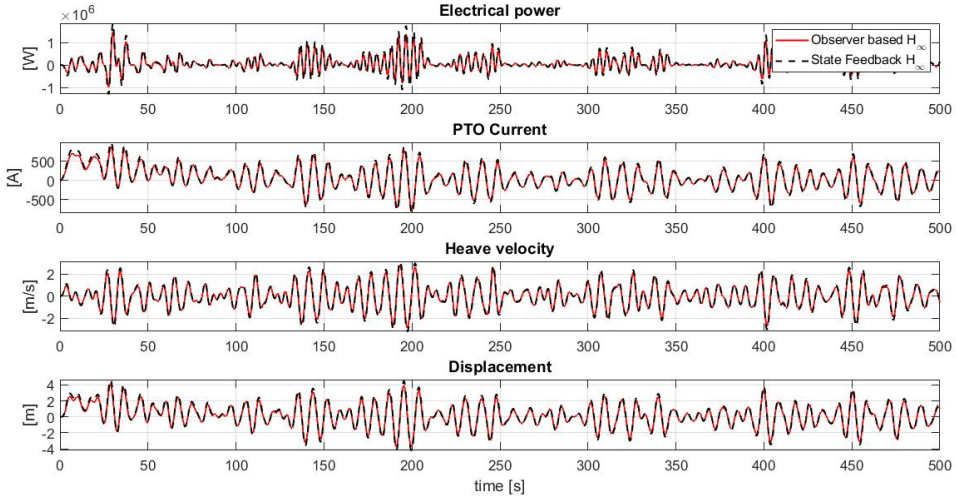

Figure 5.6: From top to bottom: time evolution of the electrical power output, PTO current, heave velocity and displacement in a sea state with significant wave height $H_s = 1.76m$ and zero-crossing period $T_p = 7.99s$ (H_∞)

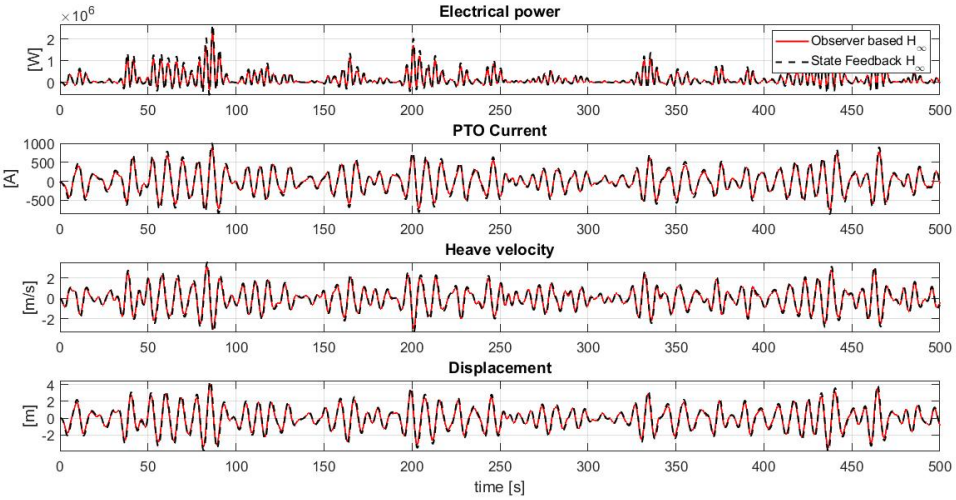

Figure 5.7: From top to bottom: time evolution of the electrical power output, PTO current, heave velocity and displacement in a sea state with significant wave height $H_s = 4.51m$ and zero-crossing period $T_p = 7.99s$ (H_∞)

instantaneous power time profile. That meant there is perhaps more expensive electrical equipment necessary to handle the spikes, probably not justifying its choice over H_2. It is now interesting to see if such behavior is repeated in presence of the observer.

In Figs. 5.6-5.7 we observe actually exactly this: compatibly with the constraints, and given the same choice of κ configuration, a slight gain over power is attained compared with H_2, at the price of higher spikes. The observer designed though shows only very marginal power reduction to the full state case, as in H_2. This suggests very encouraging results for the application of the strategy, given the not optimal nature of the observer, and the perhaps still wide research to be done on its design. A summary over the two sea states on the H_∞ case is given in Table 5.3.

	State Feedback	Observer Based
Mean Power [W]	$6.97 * 10^4$	$6.41 * 10^4$
i_{RMS} [A]	336.64	303.1
κ	1	1
Mean Power [W]	$1.95 * 10^5$	$1.72 * 10^5$
i_{RMS} [A]	328.6	292.1
κ	10^4	10^4

Table 5.3: Mean power and current rms value for sea state of $1.76m$ (top) and $4.51m$ (bottom) significant wave height (H_∞ Control)

As said, slightly higher mean power is once again observed, and also slightly less control current i_g in terms of root-mean-square value. Both valuable characteristics if it comes along with comparable power excursions. It has to be found with more investigation though, when the chosen actual machinery is to be deployed on a site, which strategy is most convenient to be employed. At that stage many other factors come into the picture which will influence the decision.

Comparisons of Currents

In order to fully appreciate the constraint handling of the observer based controllers, it was decided to run few additional simulations, with the some of the sea states derived for Chapter 4. In particular, sea states with two significant wave heights of $H_s = 1.76m$ and $H_s = 4.51m$ were run for six different zero crossing periods each. The sea states, similarly to Chapter 4 belong to six binned classes of periods where the WEC is supposed to be operational. The grouping of these classes, was based on the actual wave data measured on the site off the west coast of Ireland [135]. As already observed in Figs. 5.4-5.5-5.6-5.7 the current stays well below the limits, as it looks like the constraints on the state variables in order to be satisfied indirectly push the currents down as well. This is confirmed in Figs. 5.8-5.9 where the observer based controllers H_2 and H_∞ are run for the two significant wave heights, and varying zero-crossing periods. Between the two H_2 and H_∞ in this case it is even hard to notice any difference, which appears instead more noticeably in the power output. We can limit ourselves to say that the observer performs its desired function, and it does not downgrade the performance of the $S - H_2$ and $S - H_\infty$.

5.5 Chapter conclusions

In this Chapter, a systematic design method for observer based LTI control of a WEC is introduced. The method allows to optimize for the observer parameters with respect to the system's performance while at the same time the compliance with constraints is guaranteed. The goal is to develop an observer which can be combined to the $S - H_2$ and $S - H_\infty$ control methods in Chapter 4 without deteriorating the power performance as well. It is shown that unfortunately

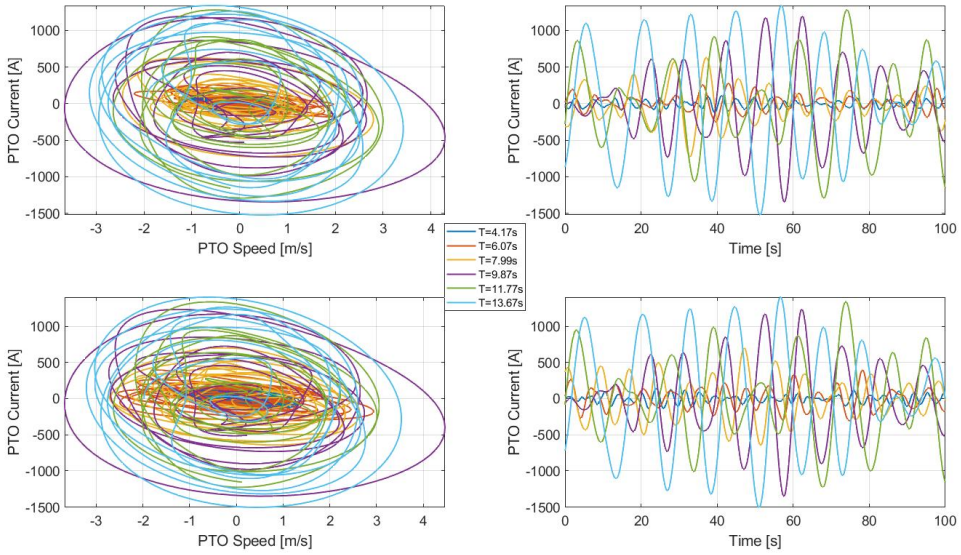

Figure 5.8: On the left-hand side: PTO current vs PTO speed. On the right hand side: PTO current over simulation time. At the top, the observer based H_∞ control, at the bottom the observer based H_2 control. Significant wave height $1.5m$.

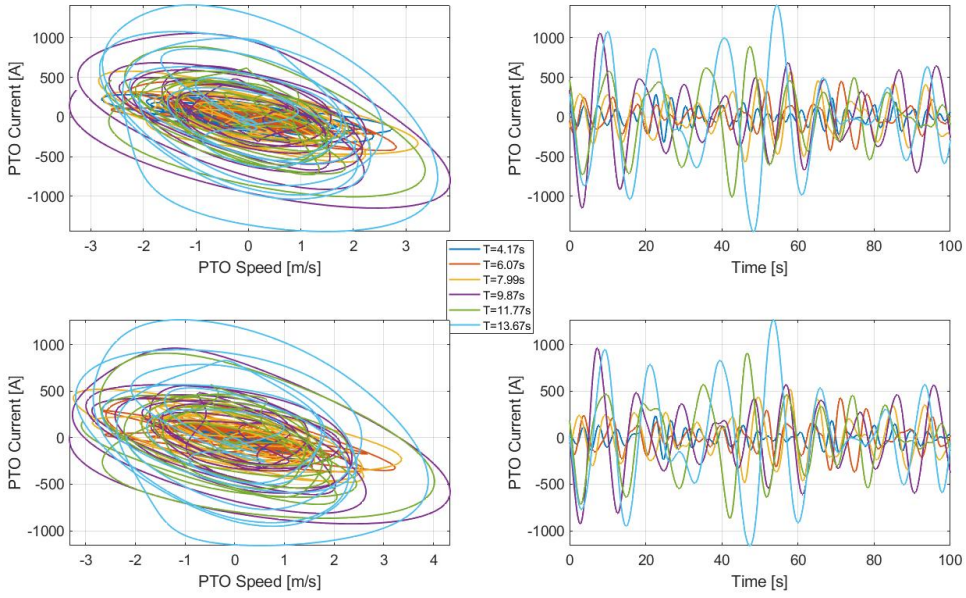

Figure 5.9: On the left-hand side: PTO current vs PTO speed. On the right hand side: PTO current over simulation time. At the top, the observer based H_∞ control, at the bottom the observer based H_2 control. Significant wave height $4.5m$.

such a formulation, compromises the standard LMI representation of the optimization problem and results in a Bilinear Matrix Inequalities setting. The desirable convexity property of the LMI is lost and a solution has to be found with alternative means. Studies on how to efficiently tackle BMIs are ongoing, but a limited literature on the matter exists and no method has proven to formally converge to a global optimum. A sequence of progressively improved solutions was found,

by virtue of a successful choice of the initial guess. Where a certain value of accuracy can be predefined, if the cost function decreases, a solution can be deemed satisfactory when the level of accuracy is achieved. At the end, the observer with desired properties was computed, and the applicability of $S - H_2$ and $S - H_\infty$ was proven, showing that the observer based strategy keeps a high power performance and does not breach constraints on a varying sea scenario. This is an open and important research question, that is now answered for the actual implementation of the strategy.

Chapter 6

Conclusions and Future Work

6.1 Summary of the Research

The main aim of this thesis was to formulate novel optimal control strategies which could be implemented in real time on point absorber WEC devices. The objectives were to develop causal strategies where forecasting techniques are not required; to develop strategies which are compatible with physical limitations; to investigate the performance and applicability based on real time observation and to develop controllers targeting nonlinear models. We summarise the work done as follows.

For the multiresolution LQ control developed, the intention was to showcase that the application of DWT in a modified linear quadratic control framework would be successful in terms of power maximization. This was shown with two separate procedures, the first employing a trajectory tracking, and the second directly maximizing power. The MRA strategies have been found to outperform the baseline LQ controllers, given their ability to assign the control weight matrices non-uniformly among the frequency bands. This is not possible for a baseline LQ control.

Multiresolution control showed its benefits also on a nonlinear model of PA. A spherical geometry was considered as case study. A novel controller, based on the solution of the Riccati differential equation forward in time, was formulated in wavelet domain. Time-frequency dependent control gains were computed online, based on the time-varying system matrices. The need for future system information is circumvented, and the fully nonlinear controller is able to effectively tackle the nonlinear effects. Moreover, due to to the MRA formulation, a further boost can be given by distributing the control weight matrices differently among the frequency bands.

Also, two novel H_2 and H_∞ methodologies were developed in this thesis to highlight the LMI-based multi-objective controller capability in the context of WEC devices and constrained optimization. The procedures are able to deal with hard constraints in the formulation and result in

a unique optimization framework together with the energy maximizing requirement. The latter is expressed as a H_2 or H_∞ norm minimization of a performance index. The index is determined following the principles of the so called MIPC, and in our particular case, a causal relationship is chosen to allow real time implementation. With these controllers, it was shown how a superior energy harnessing performance could be achieved in a varying sea scenario, when compared to an LQ strategy, given that the LQ strategy does not allow for constraint handling, nor it can be tuned with ease for changing sea conditions.

Finally, the design of an observer was undertaken for the novel H_2 and H_∞ methodologies. The goal was to determine if the design of an observer was possible at all, given the hard constraints in the control formulation. The hard constraints pose challenges to find a suitable observer gain, given that the observer design problem becomes bilinear. But, it was shown that a solution can be found for the case in consideration, confirming the applicability of the strategies with the available measuring equipment.

6.2 Main Findings

The main findings of this thesis are summarized in this section. This research has considered current challenges in control theory and wave energy conversion systems and have tried to fill some research gaps of interest. The gaps identified were mainly found in: multi-scale control, nonlinear systems, LMI-based control and observer based control. The conclusions following the results in this thesis on the control strategies mentioned follow.

Among the properties of multi-resolution controllers, the ability to target certain frequencies only and to preferentially decompose the response of a dynamic system upon the spectral distribution of a signal has shown clear benefits for broad-banded signals like the sea waves and associated responses. The application of DWT to modify the linear quadratic controller has established a clear superiority in terms of power output for a heaving point absorber described by linear dynamics, while keeping the control action restrained and smoother as compared to basic LQ. In particular, MRA-LQT shows an about 10% increase in power compared to non-MRA-LQT with equivalent control force magnitudes (and in turn currents), resulting also in a L_2 norm reduction of the error signal. The normalized value of error over the root-mean-square of the velocity drops from a peaks of over 50% to only 10%. The direct power maximizing MRA-LQ control shows more than 10% increase over the non-MRA case with an insignificant increase in the rms value of the control effort.

When the aforementioned DWT based algorithm is applied to a nonlinear type of controller, which solves forward in time the Riccati differential equation for a model of PA with varying restoring force, the benefits can be appreciated as well, guaranteeing again a power boost compared

to the non-MRA case. The nonlinear online formulation of the control ensures that the time-varying information for the state space matrices is not lost and this results in a better handling of the dynamics. In particular, it is shown that with the MRA case, the power captured is almost three fold compared to the baseline FRE control, with only a modest increase in the control force rms value. Compared to the linear MRA-LQ the improvement is even more evident, given once again an almost threefold boost in power with the control force rms value almost equivalent in the two cases.

Next, for the LMI-based control, which was hardly exploited in wave energy before as well, is known to best approach multiple objective optimization. In this thesis, it was shown how the control can successfully tackle optimization with hard constraints in a highly varying sea environment and also be tuned with ease with the changing conditions. The application of LMI-based control in this context is meant to underline the broad potential of this class of controllers in the field, given the many (often contrasting) requirements that ocean energy harnessing entails, and how substantially and effectively they are addressed with an LMI-based multi objective optimization. We could see that, by considering hard constrains, $S - H_2$ control could harness up to 45% more energy from the same sea site than an optimal LQ control, while $S - H_\infty$ in capture up to 42% more. So the two methodologies seemed almost equivalent in terms of power. Differences were observed in the peak-to-mean power ratio, which is is distinctively higher for H_∞.

Among other results in this thesis, it was also shown also BMI optimization can be nontrivial, as not always a problem can be formulated as LMI. In BMIs, the most desirable property of convexity in LMIs is indeed lost. It is shown that an LMI formulation is not possible in constrained observer design. Observers, are a necessary part of the control architecture, as no quantity in the real world can be inferred without measurements, and measurements bring inaccuracies and uncertainty. So, beside the fact that a solution to our problem was found, this is left as an open problem for future studies. One direction of research in this is regarding about targeted approximations. This has often shown to help to transform the problem and convert it to a convex one. This allows an LMI formulation. In our particular case, the designed observer has shown to reach its goal by not downgrading the power performance, and lowering the mean power output by only a marginal 7%-8% for two separate cases studied.

What is generally accomplished with the developed controllers in this thesis can be also summarized in the next four statements. (1) All of these control methods are outlined in a way that causality was always enforced, so neither future information on dynamics was never required, nor future information on excitation forces. This reduces the computational burden and operational costs in comparison to control architectures which necessitates the use of forecasting systems. (2) With similar reasoning, all of the control methods are readily applicable to real devices, given their

compatibility with processors in industry and limitations to mechanical/electrical components. (3) This is true also when it comes to measuring equipment, determining the observer configurations.

Experimental validation is the first logical step towards possible subsequent sea trial developments. Most common types of tests are wave basin/flume kind of tests. However, in Trinity College Civil Engineering department laboratories, a new type of cost-effective test is available: the so called real-time hybrid testing. This test surprisingly does not require actual waves, yet it provides incredibly accurate results on the performance of developed control algorithms. See [139] about the tests performed, and about details on the test rig.

Appendix A

Noncausal Optimal Control Algorithm

The optimal control algorithm used for the comparisons follows Pontryagin maximum principle. It combines the concepts outlined in [77] and [79] for the solution. The mechanical energy derived from the system can be obtained as integral of the mechanical power P_m

$$E_c = \int_0^{T_s} f_c(t)\dot{z}(t)dt \tag{A.1}$$

Based on Eqs. (3.1) to (3.9), it is found convenient to rewrite a state space formulation of the problem with merging the radiation states x_r in

$$\dot{x}(t) = A_o x(t) + B_o u(t) + E_o w(t) \tag{A.2}$$

with

$$x = \begin{bmatrix} x_{r1} & x_{r2} & x_{r3} & x_{r4} & z & \dot{z} \end{bmatrix}^T \tag{A.3}$$

given the order four of the approximation. The system matrices follow

$$\begin{aligned} A_o &= \begin{bmatrix} A_r & \mathbf{0}_{4\times 1} & B_r \\ \mathbf{0}_{1\times 5} & & 1 \\ -\frac{C_r}{M+m_\infty} & -\frac{K_b}{M+m_\infty} & 0 \end{bmatrix} \\ B_o &= \begin{bmatrix} \mathbf{0}_{5\times 1} \\ \frac{-1}{M+m_\infty} \end{bmatrix} \quad E_o = \begin{bmatrix} 0_{5\times 1} \\ \frac{1}{M+m_\infty} \end{bmatrix} \end{aligned} \tag{A.4}$$

The control command $u(t) = f_c(t)$ and $w(t) = f_e(t)$. As we can see the radiation force $f_r(t)$ is

approximated within the system. The optimal control problem is to find a control function $f_c(t)$ which maximizes the useful energy (A.1) over the time interval $0 < t < T$ subject to (A.2) being satisfied. The Hamiltonian of the control problem is here defined (using the variational approach) as

$$\begin{aligned} H(x(t), f_c(t), \lambda(t), t) &= f_c(t)\dot{z}(t) + \lambda(t)^T(A_o x(t) + \\ &\quad + B_o f_c(t) + E_o f_e(t)) \\ \text{where} \quad \lambda(t) &= \begin{bmatrix} \lambda_{r1} & \lambda_{r2} & \lambda_{r3} & \lambda_{r4} & \lambda_z & \lambda_{\dot{z}} \end{bmatrix}^T \\ &\Rightarrow H(x(t), f_c(t), \lambda(t), t) = f_c(t)\dot{z}(t) + \\ &\quad + \sum_{i=1}^{4} \lambda_{ri}\Big(\sum_{j=1}^{4}\big(A_{rij}x_{rj} + B_{ri}\dot{z}(t)\big)\Big) + \lambda_z \dot{z}(t) + \\ &\quad + \lambda_{\dot{z}}\Big(\frac{-1}{M + m_\infty}\big(\sum_{i=0}^{4} C_{ri}x_{ri} + K_b z(t) + f_e(t) - f_c(t)\big)\Big) \end{aligned} \tag{A.5}$$

In the above equation, (A.5), $\lambda(t)$ is the co-state vector, A_{rij},B_{ri}, C_{ri} the *i-th* and *j-th* elements of the radiation matrices A_r, B_r and C_r. The Euler-Lagrange stationarity conditions for optimal control are

$$\begin{aligned} \dot{\lambda}(t) = -\frac{\partial H}{\partial x} &= \begin{bmatrix} -A_r^T & \mathbf{0}_{4\times 1} & \frac{C_r}{M+m_\infty} \\ \mathbf{0}_{1\times 5} & & \frac{K_b}{M+m_\infty} \\ -B_r & -1 & 0 \end{bmatrix} \lambda(t) + \\ &\quad + \begin{bmatrix} \mathbf{0}_{5\times 1} \\ -1 \end{bmatrix} f_c(t) \end{aligned} \tag{A.6}$$

and

$$\begin{aligned} \lambda(T_s) = \mathbf{0} \quad (\lambda_{ri}(T_s) = \lambda_z(T_s) = \lambda_{\dot{z}}(T_s) = 0) \\ \text{for} \quad i = 1, 2, 3, 4. \end{aligned} \tag{A.7}$$

as terminal condition on the co-state vector. The algorithm solves the numerical problem iteratively ([79]).

Appendix B

State Space Balanced Realization and Henkel Singular Values

Given a state space representation for a linear system

$$\begin{cases} \dot{x}(t) &= Ax(t) + Bu(t) \\ y(t) &= Cx(t) \end{cases} \tag{B.1}$$

and a transformation P which is nonsingular, a system which is defined by the matrices $\bar{A} = PAP^{-1}$, $\bar{B} = PB$, $\bar{C} = CP^{-1}$, is equivalent to the system A, B, C. This means that the two systems have the same set of eigenvalues and same input-output transfer function. Two quantities of interest in the context, are the so called "controllability Gramian matrix W_c" and "observability Gramian matrix W_o" and they are defined such that

$$\begin{aligned} AW_c + W_cA^T &= -BB^T \\ A^TW_o + W_oA &= -C^TC \end{aligned} \tag{B.2}$$

These matrices are important because their product W_cW_o is similar to the product $\bar{W}_c\bar{W}_o$, corresponding to an equivalent state space representation $\bar{A}, \bar{B}, \bar{C}$. The meaning of similar translates in: the determinant is the same, the eigenvalues are the same and other properties.

On top of what just stated, the product W_cW_o is also similar to the Hankel matrix

$$\Sigma = diag\{\sigma_1, \sigma_2, \ldots, \sigma_n\} \tag{B.3}$$

where n is the dimensionality of the state of the system. The elements $\sigma_1 \geq \sigma_2 \geq \cdots \geq \sigma_n \geq 0$

are the Henkel singular values of the system and they represent a quantification of the energy of each state component [126].

When a state space realization of a system A, B, C is balanced when $W_c = W_o = \Sigma$.

B.1 Model Reduction Based on Henkel Singular Values

Properties of a balanced realization can be exploited to isolate the dominant dynamics of a system. The state space system in Eq. (B.1) can be decomposed as follows

$$\begin{cases} \begin{bmatrix} \dot{x}_1(t) \\ \dot{x}_2(t) \end{bmatrix} = \begin{bmatrix} A_{11} & A_{12} \\ A_{21} & A_{22} \end{bmatrix} \begin{bmatrix} x_1(t) \\ x_2(t) \end{bmatrix} + \begin{bmatrix} B_1 \\ B_2 \end{bmatrix} u(t) \\ y(t) = \begin{bmatrix} C_1 & C_2 \end{bmatrix} \begin{bmatrix} x_1(t) \\ x_2(t) \end{bmatrix} \end{cases} \tag{B.4}$$

. The Henkel matrix is easily decomposed as

$$\Sigma = diag\{\Sigma_1, \Sigma_2\} \tag{B.5}$$

, then the subsystem A_{11},B_1, C_1 is a good approximation of the original system A, B, C if the singular values in Σ_1 are much bigger than the singular values in Σ_2.

Appendix C

Design Specifications as LMI Constraints

C.1 Constraints on the H_2 norm

H_∞ and H_2 constraints can be expressed in the form of linear matrix inequalities (LMI), and efficient LMI solvers can be employed to compute controllers that satisfy those constraints. In this Appendix we will first introduce how to express design specifications in the form of linear matrix inequalities, and subsequently briefly introduce methods for computing controllers by solving the LMIs.

We address the reader to [94] for a complete exposition of the Linear Matrix Inequalities subject.

Consider a stable system with state space realization

$$\begin{cases} \dot{x}(t) &= Ax(t) + Bw(t) \\ z(t) &= Cx(t) \end{cases} \tag{C.1}$$

Let $T(s)$ denote the strictly proper transfer function matrix from w to z

$$T(s) = C(sI - A)^{-1}B \tag{C.2}$$

It is proven that the H_2 norm of $T(s)$ can be computed from

$$\|T\|_2^2 = tr(CP_0C^T) \tag{C.3}$$

where P_0 is the positive definite matrix that solves the Lyapunov equation

$$AP_0 + P_0A^T + BB^T = 0 \tag{C.4}$$

Assume now that we impose a constraint on $\|T\|_2$, say

$$\|T\|_2 < \nu \tag{C.5}$$

for some $\nu > 0$. Now, to see how (C.3)-(C.4) can be used to express the constraint, consider the solution of the following modified version of (C.4)

$$AP + PA^T + BB^T + Q = 0 \tag{C.6}$$

where $Q > 0$ is a positive definite matrix. Subtracting (C.4) from (C.6) gives

$$A(P - P_0) + (P - P_0)A^T + Q = 0 \tag{C.7}$$

Because $Q > 0$ and A is stable, this implies $P - P_0 > 0$ or

$$P > P_0 \tag{C.8}$$

The reverse also holds: if (C.8) is true then a matrix $Q > 0$ exists that satisfies (C.7), and since this is true for any $Q > 0$ then we can replace (C.8) by the matrix inequality

$$AP + PA^T + BB^T < 0 \tag{C.9}$$

and we have from (C.8) and (C.3) that

$$\|T\|_2^2 < tr(CPC^T) \tag{C.10}$$

if and only if P satisfies (C.9).

Theorem C.1 $\|T\|_2 < 0$ *if and only if there exist a positive definite matrix* P *that satisfies* (C.9) *and*

$$tr(CPC^T) < \nu^2 \tag{C.11}$$

.

In the next section we will show how to compute controllers that satisfy the constraint in $\|T\|_2$. The following equivalent formulation of the above result is used instead. Introduce a new symmetric matrix variable W (as a slack variable), then we have

Theorem C.2 $\|T\|_2 < 0$ *if and only if there exist symmetric matrices* P *and* W *that satisfy*

$$\begin{bmatrix} AP + PA^T & B \\ B^T & -I \end{bmatrix} < 0, \quad \begin{bmatrix} W & CP \\ PC^T & P \end{bmatrix} > 0 \quad and \quad tr(W) < \nu^2 \tag{C.12}$$

To see that inequalities in (C.12) are equivalent to (C.11) and (C.9), note that

$$\begin{bmatrix} M & L \\ L^T & N \end{bmatrix} > 0$$

where $M = M^T$ and $N = N^T$ is equivalent to

$$N > 0 \quad \text{and} \quad M - LN^{-1}L^T > 0$$

. This fact is often used to convert nonlinear inequalities into LMI form; where the term $M - LN^{-1}L^T$ is the Schur complement with respect to N. In the above case, this leads to $W > CPC^T$ and consequently to $tr(W) > CPC^T$ from which (C.11) and (C.12) hold.

C.2 Constraints on the H_∞ norm

Considering now a system in the form

$$\begin{cases} \dot{x}(t) = Ax(t) + Bw(t), \quad x(0) = 0 \\ z(t) = Cx(t) + Dw(t) \end{cases} \tag{C.13}$$

Assuming $T(s)$ as stable, the H_∞ norm of the system is

$$\|T\|_\infty^2 = \max_{w \neq 0} \frac{\int_0^\infty z^T(t)z(t)dt}{\int_0^\infty w^T(t)w(t)dt}$$

where we also assume $x(0) = 0$. From the above it follows that $\|T\|_\infty < \gamma$ is equivalent to

$$\int_0^\infty \big(z^T(t)z(t) - \gamma^2 w^T(t)w(t)\big)dt < 0$$

holding true for all square integrable, non-zero $w(t)$. Introducing a Lyapunov function $V(x) = x^T Px$ with $P = P^T > 0$, the constraint $\|T\|_\infty < \gamma$, as $x(0) = x(\infty) = 0$, is enforced by the existance of P such that

$$\frac{dV(x)}{dt} + \frac{1}{\gamma} z^T(t)z(t) - \gamma w^T(t)w(t) < 0 \tag{C.14}$$

for all $x(t)$, $w(t)$. To turn this into a linear matrix inequality, substitute

$$\frac{dV(x)}{dt} = x^T(A^TP + PA)x + x^TPBw + w^TB^TPx$$

and $z = Cx + Dw$ to obtain

$$\begin{bmatrix} x^T & w^T \end{bmatrix} \begin{bmatrix} A^TP + PA + \frac{1}{\gamma}C^TC & PB + \frac{1}{\gamma}C^TD \\ B^TP + \frac{1}{\gamma}D^TC & -\gamma I + \frac{1}{\gamma}D^TD \end{bmatrix} \begin{bmatrix} x \\ w \end{bmatrix} < 0$$

This must hold for any x and w. So the block matrix must be negative definite. And this can be rewritten as

$$\begin{bmatrix} A^TP + PA & PB \\ B^TP & -\gamma I \end{bmatrix} + \frac{1}{\gamma} \begin{bmatrix} C^T \\ D^T \end{bmatrix} \begin{bmatrix} C & D \end{bmatrix} < 0$$

It can be shown that the above LMI not only is a sufficient condition but also necessary for $\|T\|_\infty < \gamma$. Now, using the Shur complement, we can rewrite the condition and summarize the result as follows.

Theorem C.3 *$\|T\|_\infty < \gamma$ if and only if there exists a positive definite, symmetric matrix P that satisfies the linear matrix inequality*

$$\begin{bmatrix} A^TP + PA & PB & C^T \\ B^TP & -\gamma I & D^T \\ C & D & -\gamma I \end{bmatrix} < 0 \tag{C.15}$$

References

[1] *Ocean energy europe*, https://www.oceanenergy-europe.eu/, Accessed: 2021-08-02.

[2] A. Merigaud, J.-c. Gilloteaux, and J. Ringwood, "A nonlinear extension for linear boundary element methods in wave energy device modelling," vol. 4, Jul. 2012, pp. 615–621. DOI: 10.1115/OMAE2012-83581.

[3] M. Folley, T. Whittaker, and J. Van't Hoff, "The design of small seabed mounted bottom hinged wave energy converters," English, Medium of Output: Electronic; 7th European Wave and Tidal Energy Conference ; Conference date: 01-09-2007 Through 01-09-2007, Sep. 2007, pp. 1–10.

[4] A. Zurkinden and M. Kramer, "Numerical time integration methods for a point absorber wave energy converter," English, in *Conference: International Workshop on Water Waves and Floating Bodies*, 2012, pp. 217–220.

[5] J. V. Ringwood, "Wave energy control: Status and perspectives 2020 ∗∗this paper is based upon work supported by Science Foundation Ireland under Grant no. 13/IA/1886 and Grant No. 12/RC/2302 for the Marine Renewable Ireland (MaREI) centre.," *IFAC-PapersOnLine*, vol. 53, no. 2, pp. 12 271–12 282, 2020, 21st IFAC World Congress, ISSN: 2405-8963. DOI: https://doi.org/10.1016/j.ifacol.2020.12.1162. [Online]. Available: https://www.sciencedirect.com/science/article/pii/S2405896320315536.

[6] J. Cruz, *Ocean Wave Energy: Current Status and Future Prespectives*. Jan. 2008, ISBN: 978-3-540-74894-6. DOI: 10.1007/978-3-540-74895-3.

[7] M. Folley and T. J. T. Whittaker, "Analysis of the nearshore wave energy resource," *Renewable Energy*, vol. 34(7), 1709–1715, 2009.

[8] H. M. Deberneh and I. Kim, "Predicting output power for nearshore wave energy harvesting," *Applied Sciences*, vol. 8, p. 566, Apr. 2018. DOI: 10.3390/app8040566.

[9] J. Falnes, *Ocean Waves and Oscillating Systems: Linear Interactions Including Wave-Energy Extraction*. Cambridge University Press, 2002. DOI: 10.1017/CBO9780511754630.

[10] M. Eriksson, J. Isberg, and M. Leijon, "Hydrodynamic modelling of a direct drive wave energy converter," *International Journal of Engineering Science*, vol. 43, no. 17, pp. 1377–1387, 2005, ISSN: 0020-7225. DOI: https://doi.org/10.1016/j.ijengsci.2005.05.014.

[11] Y. Gao, S. Shao, H. Zou, M. Tang, H. Xu, and C. Tian, "A fully floating system for a wave energy converter with direct-driven linear generator," *Energy*, vol. 95, pp. 99–109, 2016, ISSN: 0360-5442. DOI: https://doi.org/10.1016/j.energy.2015.11.072. [Online]. Available: https://www.sciencedirect.com/science/article/pii/S0360544215016357.

[12] A. F. Falcão and J. C. Henriques, "Oscillating-water-column wave energy converters and air turbines: A review," *Renewable Energy*, vol. 85, pp. 1391–1424, 2016, ISSN: 0960-1481. DOI: https://doi.org/10.1016/j.renene.2015.07.086. [Online]. Available: https://www.sciencedirect.com/science/article/pii/S0960148115301828.

[13] T Setoguchi, S Santhakumar, H Maeda, M Takao, and K Kaneko, "A review of impulse turbines for wave energy conversion," *Renewable Energy*, vol. 23, no. 2, pp. 261–292, 2001, ISSN: 0960-1481.

[14] A. Falcao, "Wave energy utilization: A review of the technologies," *Renewable and Sustainable Energy Reviews*, vol. 14(3), pp. 899–918, 2010.

[15] E. Al Shami, R. Zhang, and X. Wang, "Point absorber wave energy harvesters: A review of recent developments," *Energies*, vol. 12, p. 47, Dec. 2018. DOI: 10.3390/en12010047.

[16] S. I. Mohsin and A. Al-Faruk, "Numerical simulation of an oscillating water column device and investigating the effects of lip submergence on velocity and pressure," in *American Institute of Physics Conference Series*, ser. American Institute of Physics Conference Series, vol. 2324, Feb. 2021, 040004, p. 040 004. DOI: 10.1063/5.0037586.

[17] A. F. Falcão, J. C. Henriques, and J. J. Cândido, "Dynamics and optimization of the owc spar buoy wave energy converter," *Renewable Energy*, vol. 48, pp. 369–381, 2012, ISSN: 0960-1481. DOI: https://doi.org/10.1016/j.renene.2012.05.009. [Online]. Available: https://www.sciencedirect.com/science/article/pii/S0960148112003229.

[18] K. Ruehl, "Time-domain modeling of heaving point absorber wave energy converters, including power take-off and mooring," *Master Thesis, Mechanical Engineering Department, Oregon State University*, 2011.

[19] J. Henriques, L. Gato, A. Falcão, E. Robles, and F.-X. Faÿ, "Latching control of a floating oscillating-water-column wave energy converter," *Renewable Energy*, vol. 90, pp. 229–241, 2016, ISSN: 0960-1481. DOI: https://doi.org/10.1016/j.renene.2015.12.065. [Online]. Available: https://www.sciencedirect.com/science/article/pii/S0960148115305693.

[20] R. Gomes, J. Henriques, L. Gato, and A. Falcão, "Hydrodynamic optimization of an axisymmetric floating oscillating water column for wave energy conversion," *Renewable Energy*, vol. 44, pp. 328–339, 2012, ISSN: 0960-1481. DOI: https://doi.org/10.1016/j.renene.2012.01.105. [Online]. Available: https://www.sciencedirect.com/science/article/pii/S0960148112001413.

[21] A. Falcão, L. Gato, and E. Nunes, "A novel radial self-rectifying air turbine for use in wave energy converters," *Renewable Energy*, vol. 50, pp. 289–298, 2013, ISSN: 0960-1481. DOI: https://doi.org/10.1016/j.renene.2012.06.050. [Online]. Available: https://www.sciencedirect.com/science/article/pii/S0960148112004016.

[22] ——, "A novel radial self-rectifying air turbine for use in wave energy converters. part 2. results from model testing," *Renewable Energy*, vol. 53, pp. 159–164, 2013, ISSN: 0960-1481. DOI: https://doi.org/10.1016/j.renene.2012.11.018. [Online]. Available: https://www.sciencedirect.com/science/article/pii/S0960148112007355.

[23] C. Josset and A. H. Clément, "A time-domain numerical simulator for oscillating water column wave power plants," *Renewable Energy*, vol. 32, pp. 1379–1402, 2007.

[24] W. Sheng, R. Alcorn, and A. Lewis, "On thermodynamics in the primary power conversion of oscillating water column wave energy converters," *Journal of Renewable and Sustainable Energy*, vol. 5, Mar. 2013. DOI: 10.1063/1.4794750.

[25] A. Babarit, J. Hals, M. Muliawan, A. Kurniawan, T. Moan, and J. Krokstad, "Numerical benchmarking study of a selection of wave energy converters," *Renewable Energy*, vol. 41, pp. 44–63, 2012, ISSN: 0960-1481. DOI: https://doi.org/10.1016/j.renene.2011.10.002. [Online]. Available: https://www.sciencedirect.com/science/article/pii/S0960148111005672.

[26] N. Sergiienko, B. Cazzolato, B. Ding, P. Hardy, and M. Arjomandi, "Performance comparison of the floating and fully submerged quasi-point absorber wave energy converters," *Renewable Energy*, vol. 108, pp. 425–437, 2017, ISSN: 0960-1481. DOI: https://doi.org/10.1016/j.renene.2017.03.002. [Online]. Available: https://www.sciencedirect.com/science/article/pii/S0960148117301829.

[27] J. Falnes, "Radiation impedance matrix and optimum power absorption for interacting oscillating in surface wave," *Applied Ocean Research*, vol. 2(2), pp. 75–80, 1980.

[28] D. V. Evans, "A theory for wave-power absorption by oscillating bodies," *Journal of Fluid Mechanics*, vol. 77, no. 1, 1–25, 1976. DOI: 10.1017/S0022112076001109.

[29] J. Wu, Y. Yao, D. Sun, Z. Ni, and M. Göteman, "Numerical and experimental study of the solo duck wave energy converter," *Energies*, vol. 12, no. 10, 2019, ISSN: 1996-1073. [Online]. Available: https://www.mdpi.com/1996-1073/12/10/1941.

[30] S.-J. Kim, W. Koo, and M.-J. Shin, "Numerical and experimental study on a hemispheric point-absorber-type wave energy converter with a hydraulic power take-off system," *Renewable Energy*, vol. 135, pp. 1260–1269, 2019, ISSN: 0960-1481. DOI: https://doi.org/10.1016/j.renene.2018.09.097. [Online]. Available: https://www.sciencedirect.com/science/article/pii/S0960148118311716.

[31] B. Bosma, Z. Zhang, T. K. Brekken, H. T. Özkan Haller, C. McNatt, and S. C. Yim, "Wave energy converter modeling in the frequency domain: A design guide," in *2012 IEEE Energy Conversion Congress and Exposition (ECCE)*, 2012, pp. 2099–2106. DOI: 10.1109/ECCE.2012.6342553.

[32] W. Cummins, D. T. M. B. W. D. C., and D. W. T. M. Basin, *The Impulse Response Function and Ship Motions*, ser. Report (David W. Taylor Model Basin). Navy Department, David Taylor Model Basin, 1962. [Online]. Available: https://books.google.ie/books?id=GLLANwAACAAJ.

[33] T. Pérez and T. I. Fossen, "Time- vs. frequency-domain identification of parametric radiation force models for marine structures at zero speed," *Modeling Identification and Control*, vol. 29, pp. 1–19, 2008.

[34] R. Taghipour, T. Perez, and T. Moan, "Hybrid frequency–time domain models for dynamic response analysis of marine structures," *Ocean Engineering*, vol. 35, no. 7, pp. 685–705, 2008, ISSN: 0029-8018. DOI: https://doi.org/10.1016/j.oceaneng.2007.11.002. [Online]. Available: https://www.sciencedirect.com/science/article/pii/S0029801807002363.

[35] M. Penalba, A. Mérigaud, J.-C. Gilloteaux, and J. Ringwood, "Influence of nonlinear Froude-Krylov forces on the performance of two wave energy points absorbers," *Journal of Ocean Engineering and Marine Energy*, vol. 3, no. 3, pp. 209–220, 2017.

[36] U. Korde and J. Ringwood, *Hydrodynamic Control of Wave Energy Devices*. Cambridge University Press, 2016, ISBN: 9781107079700. [Online]. Available: https://books.google.ie/books?id=VcfxDAAAQBAJ.

[37] J. Falnes, "A review of wave-energy extraction," *Marine Structures*, vol. 20, pp. 285–201, 2007.

[38] D. Valério, P. Beirão, and J. da Costa, "Reactive control and phase and amplitude control applied to the archimedes wave swing," ser. International Ocean and Polar Engineering Conference, vol. All Days.

[39] J. Hals, J. Falnes, and T. Moan, "A Comparison of Selected Strategies for Adaptive Control of Wave Energy Converters," *Journal of Offshore Mechanics and Arctic Engineering*, vol. 133, no. 3, Mar. 2011, 031101, ISSN: 0892-7219. DOI: 10.1115/1.4002735. [Online]. Available: https://doi.org/10.1115/1.4002735.

[40] P.Nebel, "Maximizing the efficiency of wave energy plant using complex conjugate control," *Proceedings of the IME. Part I: Journal of Systems and Control Engineering*, 206:225–36, 1992.

[41] N. S.H. Salter J.R.M. Taylor, "Power conversion mechanisms for wave energy," *Proceedings of the IME. Part M: Journal of Engineering for the Maritime Environment*, 216:1–27, 2002.

[42] E. Tedeschi, M. Molinas, M. Carraro, and P. Mattavelli, "Analysis of power extraction from irregular waves by all-electric power take off," in *2010 IEEE Energy Conversion Congress and Exposition*, 2010, pp. 2370–2377. DOI: 10.1109/ECCE.2010.5617893.

[43] E. Tedeschi, M. Carraro, M. Molinas, and P. Mattavelli, "Effect of control strategies and power take-off efficiency on the power capture from sea waves," *IEEE Transactions on Energy Conversion*, vol. 26, no. 4, pp. 1088–1098, 2011. DOI: 10.1109/TEC.2011.2164798.

[44] F. Fusco, J.-C. Gilloteaux, and J. Ringwood, "A study on prediction requirements in time-domain control of wave energy converters," *IFAC Proceedings Volumes*, vol. 43, no. 20, pp. 372–377, 2010, 8th IFAC Conference on Control Applications in Marine Systems, ISSN: 1474-6670. DOI: https://doi.org/10.3182/20100915-3-DE-3008.00075. [Online]. Available: https://www.sciencedirect.com/science/article/pii/S1474667016334917.

[45] F. Fusco and J. Ringwood, "A model for the sensitivity of non-causal control of wave energy converters to wave excitation force prediction errors," *Proceedings of the 9th European Wave and Tidal Energy Conference (EWTEC)*, Sep. 2011. [Online]. Available: https://mural.maynoothuniversity.ie/3551/.

[46] F. Fusco and J. V. Ringwood, "Short-term wave forecasting for real-time control of wave energy converters," *IEEE Transactions on Sustainable Energy*, vol. 1, no. 2, pp. 99–106, 2010. DOI: 10.1109/TSTE.2010.2047414.

[47] J. Scruggs, S. Lattanzio, A. Taflanidis, and I. Cassidy, "Optimal causal control of a wave energy converter in a random sea," *Applied Ocean Research*, vol. 42, pp. 1–15, 2013, ISSN: 0141-1187. DOI: https://doi.org/10.1016/j.apor.2013.03.004. [Online]. Available: https://www.sciencedirect.com/science/article/pii/S0141118713000205.

[48] M. Lopes, J. Hals, R. Gomes, T. Moan, L. Gato, and A. O. Falcão, "Experimental and numerical investigation of non-predictive phase-control strategies for a point-absorbing wave energy converter," *Ocean Engineering*, vol. 36, no. 5, pp. 386–402, 2009, ISSN: 0029-8018.

[49] M. French, "A generalized view of resonant energy transfer," *Journal of Mechanical Engineering Science*, vol. 21(4), pp. 299–300, 1979.

[50] W. Sheng, R. Alcorn, and A. Lewis, "On improving wave energy conversion, part II: Development of latching control technologies," *Renewable Energy*, vol. 75, no. C, pp. 935–944, 2015. DOI: 10.1016/j.renene.2014.09..

[51] J. Wu, Y. Yao, L. Zhou, and M. Göteman, "Real-time latching control strategies for the solo duck wave energy converter in irregular waves," *Applied Energy*, vol. 222, pp. 717–728, 2018, ISSN: 0306-2619. DOI: https://doi.org/10.1016/j.apenergy.2018.04.033. [Online]. Available: https://www.sciencedirect.com/science/article/pii/S0306261918305750.

[52] P. A. Brodtkorb, P. Johannesson, G. Lindgren, I. Rychlik, J. C. Ryden, and E. Sjö, "WAFO - a Matlab toolbox for analysis of random waves and loads," ser. International Ocean and Polar Engineering Conference, vol. All Days, 2000.

[53] J. Falnes, "Principles for capture of energy from ocean waves. phase control and optimum oscillation," 1997.

[54] J. Falnes, "A review of wave-energy extraction," *Marine Structures*, vol. 20, no. 4, pp. 185–201, 2007, ISSN: 0951-8339. DOI: https://doi.org/10.1016/j.marstruc.2007.09.001. [Online]. Available: https://www.sciencedirect.com/science/article/pii/S0951833907000482.

[55] M. Greenhow and S. P. White, "Optimal heave motion of some axisymmetric wave energy devices in sinusoidal waves," *Applied Ocean Research*, vol. 19, pp. 141–159, 1997.

[56] F. Kara, "Time domain prediction of power absorption from ocean waves with latching control," *Renewable Energy*, vol. 35, no. 2, pp. 423–434, 2010, ISSN: 0960-1481. DOI: https://doi.org/10.1016/j.renene.2009.06.003. [Online]. Available: https://www.sciencedirect.com/science/article/pii/S0960148109002730.

[57] M. Molinas, O. Skjervheim, P. Andreasen, *et al.*, "Power electronics as grid interface for actively controlled wave energy converters," in *2007 International Conference on Clean Electrical Power*, 2007, pp. 188–195. DOI: 10.1109/ICCEP.2007.384210.

[58] J Falnes and T Bjarte-Larsson, "Theoretical and experimental investigation of wave energy conversion by a phase-controlled heaving body," *Proceedings of the Institution of Mechanical Engineers, Part M: Journal of Engineering for the Maritime Environment*, vol. 220, no. 4, pp. 175–183, 2006. DOI: 10.1243/14750902JEME52. [Online]. Available: https://doi.org/10.1243/14750902JEME52.

[59] T. Bjarte-Larsson and J. Falnes, "Laboratory experiment on heaving body with hydraulic power take-off and latching control," *Ocean Engineering*, vol. 33, pp. 847–877, 2006.

[60] U. A. Korde, "Phase control of floating bodies from an on-board reference," *Applied Ocean Research*, vol. 23, no. 5, pp. 251–262, 2001, ISSN: 0141-1187. DOI: https://doi.org/10.1016/S0141-1187(01)00026-8. [Online]. Available: https://www.sciencedirect.com/science/article/pii/S0141118701000268.

[61] A. Babarit, H. Mouslim, M. Guglielmi, and A. Clément, "Simulation of the SEAREV wave energy converter with a by-pass control of its hydraulic power take off," *10th World Renewable Energy Congress*, Jan. 2008.

[62] A. Clément and A. Babarit, "Discrete control of resonant wave energy devices," *Philosophical transactions. Series A, Mathematical, physical, and engineering sciences*, vol. 370, pp. 288–314, Jan. 2012. DOI: 10.1098/rsta.2011.0132.

[63] R. Hoskin and N. Nichols, "Latching control of a point absorber," *Proceedings of the 3rd international symposium on wave, tidal, OTEC, and small scale hydro energy*, pp. 317–30, 1986.

[64] J. J. Cândido and P. A. Justino, "Modelling, control and Pontryagin Maximum Principle for a two-body wave energy device," *Renewable Energy*, vol. 36, no. 5, pp. 1545–1557, 2011. DOI: 10.1016/j.renene.2010.11..

[65] A. F. de O. Falcão, "Phase control through load control of oscillating-body wave energy converters with hydraulic pto system," *Ocean Engineering*, vol. 35, no. 3, pp. 358–366, 2008, ISSN: 0029-8018. DOI: https://doi.org/10.1016/j.oceaneng.2007.10.005.

[66] T. K. A. Brekken, "On model predictive control for a point absorber wave energy converter," *Proc. of the 2011 IEEE Trondheim PowerTech, Trondheim, Norway, Jun. 2011*, pp. 1–8, 2011.

[67] B. Finlayson and L. Scriven, "The method of weighted residuals - a review," *Appl. Mech. Rev.*, vol. 19, pp. 735–748, Jan. 1966.

[68] G. Bacelli, J. V. Ringwood, and J.-C. Gilloteaux, "A control system for a self-reacting point absorber wave energy converter subject to constraints," *IFAC Proceedings Volumes*, vol. 44, no. 1, pp. 11 387–11 392, 2011, 18th IFAC World Congress, ISSN: 1474-6670. DOI: https://doi.org/10.3182/20110828-6-IT-1002.03694.

[69] D. R. Herber and J. T. Allison, "Wave Energy Extraction Maximization in Irregular Ocean Waves Using Pseudospectral Methods," ser. International Design Engineering Technical Conferences and Computers and Information in Engineering Conference, vol. Volume 3A: 39th Design Automation Conference, Aug. 2013.

[70] G. Duclos, A. Babarit, and A. H. Clément, "Optimizing the Power Take Off of a Wave Energy Converter With Regard to the Wave Climate," *Journal of Offshore Mechanics and Arctic Engineering*, vol. 128, no. 1, pp. 56–64, Jul. 2005.

[71] J. J. Candido and P. A. P. Justino, "Frequency, stochastic and time domain models for an articulated wave power device," ser. International Conference on Offshore Mechanics and Arctic Engineering, vol. Volume 6: Nick Newman Symposium on Marine Hydrodynamics; Yoshida and Maeda Special Symposium on Ocean Space Utilization; Special Symposium on Offshore Renewable Energy, Jun. 2008, pp. 633–643.

[72] E. A. Amon, A. A. Schacher, and T. K. A. Brekken, "A novel maximum power point tracking algorithm for ocean wave energy devices," in *2009 IEEE Energy Conversion Congress and Exposition*, 2009, pp. 2635–2641. DOI: 10.1109/ECCE.2009.5316277.

[73] B. Orazov, O. O'Reilly, and Savaş, "On the dynamics of a novel ocean wave energy converter," *Journal of Sound and Vibration*, vol. 329, no. 24, pp. 5058–5069, 2010.

[74] T. Lewis, A. von Jouanne, and T. Brekken, "Wave energy converter with wideband power absorption," Oct. 2011, pp. 3844 –3851. DOI: 10.1109/ECCE.2011.6064291.

[75] M. Belmont, "Increases in the average power output of wave energy converters using quiescent period predictive control," *Renewable Energy*, vol. 35, no. 12, pp. 2812–2820, 2010, ISSN: 0960-1481. DOI: https://doi.org/10.1016/j.renene.2010.05.001. [Online]. Available: https://www.sciencedirect.com/science/article/pii/S0960148110002193.

[76] R. Genest and J. V. Ringwood, "A critical comparison of model-predictive and pseudospectral control for wave energy devices," *Journal of Ocean Engineering and Marine Energy*, vol. 2, pp. 485–499, 2016.

[77] M. Sichani, J.-B. Chen, M. Kramer, and S. Nielsen, "Constrained optimal stochastic control of non-linear wave energy point absorbers," English, *Applied Ocean Research*, vol. 47, 255–269, 2014, ISSN: 0141-1187.

[78] J. Scruggs, "Multi-objective optimal causal control of an ocean wave energy converter in random waves," in *OCEANS'11 MTS/IEEE KONA*, 2011, pp. 1–6. DOI: 10.23919/OCEANS.2011.6107113.

[79] H. Eidsmoen, "Optimum Control of a Floating Wave-Energy Converter With Restricted Amplitude," *Journal of Offshore Mechanics and Arctic Engineering*, vol. 118, no. 2, pp. 96–102, May 1996.

[80] A. Zurkinden, S. Lambertsen, L. Damkilde, Z. Gao, and T. Moan, "Fatigue analysis of a wave energy converter taking into account different control strategies," vol. 8, Jun. 2013. DOI: 10.1115/OMAE2013-10864.

[81] S. Mallat, *A Wavelet Tour of Signal Processing, Third Edition: The Sparse Way*, 3rd. USA: Academic Press, Inc., 2008, ISBN: 0123743702.

[82] S. Parvez and Z. Gao, "A wavelet-based multi-resolution pid controller," in *38th IAS Annual Meeting on Conference Record of the Industry Applications Conference, 2003.*, vol. 1, 2003, 1–5 vol.1. DOI: 10.1109/IAS.2003.1257474.

[83] A. Jayasiri, S. Ahmed, and S. Imtiaz, "Wavelet-based controller design for dynamic positioning of vessels," *IFAC-PapersOnLine*, vol. 50, no. 1, pp. 1133–1138, 2017, 20th IFAC World Congress, ISSN: 2405-8963. DOI: https://doi.org/10.1016/j.ifacol.2017.08.396. [Online]. Available: https://www.sciencedirect.com/science/article/pii/S2405896317307437.

[84] B. Basu and S. Nagarajaiah, "A wavelet-based time-varying adaptive LQR algorithm for structural control," *Engineering Structures*, vol. 30, no. 9, pp. 2470–2477, 2008. DOI: https://doi.org/10.1016/j.engstruct.2008.01.011.

[85] G. Ducrozet, F. Bonnefoy, D. Le Touzé, and P. Ferrant, "3-D HOS simulations of extreme waves in open seas," *Natural hazards and earth system sciences*, vol. 7, pp. 109–122, Jan. 2007. DOI: 10.5194/nhess-7-109-2007.

[86] M. Bhinder, A. Babarit, L. Gentaz, and P. Ferrant, "Effect of viscous forces on the performance of a surging wave energy converter," in *22nd International Conference on Ocean, Offshore and Artic Engineering (ISOPE2012)*, Rhodes, Greece, 2012.

[87] P. C. Vicente, A. F. Falcão, and P. A. Justino, "Nonlinear dynamics of a tightly moored point-absorber wave energy converter," *Ocean Engineering*, vol. 59, pp. 20–36, 2013, ISSN: 0029-8018. DOI: https://doi.org/10.1016/j.oceaneng.2012.12.008. [Online]. Available: https://www.sciencedirect.com/science/article/pii/S0029801812004179.

[88] A. Babarit, H. Mouslim, A. Cle´ment, and P. Laporte-Weywada, "On the numerical modelling of the non linear behaviour of a wave energy converter," ser. International Conference on Offshore Mechanics and Arctic Engineering, vol. Volume 4: Ocean Engineering; Ocean Renewable Energy; Ocean Space Utilization, Parts A and B, May 2009, pp. 1045–1053.

[89] G. Giorgi and J. V. Ringwood, "Implementation of latching control in a numerical wave tank with regular waves," *Journal of Ocean Engineering and Marine Energy*, vol. 2, pp. 211–226, 2016.

[90] M. P. Retes, G. Giorgi, and J. Ringwood, "A review of non-linear approaches for wave energy converter modelling," *Proceedings of the 11th European Wave and Tidal Energy Conference*, 2015. [Online]. Available: https://mural.maynoothuniversity.ie/6678/.

[91] M. Lawson, Y.-H. Yu, A. Nelessen, K. Ruehl, and C. Michelen, "Implementing nonlinear buoyancy and excitation forces in the WEC-Sim wave energy converter modeling tool," ser. International Conference on Offshore Mechanics and Arctic Engineering, vol. Volume 9B: Ocean Renewable Energy, Jun. 2014.

[92] B. Guo, R. Patton, S. Jin, J. Gilbert, and D. Parsons, "Nonlinear modeling and verification of a heaving point absorber for wave energy conversion," *IEEE Transactions on Sustainable Energy*, vol. 9, no. 1, pp. 453–461, 2018. DOI: 10.1109/TSTE.2017.2741341.

[93] S. Boyd, V. Balakrishnan, E. Feron, and L. El Ghaoui, "History of linear matrix inequalities in control theory," in *Proceedings of 1994 American Control Conference - ACC '94*, vol. 1, 1994, 31–34 vol.1. DOI: 10.1109/ACC.1994.751687.

[94] S. Boyd, L. El Ghaoui, E. Feron, and V. Balakrishnan, *Linear Matrix Inequalities in System and Control Theory*, ser. Studies in Applied Mathematics. Philadelphia, PA: SIAM, Jun. 1994, vol. 15, ISBN: 0-89871-334-X.

[95] A. Casavola, F. Iorio, and F. Tedesco, "A multiobjective H_∞ control strategy for energy harvesting in regenerative vehicle suspension systems," *International Journal of Control*, pp. 1–22, Feb. 2017. DOI: 10.1080/00207179.2017.1293298.

[96] H. Chen, P. Sun, and K. Guo, "Constrained H-infinity control of active suspensions: An LMI approach," in *The 2002 International Conference on Control and Automation, 2002. ICCA. Final Program and Book of Abstracts.*, 2002, pp. 157–157. DOI: 10.1109/ICCA.2002.1229516.

[97] Y. Lao and J. Scruggs, "Robust control of wave energy converters using unstructured uncertainty," Jul. 2020, pp. 4237–4244. DOI: 10.23919/ACC45564.2020.9148045.

[98] S. Lindroth and M. Leijon, "Offshore wave power measurements—a review," *Renewable and Sustainable Energy Reviews*, vol. 15, no. 9, pp. 4274–4285, 2011, ISSN: 1364-0321. DOI: https://doi.org/10.1016/j.rser.2011.07.123. [Online]. Available: https://www.sciencedirect.com/science/article/pii/S1364032111003704.

[99] A. Savin, O. Svensson, E. Stro¨mstedt, C. Bostro¨m, and M. Leijon, "Determining the service life of a steel wire under a working load in the wave energy converter (wec)," ser. International Conference on Offshore Mechanics and Arctic Engineering, vol. Volume 4: Ocean Engineering; Ocean Renewable Energy; Ocean Space Utilization, Parts A and B, May 2009, pp. 839–844. DOI: 10.1115/OMAE2009-79164.

[100] F. Johnson, J. Chudley, and Y. Dai, "Simulation and sea trial data analysis of a tethered multiple oscillating water column wave energy device," *MAREC 2002, International Conference on Marine Renewable Energy - Conference Proceedings*, pp. 171–181, Jan. 2002.

[101] D. Elwood, A. Schacher, K. Rhinefrank, *et al.*, "Numerical modeling and ocean testing of a direct-drive wave energy device utilizing a permanent magnet linear generator for power take-off," ser. International Conference on Offshore Mechanics and Arctic Engineering, vol. Volume 4: Ocean Engineering; Ocean Renewable Energy; Ocean Space Utilization, Parts A and B, May 2009, pp. 817–824. DOI: 10.1115/OMAE2009-79146.

[102] "Observer based controller design for linear systems with input constraints," *IFAC Proceedings Volumes*, vol. 41, no. 2, pp. 9916–9921, 2008, 17th IFAC World Congress, ISSN: 1474-6670. DOI: https://doi.org/10.3182/20080706-5-KR-1001.01678.

[103] E. Simon, P. R-Ayerbe, C. Stoica, D. Dumur, and V. Wertz, "LMIs-based coordinate descent method for solving bmis in control design," *IFAC Proceedings Volumes*, vol. 44, no. 1, pp. 10 180–10 186, 2011, 18th IFAC World Congress, ISSN: 1474-6670. DOI: https://doi.org/10.3182/20110828-6-IT-1002.00464.

[104] K.-C. Goh, M. Safonov, and G. Papavassilopoulos, "Global optimization for the biaffine matrix inequality problem," *Journal of Global Optimization*, vol. 7, pp. 365–380, Jan. 1995. DOI: 10.1007/BF01099648.

[105] Q. Tran Dinh, S. Gumussoy, W. Michiels, and M. Diehl, "Combining convex–concave decompositions and linearization approaches for solving bmis, with application to static output feedback," *IEEE Transactions on Automatic Control*, vol. 57, no. 6, pp. 1377–1390, 2012. DOI: 10.1109/TAC.2011.2176154.

[106] B. Fares, D. Noll, and P. Apkarian, "Robust control via sequential semidefinite programming," *SIAM Journal on Control and Optimization*, vol. 40, no. 6, pp. 1791–1820, 2002. DOI: 10.1137/S0363012900373483.

[107] P. Apkarian and D. Noll, "Nonsmooth H_∞ Synthesis," *IEEE Transactions on Automatic Control*, vol. 51, no. 1, pp. 71–86, 2006. DOI: 10.1109/TAC.2005.860290.

[108] M. Kheirandishfard, F. Zohrizadeh, and R. Madani, "Convex relaxation of bilinear matrix inequalities part I: Theoretical results," in *2018 IEEE Conference on Decision and Control (CDC)*, 2018, pp. 67–74. DOI: 10.1109/CDC.2018.8619567.

[109] A. Mérigaud and J. Ringwood, "Optimal trajectories, nonlinear models and constraints in wave energy device control," *IFAC-PapersOnLine*, vol. 50, no. 1, pp. 15 645–15 650, Jul. 2017.

[110] A. Babarit and G. Delhommeau, "Theoretical and numerical aspects of the open source BEM solver NEMOH," in *11th European Wave and Tidal Energy Conference (EWTEC2015)*, ser. Proceedings of the 11th European Wave and Tidal Energy Conference, Nantes, France, 2015. [Online]. Available: https://hal.archives-ouvertes.fr/hal-01198800.

[111] J. Falnes, "On non-causal impulse response functions related to propagating water waves," *Appl. Ocean Res.*, vol. 17-6, pp. 379–389, 1995.

[112] B. Guo, R. Patton, and S. Jin, "Identification and validation of excitation force for a heaving point absorber wave energy convertor," in *EWTEC 2017*, Sep. 2017.

[113] K. Hasselmann, T. Barnett, E. Bouws, *et al.*, "Measurements of wind-wave growth and swell decay during the joint north sea wave project (JONSWAP)," *Deut. Hydrogr. Z.*, vol. 8, pp. 1–95, Jan. 1973.

[114] B. Basu and S. Nagarajaiah, "Multiscale wavelet-lqr controller for linear time varying systems," *Journal of Engineering Mechanics-Asce*, vol. 136, pp. 1143–1151, Sep. 2010. DOI: 10.1061/(ASCE)EM.1943-7889.0000162.

[115] J. F.Fusco, "A simple and effective real-time controller for wave energy converters," *IEEE Transactions on Sustainable Energy*, vol. 4, 35(3/4):358–66, 2013.

[116] H. T. Banks, S. L. Keeling, R. J. Silcox, and C. Wang, "Linear quadratic tracking problems in Hilbert space - application to optimal active noise suppression," *IFAC Proceedings Volumes*, vol. 22, pp. 5–10, 1989.

[117] H. Tan, S. Shu, and F. Lin, "An optimal control approach to robust tracking of linear systems," *International Journal of Control*, vol. 82, no. 3, pp. 525–540, 2009.

[118] L. Pontryagin, *Mathematical Theory of Optimal Processes*, ser. Classics of Soviet Mathematics. Taylor & Francis, 1987, ISBN: 9782881240775. [Online]. Available: https://books.google.ie/books?id=kwzq0F4cBVAC.

[119] H. Yavuz, T. Stallard, A. Mccabe, and G. Aggidis, "Time series analysis-based adaptive tuning techniques for a heaving wave energy converter in irregular seas," *Proceedings of the Institution of Mechanical Engineers, Part A: Journal of Power and Energy*, vol. 221, no. 1, pp. 77–90, 2007. DOI: 10.1243/09576509JPE291.

[120] F. Fusco and J. V. Ringwood, "Suboptimal causal reactive control of wave energy converters using a second order system model," ser. International Ocean and Polar Engineering Conference, vol. All Days, Jun. 2011.

[121] A. Prach, O. Tekinalp, and D. S. Bernstein, "Infinite-horizon linear-quadratic control by forward propagation of the differential riccati equation [Lecture Notes]," *IEEE Control Systems Magazine*, vol. 35, no. 2, pp. 78–93, 2015. DOI: 10.1109/MCS.2014.2385252.

[122] B. Basu and A. Staino, "Control of a linear time-varying system with a forward riccati formulation in wavelet domain," *Journal of Dynamic Systems Measurement and Control-transactions of The Asme*, vol. 138, p. 104 502, 2016.

[123] M. Penalba, T. Kelly, and J. Ringwood, "Using NEMOH for modelling wave energy converters: A comparative study with WAMIT," in *12th European Wave and Tidal Energy Conference (EWTEC)*, 2017.

[124] G. Giorgi and J. Ringwood, "Comparing nonlinear hydrodynamic forces in heaving point absorbers and oscillating wave surge converters," *Journal of Ocean Engineering and Marine Energy*, vol. 4, no. 1, pp. 25–35, 2018.

[125] ——, "Computationally efficient nonlinear Froude–Krylov force calculations for heaving axisymmetric wave energy point absorbers," *Journal of Ocean Engineering and Marine Energy*, vol. 3, Feb. 2017. DOI: 10.1007/s40722-016-0066-2.

[126] C. Chen, D. Chen, and K. (Firm), *Linear System Theory and Design*, ser. Oxford series in electrical and computer engineering. Oxford University Press, 1999, ISBN: 9780195117776. [Online]. Available: https://books.google.ie/books?id=Fqi4oRgmOocC.

[127] P. Tristan and T. Fossen, "A matlab toolbox for parametric identification of radiation-force models of ships and offshore structures," *Modeling, Identification and Control*, vol. 30, Jan. 2009. DOI: 10.4173/mic.2009.1.1.

[128] M.-S. Chen and C.-y. Kao, "Control of Linear Time-Varying Systems Using Forward Riccati Equation," *Journal of Dynamic Systems, Measurement, and Control*, vol. 119, no. 3, pp. 536–540, Sep. 1997.

[129] M. Ma and H. Chen, "Constrained H2 control of active suspensions using LMI optimization," in *2006 Chinese Control Conference*, 2006, pp. 702–707. DOI: 10.1109/CHICC.2006.280723.

[130] J. Löfberg, "YALMIP : A toolbox for modeling and optimization in matlab," *In Proceedings of the 2004 IEEE International Symposium on Computer Aided Control Systems Design, IEEE*, pp. 284–289, 2004.

[131] J. F. Sturm, "Using SeDuMi 1.02, a Matlab toolbox for optimization over symmetric cones," *Optimization Methods and Software*, vol. 11, no. 1-4, pp. 625–653, 1999. DOI: 10.1080/10556789908805766.

[132] S. Lattanzio and J. Scruggs, "Maximum power generation of a wave energy converter in a stochastic environment," *Proceedings of the IEEE International Conference on Control Applications*, pp. 1125 –1130, 2011. DOI: 10.1109/CCA.2011.6044428.

[133] R. G. Coe, G. Bacelli, D. G. Wilson, O. Abdelkhalik, U. A. Korde, and R. D. Robinett III, "A comparison of control strategies for wave energy converters," *International Journal of Marine Energy*, vol. 20, pp. 45 –63, 2017. DOI: 10.1016/j.ijome.2017.11.001.

[134] "Powerpod technical datasheet," Technical report, Trident Energy. URL https://www. tridentenergy. co. uk/wp, Tech. Rep., 2014.

[135] *Foras Na Mara, Marine Data Centre*, http://www.marine.ie/Home/site-area/data-services/real-time-observations/real-time-observations, [Online; accessed 19-July-2020], 2020.

[136] M. Eriksson, J. Isberg, and M. Leijon, "Theory and experiment on an elastically moored cylindrical buoy," *Oceanic Engineering, IEEE Journal of*, vol. 31, pp. 959 –963, Nov. 2006. DOI: 10.1109/JOE.2006.880387.

[137] "A sequential LMI approach to design a BMI-based multi-objective nonlinear observer," *European Journal of Control*, vol. 44, pp. 50–57, 2018, Advanced Control and Observer Design for Nonlinear Systems via LMIs, ISSN: 0947-3580. DOI: https://doi.org/10.1016/j.ejcon.2018.09.004.

[138] L. El Ghaoui and V. Balakrishnan, "Synthesis of fixed-structure controllers via numerical optimization," in *Proceedings of 1994 33rd IEEE Conference on Decision and Control*, vol. 3, 1994, 2678–2683 vol.3. DOI: 10.1109/CDC.1994.411398.

[139] C. Signorelli, "Optimal real-time predictive control for maximising the Power-Take-Off efficiency of the WaveRAM wave energy converter. phd thesis," *Trinity College Dublin. School of Engineering. Civil, Structural and Environmental Engineering*, 2018.